Short Term Performance of Bituminous Geomembranes with Respect to Temperature Variations

A Thesis Submitted to the College
of Graduate and Postdoctoral Studies
In Partial Fulfillment of the Requirements
For the Degree of Master of Science
In the Department of Civil, Geological, and Environmental Engineering
University of Saskatchewan
Saskatoon

By:
Mitchell Lewis Rogal

Permission to Use

In presenting this thesis/dissertation in partial fulfillment of the requirements for a Postgraduate degree from the University of Saskatchewan, I agree that the Libraries of this University may make it freely available for inspection. I further agree that permission for copying of this thesis/dissertation in any manner, in whole or in part, for scholarly purposes may be granted by the professor or professors who supervised my thesis/dissertation work or, in their absence, by the Head of the Department or the Dean of the College in which my thesis work was done. It is understood that any copying or publication or use of this thesis/dissertation or parts thereof for financial gain shall not be allowed without my written permission. It is also understood that due recognition shall be given to me and to the University of Saskatchewan in any scholarly use which may be made of any material in my thesis/dissertation.

Requests for permission to copy or to make other uses of materials in this thesis/dissertation in whole or part should be addressed to:

Dean College of Graduate and Postdoctoral Studies
University of Saskatchewan
116 Thorvaldson Building, 110 Science Place
Saskatoon, Saskatchewan S7N 5C9 Canada

OR

Head of the Department of Civil, Geological, and Environmental Engineering
University of Saskatchewan
57 Campus Drive
Saskatoon, Saskatchewan S7N 5A9 Canada

Abstract

There is a significant lack of independent, peer-reviewed research on the performance of bituminous geomembranes in barrier system applications when compared to the standard barrier polymers used in industry today. The purpose of the research presented in this thesis is to help form a foundation of objective data on bituminous geomembranes (BGMs) performance in the field, as well as to compare it to polymer barriers like high density polyethylene (HDPE) geomembranes, linear low density (LLDPE) geomembranes, and other well known material types. In addition, in Saskatchewan, the temperature can vary by more than 60°C so a variety of climate conditions need to be considered when installing geomembrane covers. Due to temperature variability, the influence on temperature on the performance of bituminous geomembranes is one of the main variables considered in this research.

A variety of different testing methods were evaluated during this research including multiple ASTM standards for geomembrane puncture and tearing, and short-term performance testing; all with variations in temperature included in the testing procedures. The ASTM style testing methods used the ASTM designated apparatus, while the short-term performance testing was performed using equipment designed and manufactured in the College of Engineering Shops.

When evaluating the puncture resistances of both BGMs and HDPE geomembranes, it was found that as temperatures increase, the displacement required to cause puncture also increases. In contrast to this, the puncture resistance of the samples themselves decrease as temperatures increase. During the sub-zero experiments, it was observed that the stiffness of the geomembranes increased. Additionally, while HDPE geomembranes showed higher overall loads at the time of puncture, the BGMs deformed in much more elastic manners allowing them to reform into their original shape due to the viscosity of the bitumen binding, which could be highly beneficial in application.

When looking at the short-term performance of BGMs, in applications with the presence of aggressive over liners with the potential to cause puncture, it was found that both BGM products were able to withstand applied stresses of up to 400 kPa without any holes being caused in the barrier. Additionally, at lower temperatures there was little to no surface deformation present on the samples, with very minimal damage from the aggressive over liner.

Based on the findings of this research, it was observed that HDPE retains a higher resistance to puncture than BGMs, however the highly viscous nature of BGMs shows that it could have many advantages in short-term performance depending on the conditions in which it is used.

Acknowledgements

First, I would like to thank my supervisor, Dr. Ian Fleming, for all the guidance and support he gave me throughout the project. Whether it was a brainstorming session of how we could turn part of the lab into a temperature-controlled shed or refreshing me on a basic concept I had forgotten about that somehow solved the problem I was having immediately, I always came out of our meetings feeling motivated and confident even if I went into them feeling like I was stuck or confused. I appreciate all of the advice and lessons you gave me and will make sure to take them with me into the rest of my career. I would also like to thank the other members of my committee, Dr. David Elwood and Dr. Doug Milne for their input and advice in committee meetings and for their help in finalizing my thesis.

Next, I would like to thank Adam Hammerlindl for all the help he provided to myself, and everyone else in the lab. Adam is one of the busiest people I have ever met but would still gladly help with anything you ask him, even if it was moving a 500lb load frame into a freezer on three separate occasions. Adam was usually present during the brainstorming sessions between Ian and I, and I am glad he was. His input was always appreciated, and his knowledge of the equipment in the lab helped dramatically in experiments go as smoothly as they could. A big thank you also goes out to all the other 'Dirt Nerds' in the lab, past and present, for both the friendships, and technical help throughout the project.

I would also like to thank NSERC and Titan Environmental Containment for their financial support, and for supplying the geomembrane products for this research.

I would also like to thank my parents, Pat, and Paul, for their unending support not only during my time as a graduate student, but throughout my whole life. They have both been incredible influences in my life and I wouldn't be where I am today without them. I want to thank my sister Emily, for being an amazing editor, and an even better older sister. I want to thank my friends for all their encouragement, support, and love through all the celebrations and loss that we have gone through together. I could not ask for a better group of guys to call my friends.

Finally, I want to thank my girlfriend, Jill. Thank you for being nothing but supportive of me in everything I do both academic and not. You've always been someone I can talk to about anything

going on and I am so lucky to have you in my life. Thank you for listening to me talk about rocks and dirt for countless hours, even if it may have been boring to you some of the time. Thank you for being you.

Table of Contents

Chapter 1 – Introduction 1

1.1: Background 1

1.2: Research Objectives 2

1.3: Scope of Project 2

1.4: Organization of Thesis 3

Chapter 2 - Literature Review 4

2.1: Background on Bituminous Geomembranes 4

2.2: Causes of Geomembrane Damage 5

2.3: Long Term Flow Performance of Bituminous Geomembranes 6

2.4: Damage in Bituminous Geomembranes 9

2.5: Leakage Through Bituminous Geomembranes 11

2.6: Influence of Temperature on Bituminous Geomembranes 13

2.7: Background on Standardized Puncture and Tear Testing 14

2.7.1: ASTM Puncture Resistance (ASTM D4833) 14

2.7.2: ASTM Tear Resistance (ASTM D5884) 16

2.8: Gaps in Literature 17

Chapter 3 – Methodology 18

3.1: Testing Apparatus and Equipment 18

3.1.1: Geomembrane Selection 18

3.1.2: Testing Load Frame 19

3.1.3: Temperature Control Measures 21

3.1.4: ASTM Puncture Resistance Apparatus 21

3.1.5: ASTM Tear Resistance Apparatus 22

3.1.6: Short-Term Performance Testing Apparatus 23

3.1.7: Subgrade Material Selection 25
3.1.8: Aggregate Selection 26
3.2: Testing Procedures 27
3.2.1: ASTM Test Procedures 27
3.2.2: Large-Scale Performance Testing Procedure 28
3.2.3: Testing Plan 29
Chapter 4 - Results and Discussion 30
4.1: Puncture Resistance Results and Discussion 30
4.1.1: ES2 Puncture 30
4.1.2: ES4 Puncture 31
4.1.3: 1.5 mm HDPE Puncture 32
4.1.4: 3 mm HDPE Results 33
4.1.5: Trends in Puncture Results 34
4.1.6: Specific Case Puncture Testing 36
4.2: Tear Resistance Results and Discussion 39
4.2.1: ES2 Tear Results 40
4.2.2: ES4 Tear Results 42
4.2.3: Tear Results Discussion 43
4.3: Large Scale Performance Testing Results 45
4.3.1: Results of −15°C Performance Testing 46
4.3.2: Results of 0°C Performance Testing 47
4.3.3: Results of +20°C Performance Testing 48
Chapter 5 - Conclusion and Recommendations 51
5.1: Conclusions of the Research 51
5.2: Recommendations for Future Research 56

References 57
Appendix A: Individual Puncture Resistance Plots 59
A.1: ES2 Puncture 59
A.2: ES4 Puncture 62
A.3: 1.5 mm HDPE Puncture 66
A.4: 3 mm HDPE Puncture 69
Appendix B: Engineering Designs of Manufactured Equipment 73
B.1: Individual Component Drawings 73
B.1.1: Load Apparatus Lower Body 73
B.1.2: Load Apparatus Upper Body 74
B.1.3: O-Ring Placeholder 75
B.1.4: Upper Cap Plate 76
B.1.5: Lower Base Plate 77
B.1.6: Load Plate Top 78
B.1.7: Load Plate Body 79
B.1.8: Load Plate Bottom 80
B.1.9: Load Point Attachment 81
B.2: Assembly Design Drawings 82
B.2.1: Upper Body Assembly 82
B.2.2: Lower Body Assembly 83
B.2.3: Load Plate Assembly 84
Appendix C: Extra Large Scale Sample Photos 85
C.1: ES2 Samples Photos (−15°C) 85
C.2: ES4 Samples Photos (−15°C) 87
C.3: ES2 Samples Photos (0°C) 90

C.4: ES4 Samples Photos (0°C) 92
C.5 ES2 Samples Photos (+20°C) 94
C.6: ES4 Samples Photos (+20°C) 96
Appendix D: Bituminous Geomembrane Datasheets 98
D.1: ES2 Datasheet 98
D.2: ES4 Datasheet 99

List of Figures

Figure 2.1 Stainless Steel Pressure Cell (Touze-Foltz et al. 2015) 7
Figure 2.2 Elastomeric BGM Upstream and Downstream Flow Rate Measurements (Touze-Foltz et al. 2015) 8
Figure 2.3 Oxidized BGM Upstream and Downstream Flow Rates (Touze-Foltz et al. 2015) 8
Figure 2.4 Chromatograms of extracted bitumen (Touze-Foltz et al. 2015) 9
Figure 2.5 Geosynthetic Liner Longevity Simulator (GLLS) (Clinton & Rowe, 2017) 10
Figure 2.6 Interface Transmissivity Apparatus (Bannour et al., 2013) 12
Figure 2.7 Flow Rate Comparison of BGM Interfaces (Bannour et al., 2013) 13
Figure 2.8 ASTM Puncture Frame Schematics (ASTM, 2010) 15
Figure 2.9 Tear Sample Cut Guidelines (ASTM, 2012) 16
Figure 3.1 ES2 Sample Thickness Profile 19
Figure 3.2 E42 Sample Thickness Profile 19
Figure 3.3 Air Cylinder Frame with Control Valves 21
Figure 3.4 (Left) BGM mounted in Puncture Frame (Right) Puncture Apparatus in Load Frame 22
Figure 3.5 Tear Apparatus in Load Frame 23
Figure 3.6 (a) Upper Body Assembly (b) Lower Body Assembly (c/d) Load Plate Assembly 24
Figure 3.7 Full Load Assembly mounted in Air Frame 25
Figure 3.8 Glass Bead Subgrade SWCC 26
Figure 3.9 (Left) Coarse Aggregate with 30cm ruler for scale (Right) Aggressive Aggregate Fragments used to force puncture 27

Figure 4.1 ES2 Puncture Curves 31
Figure 4.2 ES4 Puncture Curves 32
Figure 4.3 1.5mm HDPE Puncture Curves 33
Figure 4.4 3mm HDPE Puncture Curves 34
Figure 4.5 BGM Displacement Vs Temperature Plot 35
Figure 4.6 BGM Puncture Resistance Vs Temperature Plot 36
Figure 4.7 ES2 Glycol Puncture Curves with Standard Baseline Reference Test (+10°C) 37
Figure 4.8 ES4 Glycol Puncture Curves with Standard Baseline Reference Test (+10°C) 37
Figure 4.9 ES2 Subgrade Puncture Curves with Standard Baseline Reference Test (+20°C) 38
Figure 4.10 ES4 Subgrade Puncture Curves with Standard Baseline Reference Test (+20°C) ... 39
Figure 4.11 ES2 −20°C Tear Curves 40
Figure 4.12 ES2 0°C Tear Curves 40
Figure 4.13 ES2 +20°C Tear Curves 41
Figure 4.14 ES2 +30°C Tear Curves 41
Figure 4.15 ES4 −20°C Tear Curves 42
Figure 4.16 ES4 0°C Tear Curves 42
Figure 4.17 ES4 +20°C Tear Curves 43
Figure 4.18 ES4 +30°C Tear Curves 43
Figure 4.19 Average Large-Scale Load Profile 45
Figure 4.20 ES2 Sample with Significant Deformation Points (-15°C) 47
Figure 4.21 ES2 Sample with Significant Deformation Points (0°C) 48
Figure 4.22 ES2 Sample with Significant Deformation (+20°C) 49
Figure 4.23 ES4 Sample with Significant Deformation (+20°C) 50
Figure 4.24 ES4 0°C Trial #2 Load Profile 50
Figure 5.1 Boussinesq's Equation in Application (Murthy, 2002) 55

List of Tables

Table 2.1 BGM Properties (Clinton & Rowe, 2017) 10
Table 2.2 Leakage Rates (Clinton & Rowe, 2017) 11
Table 2.3 Final Flow Rate and Transmissivity Values of BGM Interfaces (From Bannour et al., 2013) 13
Table 3.1 ES2 Physical and Technical Specs (Axter Coletanche, 2009) 19
Table 3.2: ES4 Physical and Technical Specs (Axter Coletanche, 2009) 19
Table 3.3 Testing Plan 29
Table 4.1 ES2 Puncture Values 31
Table 4.2 ES4 Puncture Values 32
Table 4.3 1.5mm HDPE Puncture Values 33
Table 4.4 3mm HDPE Puncture Values 34
Table 4.5 Significant Deformation Distribution (-15°C) 46
Table 4.6 Significant Deformation Distribution (0°C) 47
Table 4.7 Significant Deformation Distribution (+20°C) 48
Table 5.1 Puncture Test Value Summary 52
Table 5.2 Boussinesq's Evaluation of BGM Vertical Stress 55

List of Equations

Equation 5-1 Boussinesq's Equation 55
Equation 5-2 Definition of I_B 55

List of Abbreviations

Abbreviation/Acronym	Full Wording
BGM	Bituminous geomembrane
HDPE	High-Density polyethylene
LLDPE	Linear low-density polyethylene
PVC	Polyvinyl chloride
EPDM	Ethylene propylene diene terpolymer
GLLS	Geosynthetic Liner Longevity Simulator
GCL	Geosynthetic clay liner
CCL	Compacted clay liner
DI	De-ionized
P/V Controller	Pressure/Volume Controller
NPT	National Pipe Thread
LVDT	Linear variable differential transformer
SWCC	Soil Water Characteristic Curve

Chapter 1 – Introduction

1.1: Background

Bituminous geomembranes (BGMs) are an alternate type of geomembrane barrier that can be used in practice in landfills, waste covers, lagoons, and other various geotechnical engineering applications. There are a variety of traditional geomembrane polymers used in current engineering practices including high-density polyethylene (HDPE), linear low-density polyethylene (LLDPE), polyvinyl chloride (PVC), polypropylene (PP), and ethylene propylene diene terpolymer (EPDM) (Fleming, 2019). These polymers have their own physical and chemical properties that may be favourable for specific purposes and applications. There has been a large amount of peer reviewed research completed on standard geomembrane polymers, by a variety of academic institutions, however there is little research on bituminous geomembranes.

The benefit to using BGMs over standard geomembranes is that they are considered to have high puncture resistance, high strength, high interface shear resistance, high density, and are resistant to wrinkling from UV/solar radiation due to the bitumen binding. While all of these factors are positive, the low amount of peer reviewed research on these barriers are cause for doubt under field conditions.

Overall, bituminous geomembranes lack large amounts of independent research to reinforce the manufacturers' performance specifications. There are small amounts of research ongoing at different institutions, but the available data is still minimal when compared to traditional polymer barrier materials. Queen's University in Ontario has previously conducted research on the effects of aggregate loading and leakage through BGMs (Clinton and Rowe, 2017), however, the effects of temperature variation on the material are still limited. In semi-arid climates like Saskatchewan, where the temperature variation between seasons can reach 60°C, which is an important factor to consider when installing these types of products.

1.2: Research Objectives

The objective of this research is to conduct reliable, independent research and testing on the short-term performance of bituminous geomembranes with respect to variations in temperature, and evaluate how they perform in differently.

In the case of this project, the testing consisted of puncture and tear index testing, and vertical loading of the BGM with aggressive, angular aggregate in place to try and force puncture in the sample. These tests were conducted at a range of different ambient temperatures to compare the performance of the BGM under different conditions and determine if there could be significant variations in the reliability of BGMs based on the temperature they are installed at. The aspect of temperature influence on the BGM performance can be considered the priority of this research.

By conducting a variety of performance and index tests on different BGMs, and comparing their performance at different temperatures, geotechnical engineers will be able to make educated decisions about choosing bituminous geomembranes to fit the needs of their specific project. The purpose of this research is not to overshadow the existing geomembranes used in practice, but to expand the options of well researched materials available to the industry. The aspect of temperature influence will be particularly important for semi-arid regions such as Saskatchewan, where seasonal temperatures can vary significantly between winter and summer months.

1.3: Scope of Project

The purpose of this research is to create reliable, independent data on different short-term performance characteristics of bituminous geomembranes with respect to variations in temperature. The specific properties being tested include:

- Variation in short-term puncture and tear resistance across a temperature range of −20°C through +30°C
- Evaluate ASTM Puncture resistance for HDPE and BGM
- Evaluate ASTM Tear resistance for BGM
- Evaluate short term durability and performance for BGM under loads
- Monitor for any leakage through the BGM as it is loaded/damaged

These properties have been tested using a variety of load application equipment, which is detailed further in Chapter 3. The different apparatus includes equipment designed as part of this research project, as well as other pieces of equipment previously used for similar testing at the University of Saskatchewan.

Overall, this project is focused on the short-term loading performance of bituminous geomembranes, and how it varies under the influence of the ambient temperature, as during construction, temperatures can vary drastically from season to season in semi-arid regions like Saskatchewan. Some of these results are compared to HDPE geomembranes in order to show scenarios where BGMs may be a preferred polymer for a barrier system.

1.4: Organization of Thesis

This thesis consists of five major chapters, along with a collection of appendices:

1) Chapter 1 is the introduction to the research, along with its purposes and objectives.
2) Chapter 2 is a summary of basic literature related to the project and its objectives.
3) Chapter 3 details the methodology, equipment, and approaches used to testing and data collection.
4) Chapter 4 discusses the results of the testing stages.
5) Chapter 5 summarizes the performance testing and results. It also draws conclusions from this work and lists a set of recommendations for future work in this area.

Chapter 2 - Literature Review

2.1: Background on Bituminous Geomembranes

Geomembranes are a non-porous media, meaning that there are no void spaces present within the material. Even with no void spaces present, transport still occurs through the material at the molecular level through diffusion (Lambert et al. 2000). Factors driving this diffusion include: concentration, temperature gradients, and hydraulic gradients (Touze-Foltz et al. 2015).

Bituminous geomembranes as explained by Touze-Foltz and Farcas (2017), typically consist of a core layer made of a non-woven geotextile that has been coated with a waterproof bitumen binder, and a surface treatment to finish the product. The treatment process in most modern BGMs is usually an elastomer like Styrene-Butadiene-Styrene (SBS). This variation of geomembranes is referred to as elastomeric BGMs. Elastomeric BGMs tend to have low temperature brittleness ranges starting at −20°C to −30°C, maximum elastic strain of roughly 10%, and a max break elongation of around 1500% (Touze-Foltz et al. 2015). Oxidized BGMs undergo the same initial bitumen binding as elastomeric BGMs. However instead of receiving an elastomeric coating, the surface is oxidized by being exposed to hot air ranging from of 260°C to 320°C. The use of elastomeric BGMs have gradually been replacing oxidized BGMs over time due to their superior UV resistance (Touze-Foltz et al. 2015).

The core layer present in a BGM act as the main reinforcement that resist the mechanical stress applied to the geomembrane through an administered load. The three main types of core materials consist of:

1. A glass fibre reinforcement
2. A nonwoven polyester geotextile
3. A composite consisting of both a glass veil and a geotextile

As previously mentioned, the core layers undergo two levels of treatment to create a complete BGM. The first consists of a treatment that impregnates the core layer in an elastomeric bitumen resin binder. The second treatment coats the material again with the same binder in the case of elastomeric BGMs. The purpose for the double coating is to reduce the void space present as much

as possible, and to increase the bond strength between individual pieces. These elastomeric coatings act as a waterproofing for the core material present, while the core materials provide the mechanical properties of the BGM.

In Touze-Foltz et al. (2015), the performance of two bituminous geomembranes, one oxidized and one elastomeric, which had been in service for 15 years were evaluated based on their potential degradation. The paper is concerned with two out of the nine the Bazancourt sugar refinery retention ponds in Marne, France (Touze-Foltz et al. 2015). Both ponds were lined in 1997, and the samples were taken in 2013.

One pond was originally lined with an oxidized BGM, with a 300 g/m^2 geotextile underlain with a compacted chalk subgrade. Over the 15 years, the average coldest, and warmest temperatures of the two ponds were 6.1°C and 15.1°C, and -13°C and 39°C respectively, with annual sunshine hours ranging from 1274-2026 hours (Touze-Foltz et al. 2015).

At the end of the investigation, both the oxidized and elastomeric BGMs had noticeable visual differences from their installation condition. The oxidized BGM showed wearing away of the bitumen binder, and the reinforcement layer was visible at surface. The elastomeric BGM also showed signs of degradation, however it was purely surficial, and the reinforcement had not been exposed at all. Overall, the elastomeric BGM showed better hydraulic performance, and overall better conservation of its original properties after the 15-year trial compared with the oxidized BGM. The leakage rate through each BGM increased however for the oxidized BGM the flow rate was around one order of magnitude higher than that of the elastomeric BGM (4.5×10^{-5} m^3/m^2/d compared to 1.9×10^{-6} m^3/m^2/d). This was attributed to the reduction of bitumen present on the liner after its 15-year exposure. Based .on this information, it was advised by the researchers that if oxidized BGMs are used, it is best to limit exposure to UV radiation to reduce the degradation of the bitumen binder, as the UV radiation was considered to be a leading cause of the degradation.

2.2: Causes of Geomembrane Damage

As stated by Hornsey and Wishaw (2012), a coarse aggregate is commonly used as a drainage layer overlying a geomembrane with a geotextile used as a protection layer. Due to the nature of

most coarse aggregates, points of high local stress can be present, which can lead to damage and stress cracking. To combat this, protection layers have been developed that can consist of a variety of materials depending on project requirements. Protection layers can include sand cushions, tyre shreds, geotextiles, geo-composites, and compacted clay layers.

Additionally, in Marcotte's thesis (2021), he went into extensive detail on the major causes of geomembrane damage and came to the conclusion that the damage occurs in two main ways. The first is short term puncture damage, and the second is long term high localized strain damage. The short-term puncture damage is mainly caused by a combination of the angularity of the overlying gravel aggregate, along with potentially insufficient protection layers on the barrier material. There is also a potential for short-term strain deformations in geomembranes, however the major issues caused by strain usually occur in the long term.

2.3: Long Term Flow Performance of Bituminous Geomembranes

In the test described in Touze-Foltz et al. (2015), a two part cell was used to test the flow rates through a BGM. The cell was made of stainless steel with resistance to oxidation. In each of the two parts of the cell, there are small inlets to allow for the application of hydraulic pressure, as well as a porous disc in the downstream cavity to prevent unwanted deformation of the BGM (Figure 2.1). The two halves of the cell clamp together in order to hold the sample in place, with no additional tightening mechanisms required. Both the upstream and downstream sides have an inlet and outlet valve respectively, in order to allow draining of the system when necessary. Finally, the volume can be maintained on both sides using pressure-volume controllers. The apparatus is able to measure flow accurately to 10^{-6} m^3/m^2/day.

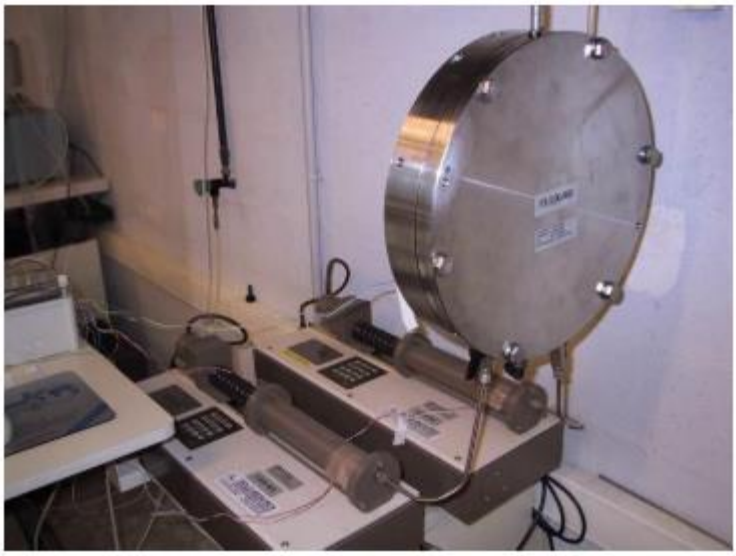

Figure 2.1 Stainless Steel Pressure Cell (Touze-Foltz et al. 2015)

The elastomeric and the oxidized BGMs were both tested using this apparatus. For the purposes of this study, the head differential applied across the geomembrane was set to 5m. The final equilibrium flux found on the upstream side of the geomembrane was 1.9×10^{-6} $m^3/m^2/d$ (Touze-Foltz et al. 2015). The fluctuations in the elastomeric BGM were due to temperature changes in the room during testing (Figure 2.2).

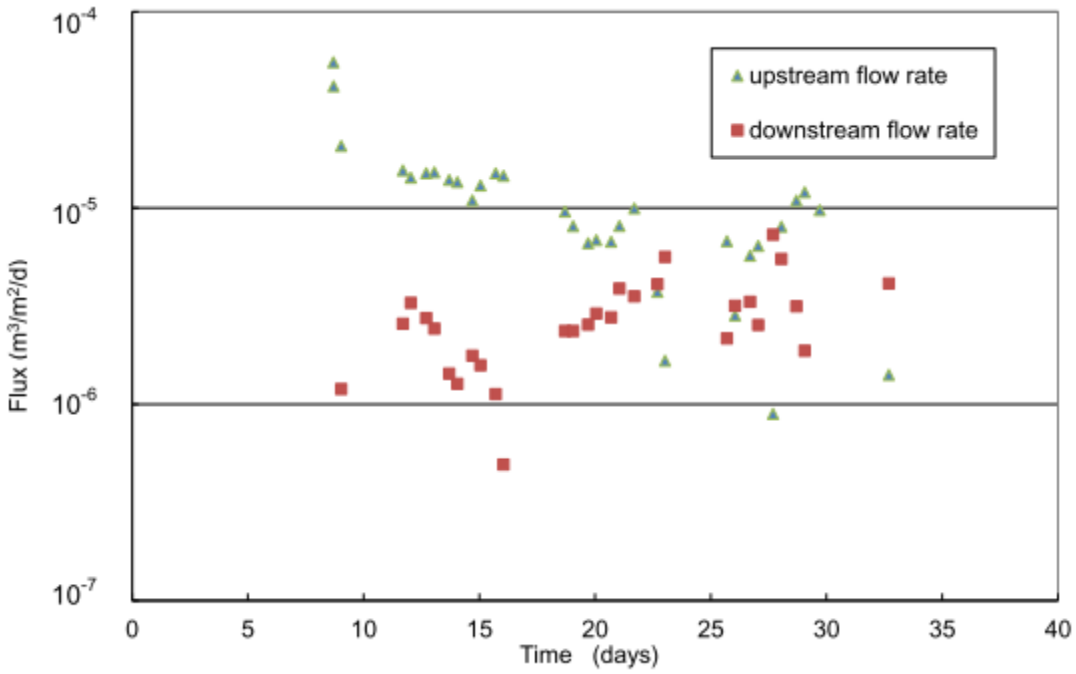

Figure 2.2 Elastomeric BGM Upstream and Downstream Flow Rate Measurements (Touze-Foltz et al. 2015)

After running the same test on the oxidized BGM, the final flow rates on the upstream and downstream sides were found to be 4.65×10^{-5} and 4.49×10^{-5} $m^3/m^2/d$ respectively. These flow rates are about an order of magnitude higher than that of the elastomeric BGM (Figure 2.3).

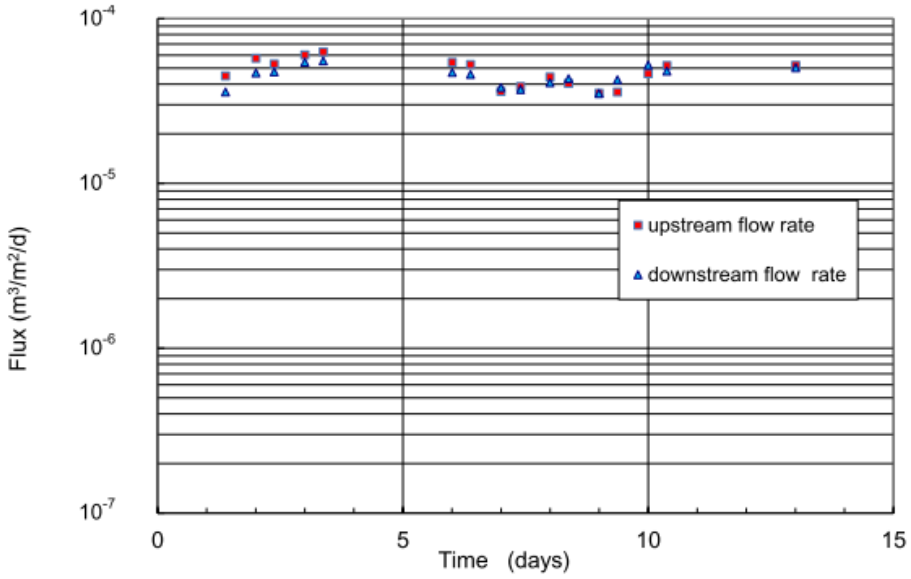

Figure 2.3 Oxidized BGM Upstream and Downstream Flow Rates (Touze-Foltz et al. 2015)

After observing the variation in flux through the BGMs, a chromatography analysis of extracted binders from both BGM samples was conducted to evaluate potential degradation of the bitumen

binding. It was found that there was a lack of a polymer resistivity peak when looking at the oxidized BGM (Figure 2.4). It was hypothesized that the presence of larger oxidized chemical reactions leads to increased embrittlement of the BGM, which had a factor in the increased hydraulic conductivity (Touze-Foltz et al. 2015).

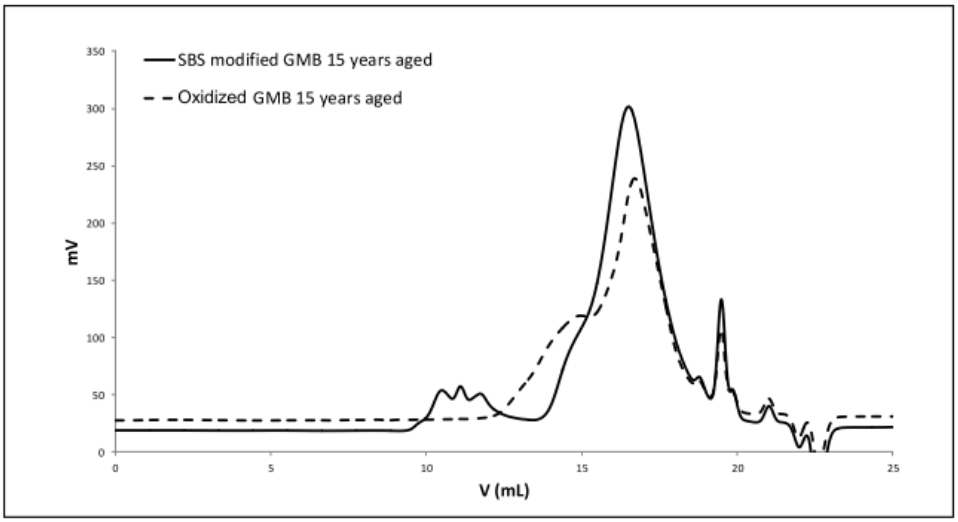

Figure 2.4 Chromatograms of extracted bitumen (Touze-Foltz et al. 2015)

This paper stated that after 15 years in service, the elastomeric BGM performed better as a hydraulic barrier than the oxidized BGM when both were left exposed, and although there was surface degradation of the surface of the bitumen, the internal core was unaffected and still maintained its hydraulic properties. It is worth noting that the hydraulic conductivity of the BGM samples is nearly out of the accuracy of the pressure cell used, which could have an impact on the results.

2.4: Damage in Bituminous Geomembranes

Clinton and Rowe (2017) look at the use of bituminous geomembranes as a barrier in heap leach pads. Heap leach pads are somewhat challenging with respect to geomembrane use, as the coarse aggregates are generally placed directly on top of the geomembranes, leading to increased risk of damage and leakage (Clinton and Rowe 2017). Some properties of the BGM used can be seen in Table 1:

Table 2.1 BGM Properties (Clinton & Rowe, 2017)

Property[2]	Value	Units
Avg. Thickness	4.0	mm
Tensile Strength MD (XD)	23 (20)	kN/m
Break Elongation MD (XD)	45 (48)	%
Static Puncture Resistance	460	N
Cold Bend Test	-25	°C

Values from manufacturer data sheet
[2] From applicable ASTM standards

The testing method consisted of a steel load cell with dimensions d= 590mm and h= 500mm (Figure 2.5). The cell can apply loads up to 3000kPa with minimal horizontal strain due to the thickness of the cell walls.

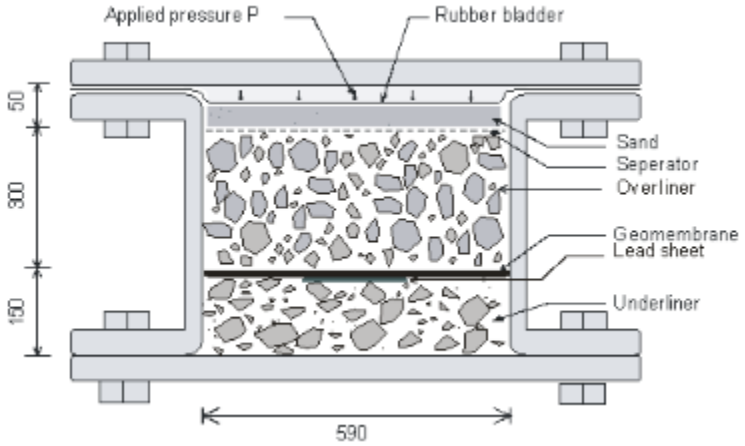

Figure 2.5 Geosynthetic Liner Longevity Simulator (GLLS) (Clinton & Rowe, 2017)

The results of the BGM testing are compared with the previous testing completed by Rowe (2013) where the same apparatus was used to test a variety of high-density polyethylene (HDPE) geomembranes. In these tests, the performance of geomembranes in heap leach pads was investigated. The setup consisted of 1.5mm HDPE GM with a 300mm coarse gravel overburden placed on top. The cell was then pressurized at 200 kPa at 10-minute increments until a 2000 kPa water pressure was reached and let stand for 100 hours. After this process was complete, the cell was depressurized and the individual components were analyzed (Rowe et al. 2013).

When calculating the strain of the geomembrane, a laser profiler was used to analyze the indentations across the surface, and then evaluated using the Tognon method (Tognon, 2000). The Tognon method calculates the "peak local strain" instead of taking the average strain across the indentation surface, which has been found to underestimate the peak strain (Tognon, 2000). For

BGMs, the assumption of 'plane strain' does not reflect what is happening like it does for conventional geomembranes as the BGM is made up of two components: the outer bitumen coating, and the central core geosynthetic, and does not behave like a homogeneous material. The mechanical stiffness along the neutral bending axis of the outer bitumen coating is nearly zero when compared to that of the geosynthetic core, meaning that the observed strains can be almost completely assumed to be present in the geosynthetic (Clinton and Rowe 2017).

The paper conclusions stated that the BGM experienced a higher volume of damage in the form of punctures (9 in the HDPE geomembrane and 115 in the BGM). To analyze the leakage through the BGM, constant heads were applied over the surface in different stages (Table 2.2).

Table 2.2 Leakage Rates (Clinton & Rowe, 2017)

Head (m)	Leakage (L/hr)	(L/ha/d)
0.3	0	0
1	0	0
10	0.0012	1136
30	0.004 -> 0.010	3545 -> 8900

The initial leakage through the BGM was substantially less than that of the HDPE geomembrane. This was thought to be the result of a 'self-sealing' effect caused by the ductility of the bitumen in the BGM. The sudden increase in leakage with the 30m applied head is thought to be caused by time dependent crushing and fracture of the gravel (Clinton and Rowe 2017).

2.5: Leakage Through Bituminous Geomembranes

An experiment regarding leakage through BGMs was conducted by Bannour et al. (2013). Its purpose was to quantify flow through a composite liner system consisting of a geosynthetic clay liner (GCL), and a BGM that has been ruptured in operation. In the testing, two different GCLs were tested along with one BGM, however both the "smooth side" and "rough side" were evaluated by flipping the BGM over for different tests. The "smooth side" is the side of the BGM with a polymeric film coating, while the "rough side" is faced with a sanded layer. All tests were run under a 50 kPa confining pressure, with 0.3m of hydraulic head constantly applied. Additionally,

in these tests all gathered data was from below the BGM-GCL contact, assuming that the compatibility between the leachate and BGM on the top side was ideal.

The two GCLs tested both have slightly different compositions. GCL 1 is a needle punched sodium bentonite, with an upper layer woven geotextile layer. GCL 2 is an activated calcium bentonite, with woven geotextiles on both faces. The bentonite is embedded within the geotextiles via stitching.

The experimental setup consists of a BGM with a 4mm hole in the centre of the surface coating to simulate a puncture. The BGM overlays the GCL being tested, with an underlying simulated compacted clay liner (CCL) layer (Figure 2.7). The cell walls are lubricated to reduce any sidewall friction during the tests.

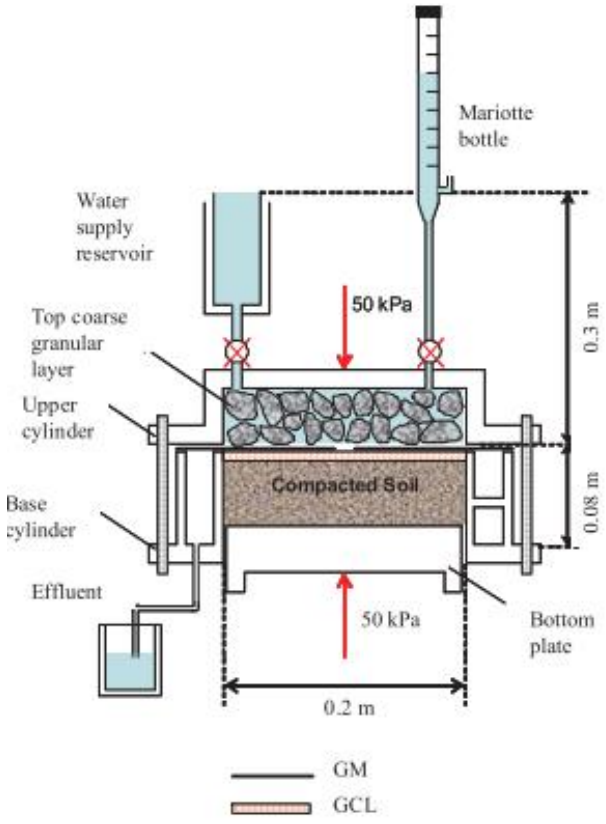

Figure 2.6 Interface Transmissivity Apparatus (Bannour et al., 2013)

It is seen that the flow rate at the interface gradually decreases over time, until steady state conditions are eventually reached around 300 hours of exposure in all scenarios (Figure 2.8).

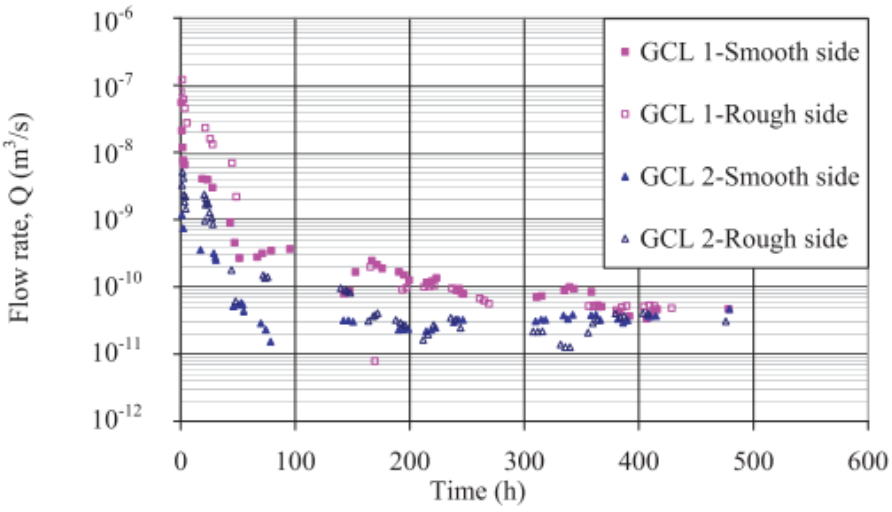

Figure 2.7 Flow Rate Comparison of BGM Interfaces (Bannour et al., 2013)

In addition to the visual representation of the data, the evaluated flow values as well as the calculated interface transmissivities between the GCLs and the BGMs were found. The rough/sanded side and smooth underside were tested with the GCLs and had their transmissivities compared (Table 2.3).

Table 2.3 Final Flow Rate and Transmissivity Values of BGM Interfaces (From Bannour et al., 2013)

Test	Q (m^3/s)	K_{GCL} (m/s)	R (m)	θ (m^2/s)
GCL 1- smooth side	5.22×10^{-11}	1.77×10^{-11}	0.1	1.08×10^{-10}
GCL 1- rough side	5.04×10^{-11}	1.77×10^{-11}	0.1	1.04×10^{-10}
GCL 2- smooth side	3.14×10^{-11}	6.90×10^{-10}	0.1	5.96×10^{-11}
GCL 2- rough side	2.69×10^{-11}	6.90×10^{-10}	0.1	5.03×10^{-11}

Q, the flow rate; K_{GCL}, hydraulic conductivity of the GCL in steady-state; R_c, radius of the wetted area; θ, interface transmissivity calculated by the analytical solution.

The results were then compared with a variety of other similar research done by other individuals on HDPE GM-GCL barriers and showing comparisons between the BGM-GCL barrier flow rates done in this study. The BGM-GCL barrier performs similarly, if not slightly better than that of a standard HDPE GM-GCL barrier, when the mechanical/chemical compatibilities are assumed to be ideal.

2.6: Influence of Temperature on Bituminous Geomembranes

In Samea and Abdelaal (2022), the effect of elevated temperatures on the degradation of elastomeric BGMs was investigated. The tests were completed with the sample either immersed in air or deionized water. Both physical and chemical degradations were evaluated to assess

environmental effects. The samples were aged using a jar immersion technique in which the samples are placed in the medium they are to be tested in (air or deionized water) at the temperature at which they were simulating. The temperatures were 40, 55, and 70°C, and for the deionized water solutions, the water was changed every two months of the aging process. The time for which the samples were incubated ranged from 2 months to 29 months. It is worth noting that in the DI water cases, the sample was sealed along the cut edges, to help prevent rapid degradation of the core interior non-woven geotextile due to being exposed to the submersion medium, when in normal cases it wouldn't be.

The main takeaways from this research can be summarized as follows:

1. The rate of degradation of the BGM's components varied with different test temperatures, as well as the different medias it was exposed to
2. For the samples kept in 40, 55, and 70°C air, the degradation of the physical bitumen coat occurred faster than that of the chemical and rheological properties of the sample. Overall, the BGM's bitumen coating became more brittle with exposure time and temperature. The mechanical strength of the samples was unchanged, however the maximum elongation strength of the BGM was reduced.
3. In the deionized water case, there was substantially less change in the chemical and rheological properties of the BGM, however the interior core geotextile and the bituminous coating both physically degraded much more than the samples kept in air.

Points 2 and 3 provide key information on whether BGMs would be suitable or not for different applications in the field depending on what properties are most important. The consideration of what media the BGM will be present in, along with what properties are a priority of utmost importance when selecting a geomembrane barrier to use and this provides additional information that could allow for BGMs to be used more frequently in the field.

2.7: Background on Standardized Puncture and Tear Testing

2.7.1: ASTM Puncture Resistance (ASTM D4833)

ASTM D 4833 (2010) was used to measure the index puncture resistance, being the downward force required to puncture completely through the sample, of geomembranes and products with a

similar function based on a standard criterion. When conducting this test procedure, the use of the apparatus provided in the ASTM standard is required as to keep consistency between tests conducted at different institutions (Figure 2.9).

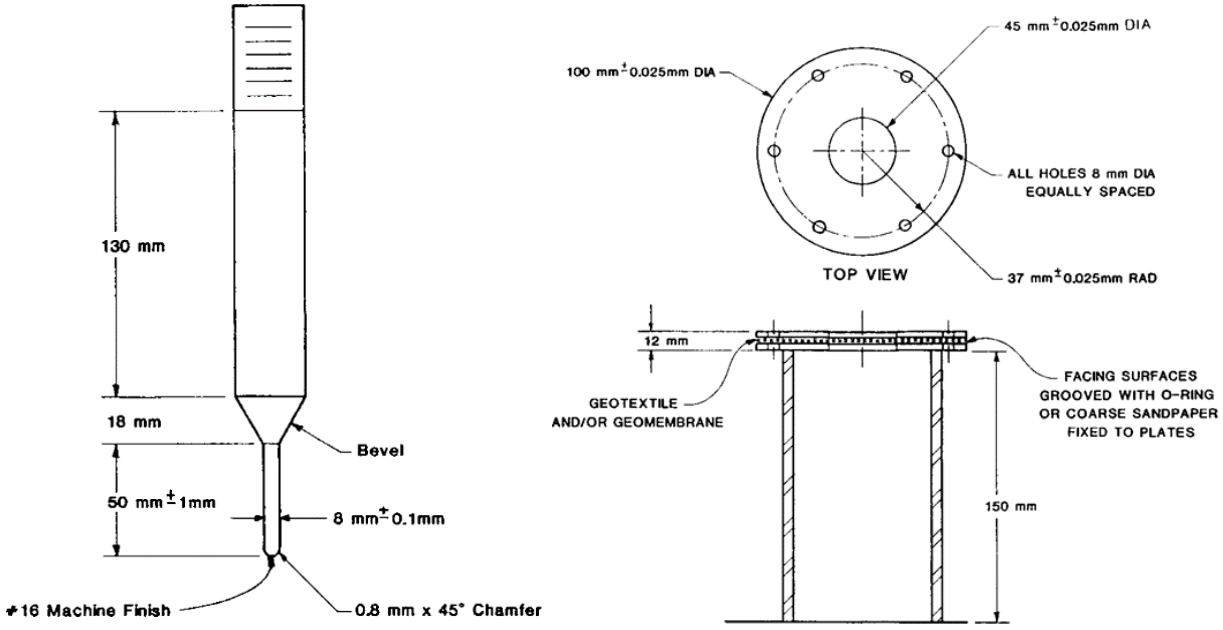

Figure 2.8 ASTM Puncture Frame Schematics (ASTM, 2010)

The samples used in testing are cut into a square with a minimum of 100 mm side length, as to ensure they can be clamped into the apparatus sufficiently. The sample is then centred under the puncture probe, and the test can begin. The machine used to apply the load should be set to a displacement rate of 300 mm/min +/- 10 mm and ran until the rod completely punctures the sample. The load and displacement reached at the time of puncture are then read and recorded directly from the recording instrument. After enough tests have been completed (3-5), the average response of the tests is calculated and presented (ASTM, 2010). This test only provides data for the load applied in newtons and displacement of the sample before puncture in millimetres during the trial. These tests were conducted on both BGM and HDPE sample. The evaluation of puncture resistance is easily accessible to perform, however the aspect of temperature variation has not been applied to this type of research before, which is one of the main goals of this research.

2.7.2: ASTM Tear Resistance (ASTM D5884)

The ASTM D5884 is used for determining the tearing resistance of internally reinforced geomembranes, such as bituminous geomembranes reinforced by a geotextile. Due to this test being a measure of index tearing properties, results from this test are used purely for comparison between materials under these same circumstances and are not suitable for in-field evaluations (ASTM, 2012).

To prepare for the test, samples are cut into 200 mm x 200 mm squares, with a centred 75mm cut made on one of the 4 sides, either across or with the machine direction (Figure 2.10). Five samples of each variation are cut and used per test cycle, with the average maximum response being recorded.

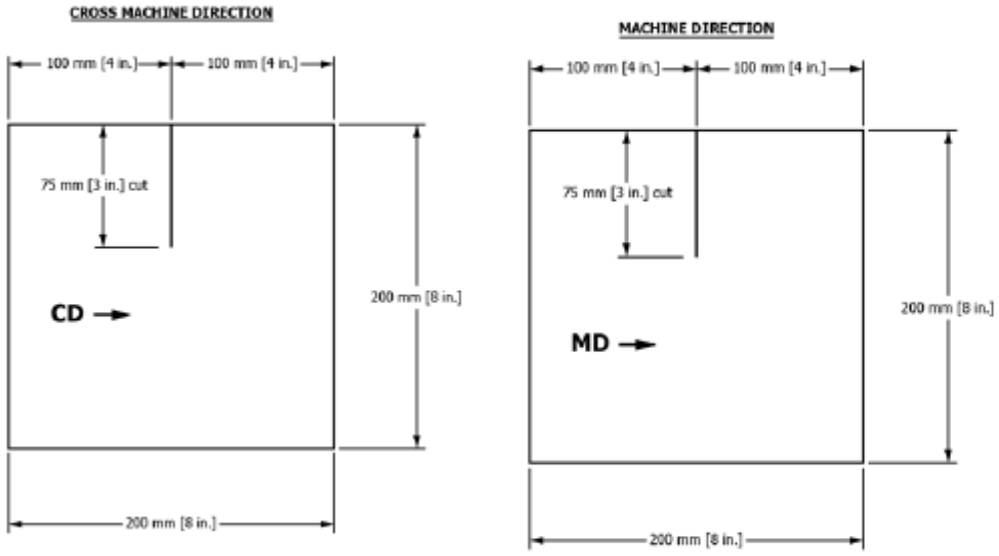

Figure 2.9 Tear Sample Cut Guidelines (ASTM, 2012)

The samples are then placed in the testing machine with one ‘tongue’ clamped in each of the grips above and below the sample with a grip spacing of 75 mm. The 100 mm ‘tongues’ should be fully gripped by the clamps being used. The sample is then torn completely, with the peak tear resistance profile recorded and presented. Only tearing resistance and time are recorded from this test, as the displacement is constant throughout each test trial. These tests were conducted on BGM samples.

2.8: Gaps in Literature

There has been relatively little research carried out regarding the performance of bituminous geomembranes, and how temperature can influence degradation of these BGMs. Additionally, there is little to no research on the performance of BGMs at sub-zero temperatures, and how that performance differs from temperatures above zero. The research being presented discusses experimentation that simulates the early stages of construction, and how the temperature in which a BGM is installed can impact how effective it is in the field.

Chapter 3 – Methodology

3.1: Testing Apparatus and Equipment

A variety of equipment was used in the ASTM and large-scale testing stages. The equipment used in the ASTM D 4833 (Geomembrane puncture resistance) testing stage was fabricated by Engineering Shops at the University of Saskatchewan to the specifications of the ASTM standard for this research and was used to evaluate puncture resistance of HDPE geomembranes and BGM. The equipment used in the ASTM D 5884 (Tearing resistance of geomembranes) had been previously acquired and was available for use at the time of testing, and was used to evaluate BGM tear resistance. The large-scale performance apparatus was designed and then fabricated in the College of Engineering Design Shops for the specific purpose of testing the short-term performance of BGMs under high loads.

3.1.1: Geomembrane Selection

Two versions of the manufacturer supplied Coletanche elastomeric BGMs were selected for use, the ES2 and ES4 products (figures 3.6 and 3.7). These were recommended by Titan Environmental as they are the two most popular variations of the product that they carry. They are also close to the average specifications of the ES line of products in terms of properties Coletanche Inc. (2020). The exact specifications can be seen in tables 3.1 and 3.2. The 1.5 mm and 3 mm variations of Solmax HDPE geomembranes were also selected and compared against the BGMs in the ASTM index testing stages.

Table 3.1 ES2 Physical and Technical Specs (Axter Coletanche, 2009)

Material	Value (g/m^2)	Purpose
Glass Mat	50	Reinforcement
Non-woven Geotextile	250	Reinforcement
Elastomeric SBS	4300	Binder
Sand	200	Surface Finish
Polyester Anti-root film	15	Surface Finish

Characteristic	Value	Units
Thickness	4.0	mm
Surface Mass	4.85	kg/m^2
Tearing Res. (MD/XD)[3]	825/700	N
Max Tensile Str. (MD/XD)[1]	27/24	kN/m
Elongation (MD/XD)[1]	60/60	%
Static Puncture Res.[2]	530	N

[1] As per ASTM D 7275
[2] As per ASTM D 4833
[3] As per ASTM D 4073

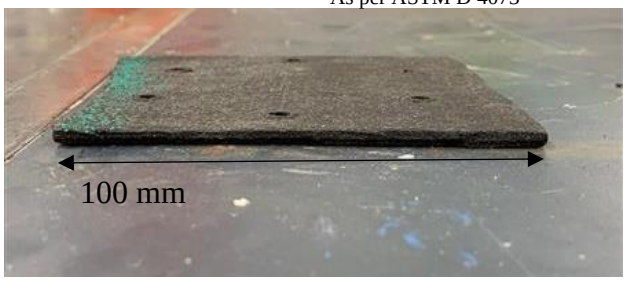

Figure 3.1 ES2 Sample Thickness Profile

Table 3.2: ES4 Physical and Technical Specs (Axter Coletanche, 2009)

Material	Value (g/m^2)	Purpose
Glass Mat	50	Reinforcement
Non-woven Geotextile	400	Reinforcement
Elastomeric SBS	5400	Binder
Sand	200	Surface Finish
Polyester Anti-root film	15	Surface Finish

Characteristic	Value	Units
Thickness	5.60	mm
Surface Mass	6.40	kg/m^2
Tearing Res. (MD/XD)[3]	1225/1025	N
Max Tensile Str. (MD/XD)[1]	39/31	kN/m
Elongation (MD/XD)[1]	60/60	%
Static Puncture Res.[2]	650	N

[1] As per ASTM D 7275
[2] As per ASTM D 4833
[3] As per ASTM D 4073

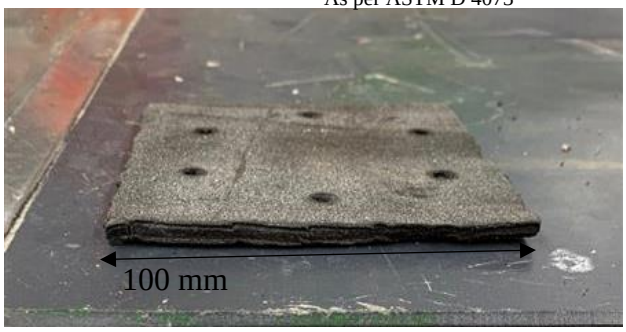

Figure 3.2 E42 Sample Thickness Profile

3.1.2: Testing Load Frame

The testing frame, which was used for all testing (puncture, tear, and performance testing), incorporates a Parker Hannifin 10 inch (0.25 m) pneumatic cylinder frame with a maximum operating pressure of 1700 kPa, which corresponds to maximum applied force of 544 kN (Figure

3.3). For some of the testing, particularly those carried out at sub-zero temperatures, constraints in compressed air supply limited the cylinder pressure to approximately 660 kPa corresponding to a vertical force of 34 kN. At sub-zero temperatures, the air-cylinder seals leaked enough that with 250 psi of internal pressure, an entire compressed air was completely emptied in less than an hour. Due to this issue, the building compressed air system was used which can supply an essentially unlimited amount of compressed air at 700 kPa. Although there are some disadvantages to using an air cylinder compared to hydraulic such as the potential of leakage, the mobility of the unit makes it easy to move in and out of the temperature-controlled environments. A desiccator was attached to the air line during the sub-zero testing to eliminate the risk of moisture in the air line freezing and interrupting the testing.

For the puncture and tear testing, air pressure was controlled using the Alicat P-series electronic air regulator yielding a displacement-controlled loading system, along with an linear variable differential transformer (LVDT) to monitor displacements in real time. The puncture and tear tests were dictated by displacement, not applied load, therefore the pneumatic cylinder with the electronic regulator was able to operate based on a displacement-controlled program.

For the performance tests, the goal was to simulate gravity acting on a sample with diameter 0.34m. Using the 660 kPa air pressure within the cylinder, this corresponds to an applied vertical load of 34 kN, and roughly 360 kPa of applied vertical stress onto the sample. An Artech 2021-15K load cell was used to verify this average applied stress. The air flow in the frame is controlled using the Alicat P-series electronic air regular which can be programmed to maintain, increase, and decrease the airflow applied to the system at specific time intervals via a python script This allows for multi-stage tests that run for days at a time. The data is sent to and compiled by a VLab software program that can calibrate the data based on the defined specifications of the load cell itself. Additionally, a GDSLabs P/V controller was used to apply a constant head to the system and monitor for leakage during the performance testing.

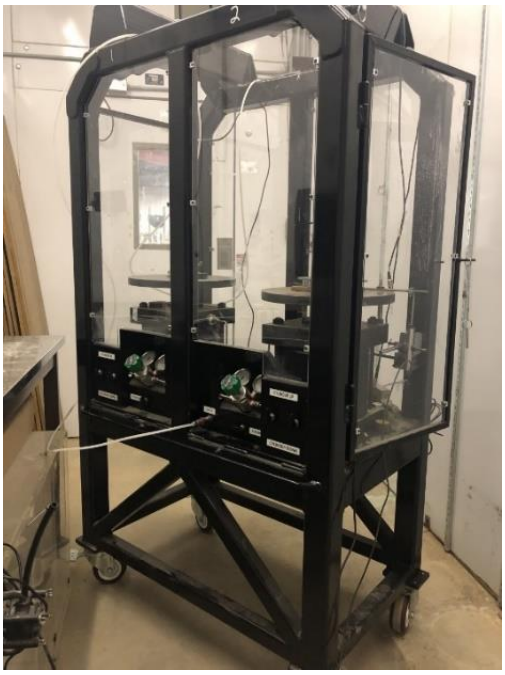

Figure 3.3 Air Cylinder Frame with Control Valves

3.1.3: Temperature Control Measures

To monitor and maintain the temperatures during the tests, both the heated climate chamber and walk-in freezer unit both have external temperature control dials, which displays the current interior temperature. An additional manually read thermometer was placed inside the heated climate chamber to ensure temperature accuracy. The walk-in freezer unit had a second digital temperature display inside the unit to monitor and maintain the internal temperature.

3.1.4: ASTM Puncture Resistance Apparatus

The second piece of equipment used in this testing was a puncture apparatus specified by ASTM D 4833 (2010). The setup consists of three pieces: the probe which used for puncture, the mounting frame used to hold the geomembrane sample, and the mounting cap used to secure the sample in place. The probe consists of a machined rod base, beveled into a 50mm long, 8mm diameter tip with a 0.8mm, 45° chamfer to the tip. The probe also has a threaded base to allow it to be connected to the load cell used in the tests.

The base of the apparatus consists of a hollow cylindrical body welded to a base plate for stability. Attached to the top of the cylinder is a 4mm thick, 100mm diameter annulus with a 37mm diameter opening in the center. Equally spaced around the disc on a 45mm diameter placement are 6, 8mm

machined holes used to bolt the BGM in place. The mounting cap with identical dimensions to the top of the body cylinder is mounted on top of the BGM and screwed together to secure it in place (Figure 3.2). The test operates at a penetration rate of 300 +/- 10 mm/min.

Figure 3.4 (Left) BGM mounted in Puncture Frame (Right) Puncture Apparatus in Load Frame

3.1.5: ASTM Tear Resistance Apparatus

The equipment used to perform the tear testing uses the same pneumatic cylinder frame as the puncture apparatus. There are two custom clamp grips that attach to the top and bottom of the cylinder assembly frame. The top clamp remains static, while the lower clamp can raise and lower with the stroke of the cylinder for both compression and tension (Figure 3.3).

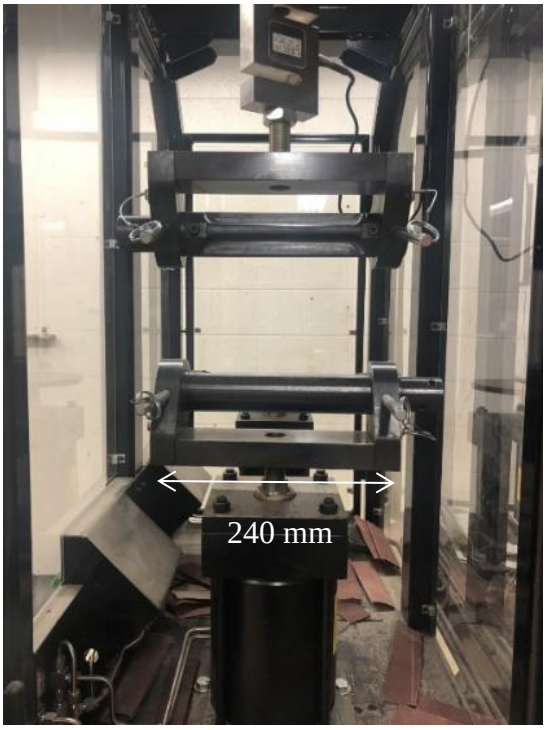

Figure 3.5 Tear Apparatus in Load Frame

3.1.6: Short-Term Performance Testing Apparatus

The large-scale test apparatus uses the same pneumatic cylinder frame to apply and maintain load on BGM samples for short-term testing to simulate the early stages of construction, however the apparatus is a custom fabricated load assembly. The apparatus was designed by the author and was manufactured by the U of S Engineering Shops. The assembly consists of three main steel fabricated pieces, as well as connections for various equipment. The three main pieces are the lower body cylinder, the upper body cylinder, and the load cap plate (Figure 3.6).

Figure 3.6 (a) Upper Body Assembly (b) Lower Body Assembly (c/d) Load Plate Assembly

The two body cylinders are stacked on top of each other over an o-ring, which is sealed with vacuum grease. The o-ring sits in a groove that is present in both the upper and lower body pieces, so they remain flush with each other even with the o-ring present. The body contains the subgrade, the barrier material being tested, and the overburden aggregate. The load plate is a shallow, hollow cylinder with an ¼ inch NPT fitting on top, and three o-ring grooves along the outer wall to seal to the inside of the main body and is used to apply the load to the system. Water can be pumped into the plate from the top of the hollow body, and then flow freely out through the drainage holes in the bottom of the plate to enter the system. The exact dimensions of the apparatus can be seen in Appendix B.

Figure 3.7 Full Load Assembly mounted in Air Frame

3.1.7: Subgrade Material Selection

The subgrade used in the large-scale performance testing was a multipurpose abrasive blasting glass bead media. The beads were specified by the manufacturer to have a 100–170 micron diameter, which was verified using a sieve analysis and were uniform and spherical in shape. These glass beads were selected as they are a yielding subgrade which allows for deformation. This allows for water to flow more freely through and to reduce test times. As the glass beads do not absorb moisture, the saturated water content was very easy to obtain as it just filled the void space between the particles. The water content of the glass beads was found to be 20% by drying a saturated sample in standard drying oven and measuring the difference in mass, the porosity was found to be roughly 0.3, and the void ratio was found to be roughly 0.25. Using a tempe cell, a soil water characteristic curve (SWCC) was created, and the air entry value of the glass bead medium was found to be around 12-15 kPa (Figure 3.8).

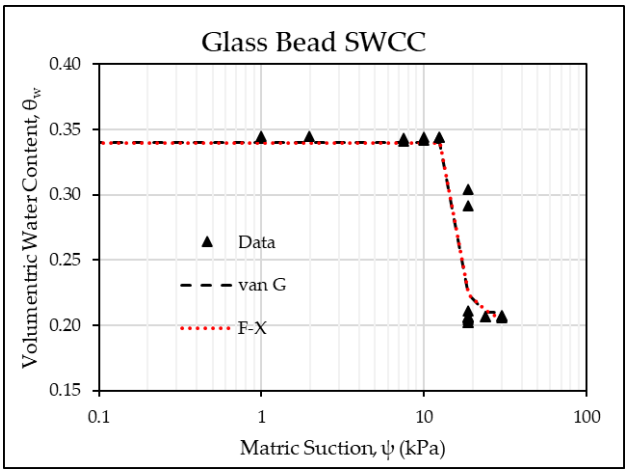

Figure 3.8 Glass Bead Subgrade SWCC

In the sub-zero testing of the BGMs, the issue of the subgrade freezing had to be addressed. To combat this issue, the pore fluid used in these test stages was a 40% propylene-glycol, 60% water solution. With these proportions in the fluid mixture, the viscosity of the fluid was still very close that of water, however the glycol fraction lowered the freezing temperature of the mixture to slightly below −20°C, thus preventing freezing at any point during the testing procedure. The pore fluid was used to both properly saturate the subgrade material, as well as simulate leachate/surface water to monitor potential leaks through the BGM during testing. The use of this glycol mixture did necessitate the evaluation of the effect of glycol on the physical properties of the BGM, thus the puncture potential of the BGM after it had been soaked in the glycol mixture was tested following the same ASTM standards as the general puncture resistance testing.

3.1.8: Aggregate Selection

The aggregate chosen to use as a cover for the BGM during the large-scale tests was a Saskatchewan Type 32 aggregate. This material was then sieved to eliminate the fines present in the aggregate, and only materials retained above the 16.0 mm sieve were retained and used in the experiments. Due to the aggregate being fairly rounded with only minimal aggressive/angular pieces, igneous rock cores were fractured into multiple highly angular pieces (Figure 3.9). These pieces were integrated into the material along the BGM surface to simulate a more angular aggregate. The angular aggregate was roughly 70-80mm in diameter, with 8-10 used in each test.

Figure 3.9 (Left) Coarse Aggregate with 30cm ruler for scale (Right) Aggressive Aggregate Fragments used to force puncture

3.2: Testing Procedures

3.2.1: ASTM Test Procedures

The testing procedure for the ASTM D 4833 (2010) and ASTM D 5884 (2012) were followed for the tests with one required modification. As the testing is based on temperature variations, the samples were left in the climate chamber/freezer for 24 hours at the specified temperatures prior to testing to ensure that the samples have equilibrated to the testing temperature. During the ASTM testing, unless otherwise stated by the ASTM standards, 3 tests were run on each sample at each temperature, with an average performance from those trials being presented. In ASTM D 4833, puncture resistance and displacement were recorded, and in ASTM D 5884, tearing resistance was recorded. Additionally, there were 2 other variations of the ASTM D 4833 puncture test conducted to evaluate changes in the BGM puncture resistance. The first involved soaking the BGM samples in propylene-glycol, as the glycol was used as an anti-freeze solution for the sub-zero performance testing. The other was puncturing the BGMs with a subgrade present to evaluate changes in resistances.

In the puncture testing stages, the plots recorded from VLab show displacement versus puncture resistance which presents a real time response of the sample during puncture. It can be noted that the ‘noise’ present in some of the data was caused by slight variations in test length, or movement of the sample before logging was stopped, but after the sample has been fully punctured. For each temperature, 3-4 tests were completed for each sample type and the average response was

calculated based on those tests as per ASTM D 4833. The results of the ES2, ES4, 1.5mm HDPE, and 3mm HDPE puncture testing will be presented for various temperatures. It is worth noting that no subgrade is present beneath the samples during these puncture tests.

3.2.2: Large-Scale Performance Testing Procedure

Test Preparation

The first step of the process was to cut the BGM into 340mm diameter samples to match the interior diameter of the load apparatus using a handheld utility blade. The samples were then placed in the climate chamber at the testing temperature. The load frame and large-scale apparatus were also set in the climate chamber/freezer unit at the set testing temperature, which was maintained for the entirety of each test. The lower assembly was placed into the load frame and lined on the bottom with a non-woven geotextile to allow for filtration/drainage to the outlet port on the assembly. The area of the samples used in the tests is measured to be 0.085m^2.

Once the samples had equilibrated, the subgrade was prepared and hydrated and added to the lower body assembly in the load frame in 10 cm lifts until it reached just below the upper ridge of the lower assembly. The BGM sample was then placed on top of the subgrade and sealed around the edges with a hydrated bentonite slurry to prevent leakage around the edges.

The next step was to secure the o-ring in place along the groove in the assembly, and seal it with vacuum grease. Then the upper body assembly was placed on top and centred. The aggregate was then loaded into the upper assembly, with roughly 10 special angular fragments placed on the BGM with the angular points directly in contact with the liner, and covered with the base aggregate to ensure they remained in contact with the sample. The aggregate was filled to 50 mm below the upper edge of the top assembly and compacted to a level surface. The load plate and exposed inner edge of the assembly were then greased to reduce sidewall friction, and the load plate was lowered into the assembly on top of the aggregate. A 5 kN load was then applied to the system to secure the load plate and ensure it rested evenly on of the aggregate, with the o-rings sealed to the sidewalls of the upper apparatus body.

The GDSLabs P/V controller was then prepared to monitor changes in pressure head, set to a 96-hour test time, and connected to the top of the load plate via the National Pipe Thread (NPT) fitting. The electronic pressure transducer was then set to the air flow pattern for the tests using a custom Raspberry Pi program, which increased the applied air pressure over the course of 12-18 hours when it was engaged. Finally, the VLab data logger was prepped to monitor the applied load on the system.

Beginning the Test

All three systems were turned on simultaneously to begin the test. The load was incrementally increased rather than applied all at once to allow for shifting in the aggregate that could occur. After roughly 96 hours, the programs were stopped and the apparatus was taken apart and the BGM was examined, photographed, and stored. The subgrade was removed, dried, and re-mixed for the next test. The aggregate was also replaced for each test. This process is repeated 2-3 times at −15°C, 0°C, and +20°C for each of the ES2 and ES4 trials which were then analyzed and presented. Each test sample was cleaned then photographed after each test, the load profiles and photographs are presented along with the performance/trends.

3.2.3: Testing Plan

A breakdown of the testing plan can be seen in Table 3.3. The tests follow all previously mentioned procedures and were not conducted in any particular order.

Table 3.3 Testing Plan

Sample Type	**ES2**								**ES4**							
Temperature	−20°C	−15°C	−10°C	0°C	5°C	10°C	20°C	30°C	−20°C	−15°C	−10°C	0°C	5°C	10°C	20°C	30°C
ASTM Puncture[1]	X		X	X	X	X	X	X	X		X	X	X	X	X	X
ASTM Tear[2]	X			X			X	X	X			X			X	X
Large-Scale Performance[3]		X		X			X			X		X			X	
Sample Type	**1.5mm HDPE**								**3mm HDPE**							
Temperature	−20°C	−15°C	−10°C	0°C	5°C	10°C	20°C	30°C	−20°C	−15°C	−10°C	0°C	5°C	10°C	20°C	30°C
ASTM Puncture[1]	X		X	X	X	X	X	X	X		X	X	X	X	X	X
ASTM Tear[2]																
Large-Scale Performance[3]																

1: Puncture tests consists of 3 replicate tests, then presented as an average response for each temperature, as per ASTM D 4833 (2010)

2: Tear tests consist of 3-4 replicate tests, presented on a single graph, as per ASTM D 5884 (2012)

3: Each performance test consists of 2-3 independent trials at each temperature

Chapter 4 - Results and Discussion

There was a variety of testing completed for this project including ASTM puncture resistance testing, ASTM tear resistance testing, and the large-scale performance testing. All the testing was completed between −20°C and +30°C and have been separated by test type, geomembrane used, and the test temperatures. This is to show the individual performance of each sample/temperature scenario. To recall, the research objectives of this thesis are to analyze the following:

- Variation in performance across a temperature range of −20°C through +30°C
- Puncture resistance for HDPE and BGM
- Tear resistance for BGM
- Short term performance for BGM
  Monitor for leakage through the BGM as it is loaded/damaged

4.1: Puncture Resistance Results and Discussion

All results shown for puncture resistance and displacement are the average of three replicate tests at the specified temperature.

4.1.1: ES2 Puncture

The first sample tested was the ES2 BGM sample, the thinner of the two being BGM being tested (Figure 4.1), being the thinner of the two BGM types. There weren't any major differences between the performances of the BGM at the temperatures above zero degrees. In terms of displacement in the ES2 testing, the highest displacements occurred in the warmer +20-30°C tests, with the displacement values decreasing with the temperature. The full displacement versus resistance plot can be seen below, along with a table with the breakdown of the puncture resistances and displacements for each temperature trial. The individual plots of load versus displacement are available in Appendix A.

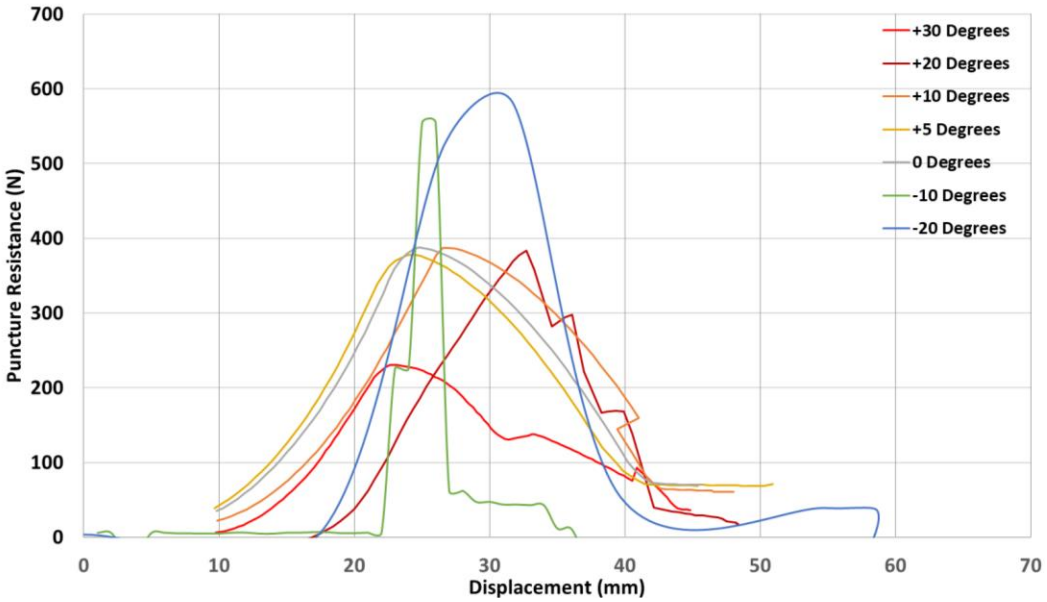

Figure 4.1 ES2 Puncture Curves

Table 4.1 ES2 Puncture Values

Temperature (°C)	Puncture Resistance (N)	Displacement (mm)
-20	590	9.3
-10	555	12.0
0	427	24.7
+5	426	25.6
+10	392	25.4
+20	469	34.5
+30	337	33.3

4.1.2: ES4 Puncture

The puncture responses for the ES4 samples follow similar trends to the ES2 samples, however due to the increased thickness of the ES4 material, the exact values are higher. Overall, the displacements of the ES4 tests were like those of the ES2 tests, while the puncture resistances were substantially higher. Again, the full displacement versus resistance plot is shown (Figure 4.2) along with a table with the breakdown of the puncture resistances and displacements for each temperature trial with the individual plots available in Appendix A.

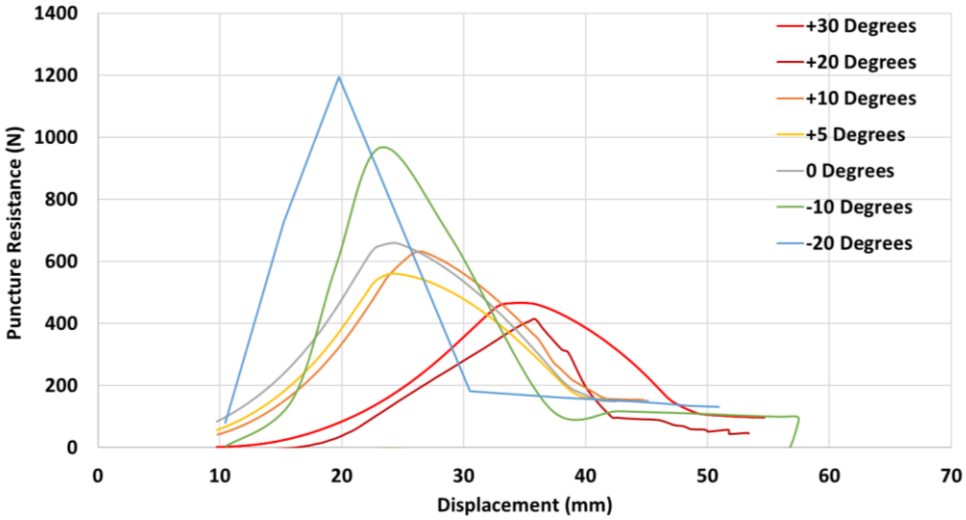

Figure 4.2 ES4 Puncture Curves

Table 4.2 ES4 Puncture Values

Temperature (°C)	Puncture Resistance (N)	Displacement (mm)
-20	1195	9.8
-10	967	13.2
0	732	24.0
+5	601	24.3
+10	679	24.5
+20	454	36.4
+30	498	33.3

4.1.3: 1.5 mm HDPE Puncture

The Solmax HDPE geomembranes both followed similar trends to that of the ES line of BGMs, with the main difference being less variation when it comes to the actual puncture resistance of the materials. For HDPE the effect of temperature was less pronounced with resistance, but was more pronounced when looking at displacement, as shown in Figure 4.3.

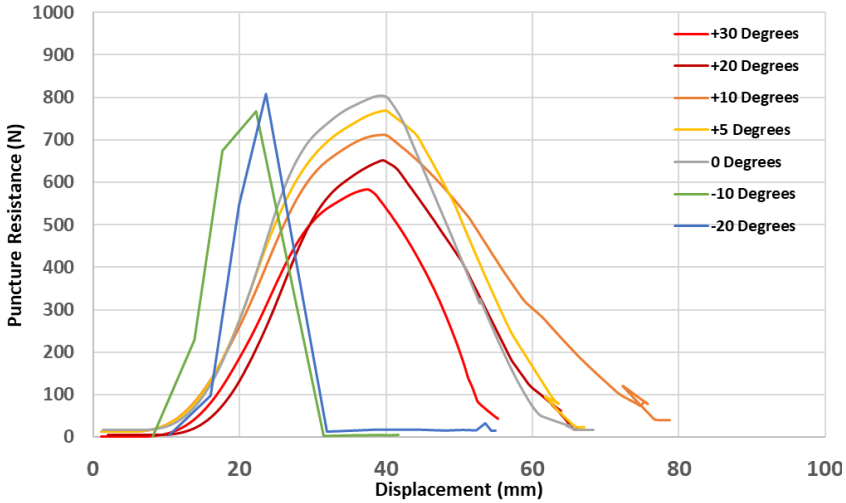

Figure 4.3 1.5mm HDPE Puncture Curves

Table 4.3 1.5mm HDPE Puncture Values

Temperature (°C)	Puncture Resistance (N)	Displacement (mm)
-20	807	13.2
-10	768	14.1
0	809	39.6
5	809	41.0
10	724	42.6
20	675	40.5
30	590	37.8

4.1.4: 3 mm HDPE Results

It was observed that the puncture resistance has a visible negative correlation with testing temperature, similarly to the BGM samples (Figure 4.4). Additionally, as temperatures increased, the responses of the HDPE transitioned from more brittle to more ductile response, as seen by the smoothing of the curves.

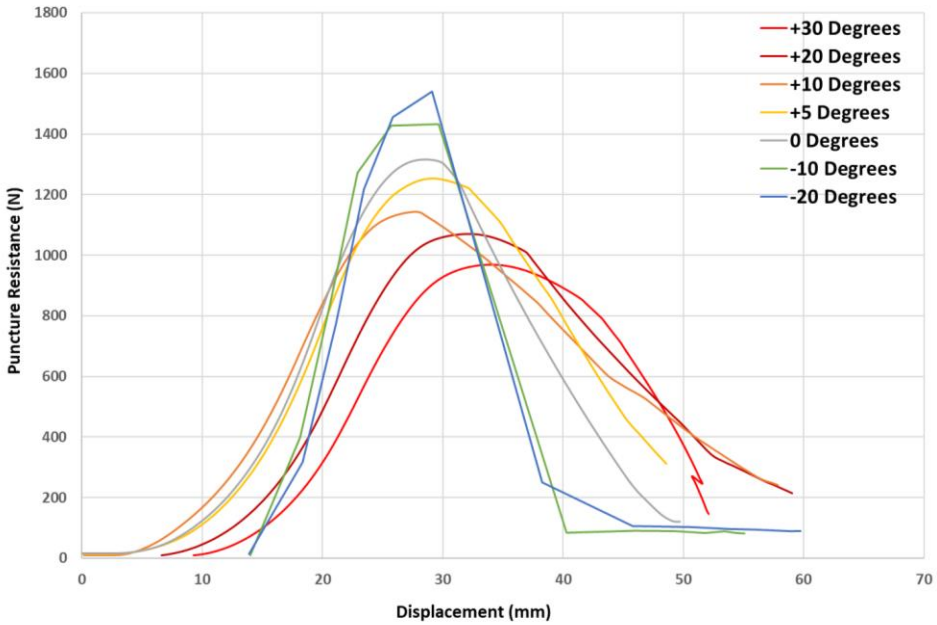

Figure 4.4 3mm HDPE Puncture Curves

Table 4.4 3mm HDPE Puncture Values

Temperature (°C)	Puncture Resistance (N)	Displacement (mm)
-20	1541	15.2
-10	1432	15.7
0	1339	28.5
+5	1320	28.4
+10	1192	28.0
+20	1091	31.5
+30	989	33.9

4.1.5: Trends in Puncture Results

The puncture resistance responses of the ES2, ES4, 1.5 mm HDPE, and 3 mm HDPE all showed very similar trends. All four sample types exhibit higher puncture resistance at lower temperatures and exhibit higher displacements at higher temperatures. It is worth noting that in the peak puncture resistance versus temperature plots, the ES2 sample did not show as clear of a correlation as the ES4 samples, and the ES line in general didn't show as clear of a correlation as the HDPE samples. For both material types, BGM and HDPE, the displacement at the highest temperatures were around 3x larger than the displacements at the lowest temperatures. Some samples also showed puncture resistances nearly doubling from the lowest to highest temperature testing. In addition, the material responses in the sub-zero testing all displayed brittle behaviour as they were being punctured. Overall, both sets of products (ES line and HDPE) showed a positive correlation

between temperature and displacement, and a negative correlation between temperature and puncture resistance (Figures 4.5 and 4.6). It is worth noting that the correlations are slightly more defined in the ES4 product, which could be due to the increase in material mass being more heavily influenced by the variation in temperature. Additionally, the puncture resistances provided by the suppliers at +20°C were found to be slightly overstated compared to the values found during this experimentation. Additionally, in practice the displacements seen in this testing may not be possible due to the addition of a subgrade. Because of this, these high displacements in warmer temperatures may translate to high contact strains when displacement isn't as possible. Overall, the responses of both the BGMs and HDPE match the expected responses, being more brittle responses at sub-zero temperatures, and more ductile responses at positive temperatures

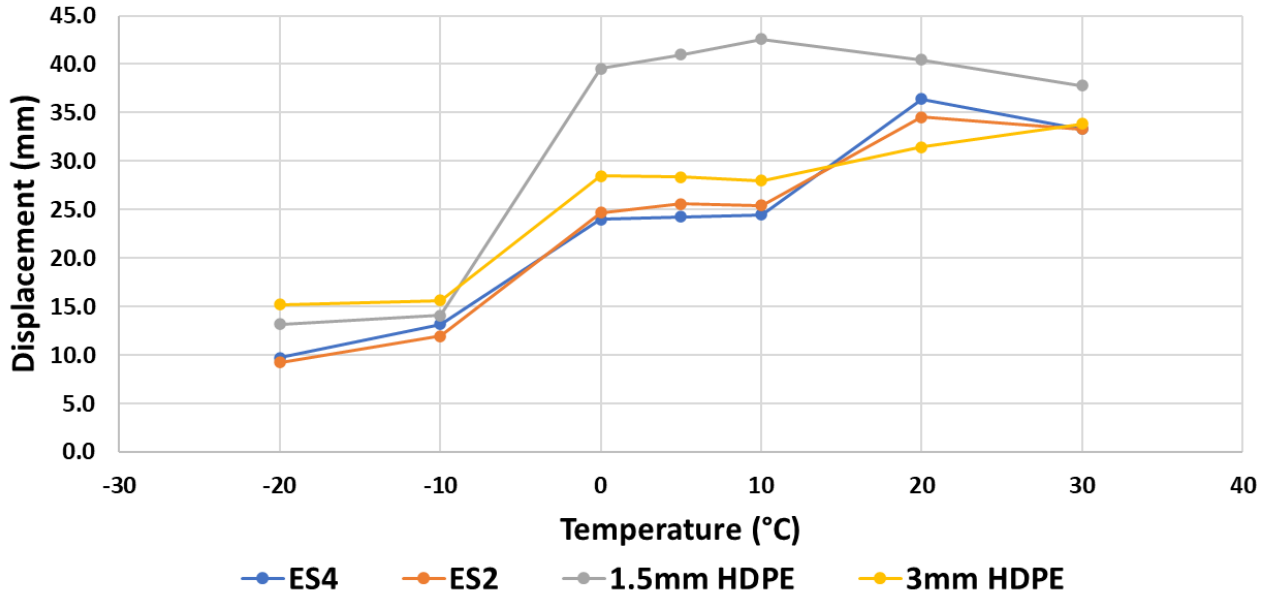

Figure 4.5 BGM Displacement Vs Temperature Plot

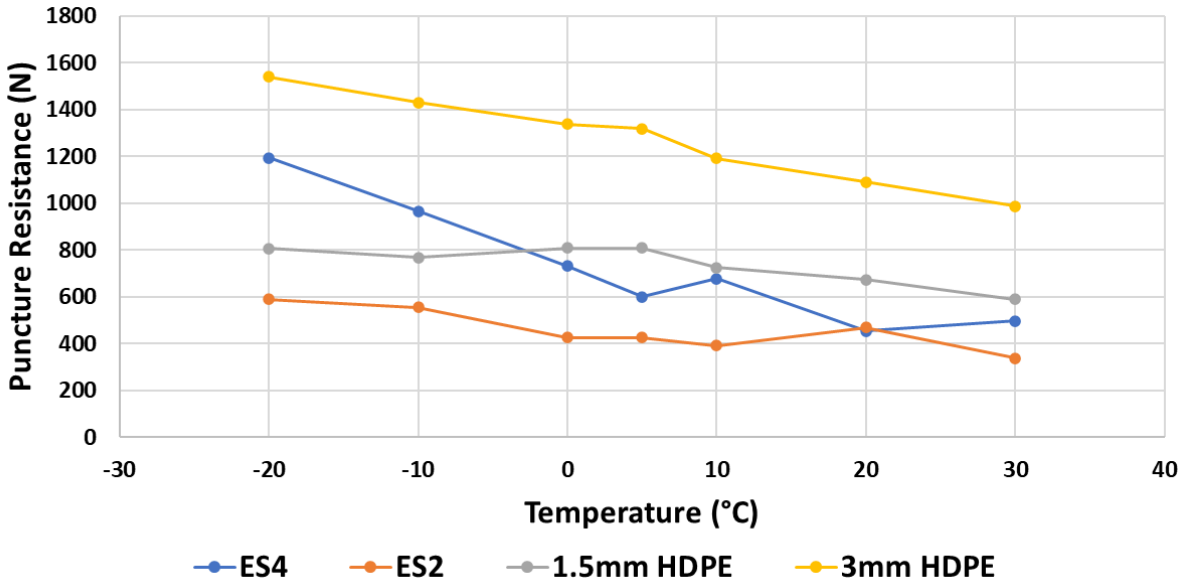

Figure 4.6 BGM Puncture Resistance Vs Temperature Plot

4.1.6: Specific Case Puncture Testing

The specific case preliminary testing includes two variations on the ASTM D 4833 that were used to confirm whether the BGM being exposed to propylene-glycol, or having a subgrade present in the large-scale test setup would impact the results of the large-scale testing. The first case to be covered was evaluating puncture resistance on BGM samples that had been soaked in propylene-glycol, which is the fluid used as an anti-freeze to prevent freezing in sub-zero tests. This was to determine if a BGM that had been soaked in propylene-glycol would show significant deterioration in puncture resistance (Figures 4.7 and 4.8). The second case was puncture resistance testing completed on BGM samples with a glass bead subgrade present under the sample to measure the influence of the subgrade on the puncture resistance at +10°C (Figures 4.9 and 4.10). The baseline values included are the values obtained from the standard ASTM D 4833 tests at +10°C.

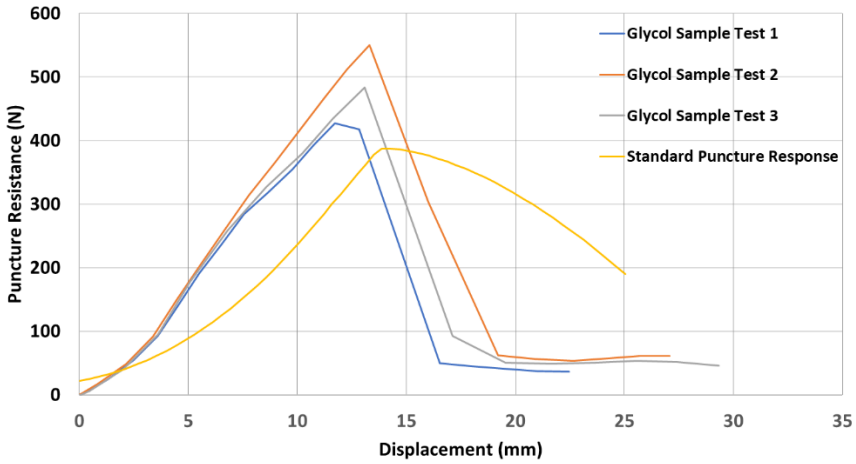

Figure 4.7 ES2 Glycol Puncture Curves with Standard Baseline Reference Test (+10°C)

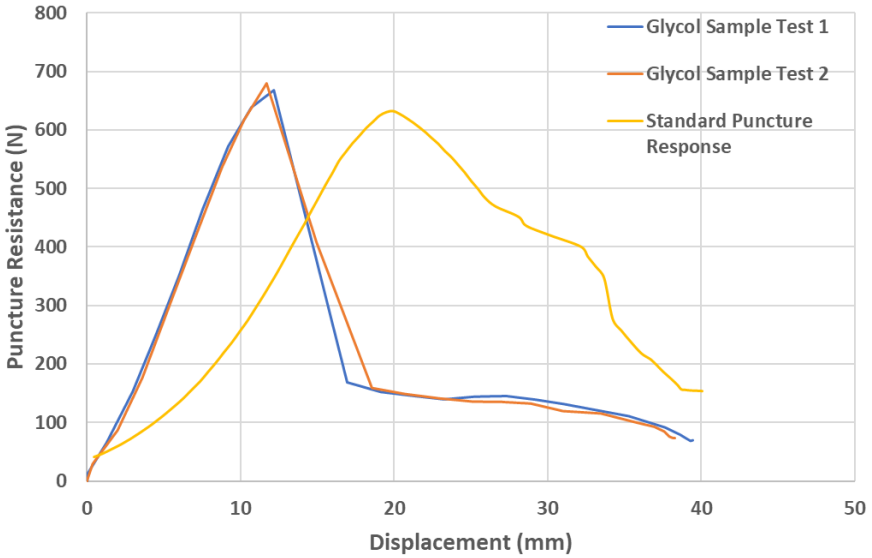

Figure 4.8 ES4 Glycol Puncture Curves with Standard Baseline Reference Test (+10°C)

It was found that there was a slight increase on the average puncture resistance of the BGM when it had been soaked in glycol in these puncture tests, specifically in the ES2 samples with an increase of around 0.2x resistance at the high end, however overall, there was no major change in the response of the material, simply an increase in puncture resistance and displacement. It is also worth noting that the glycol solution is only used to saturate the glass beads in the sub-zero testing and was not present in any of the other large-scale testing procedure, meaning it is unlikely for the BGM to be fully saturated with glycol in the performance testing.

The second trial involved puncture testing with a saturated subgrade present underneath, which is not present in the standard ASTM D 4833 trials, to see if there was any significant change in performance. The testing results can be seen below alongside the baseline puncture test with no subgrade present (Figures 4.9 and 4.10). The ASTM puncture assembly was filled and compacted to the brim of the apparatus for each test and hydrated to 20% water content. The conditions were intended to be identical for each trial, however due to the irregular shape of the puncture apparatus, there may have been slight error in the compaction levels. The baseline values included are the values obtained from the standard ASTM D 4833 tests at +20°C.

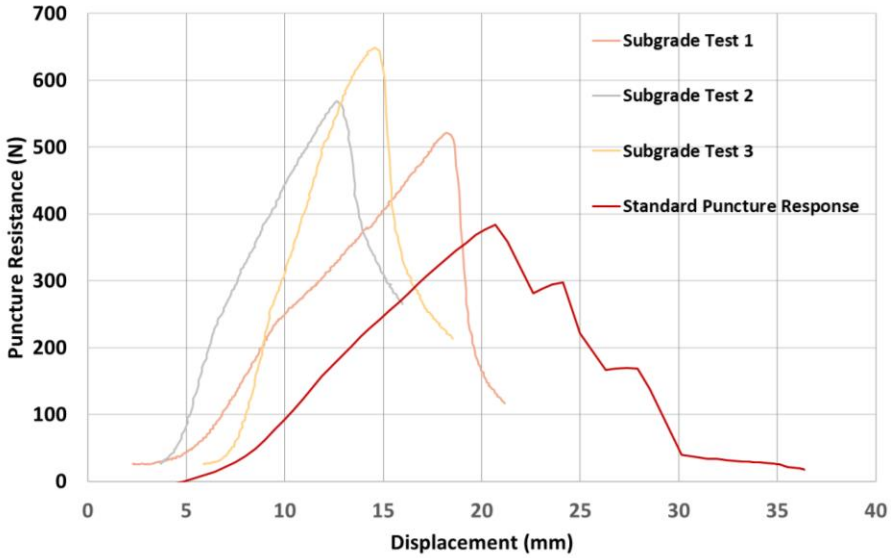

Figure 4.9 ES2 Subgrade Puncture Curves with Standard Baseline Reference Test (+20°C)

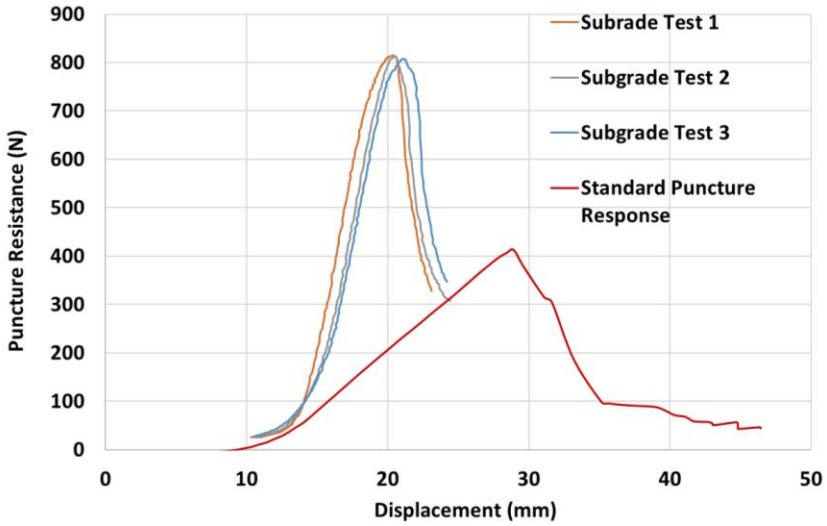

Figure 4.10 ES4 Subgrade Puncture Curves with Standard Baseline Reference Test (+20°C)

There were clear decreases in the displacements present with the subgrade, however this is expected. The load required for puncture in these tests are noticeably higher than that of the baseline testing results, which again was to be expected.

4.2: Tear Resistance Results and Discussion

For tearing results, each replicate test is shown separately. The following graphs (Figures 4.11 to 4.18) show the results of the ASTM D 5884 tear testing of both the ES2 (Section 4.2.1) and ES4 (Section 4.2.2) samples at −20°C, 0°C, +20°C, and +30°C, with the discussion presented afterwards. There were 3-4 replicate trials of each sample at each temperature.

4.2.1: ES2 Tear Results

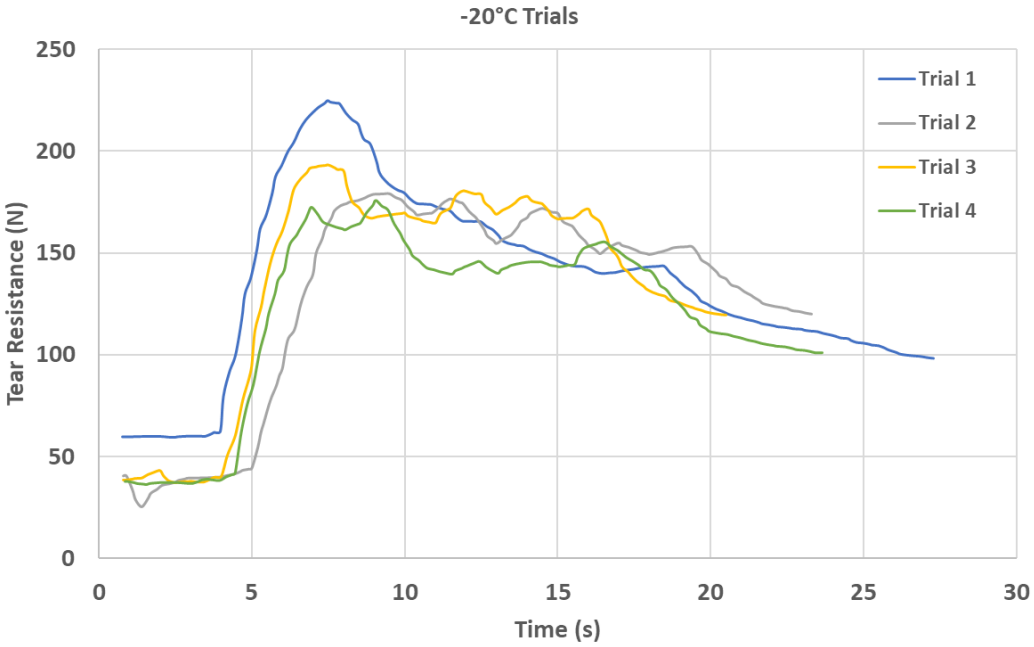

Figure 4.11 ES2 −20°C Tear Curves

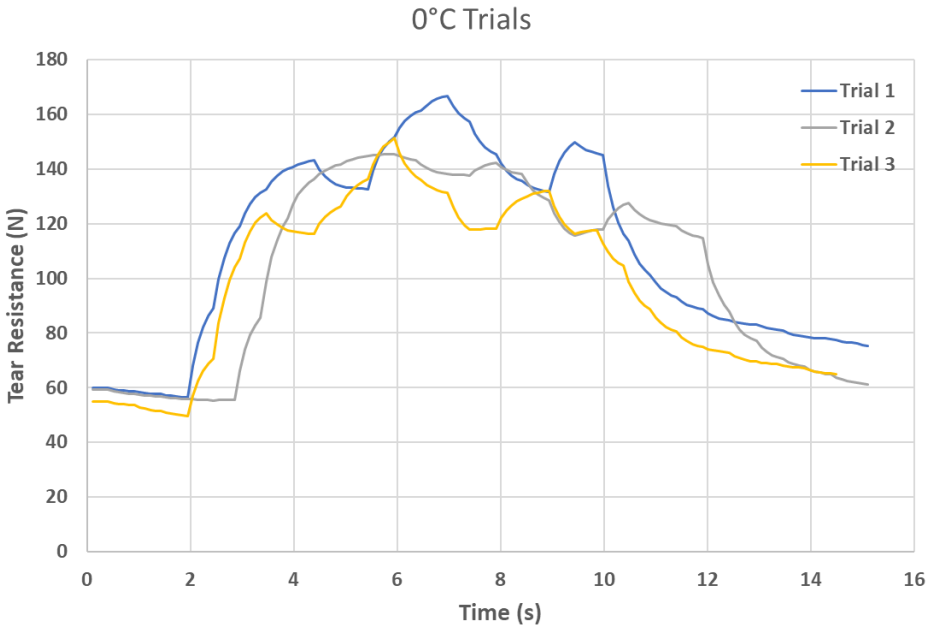

Figure 4.12 ES2 0°C Tear Curves

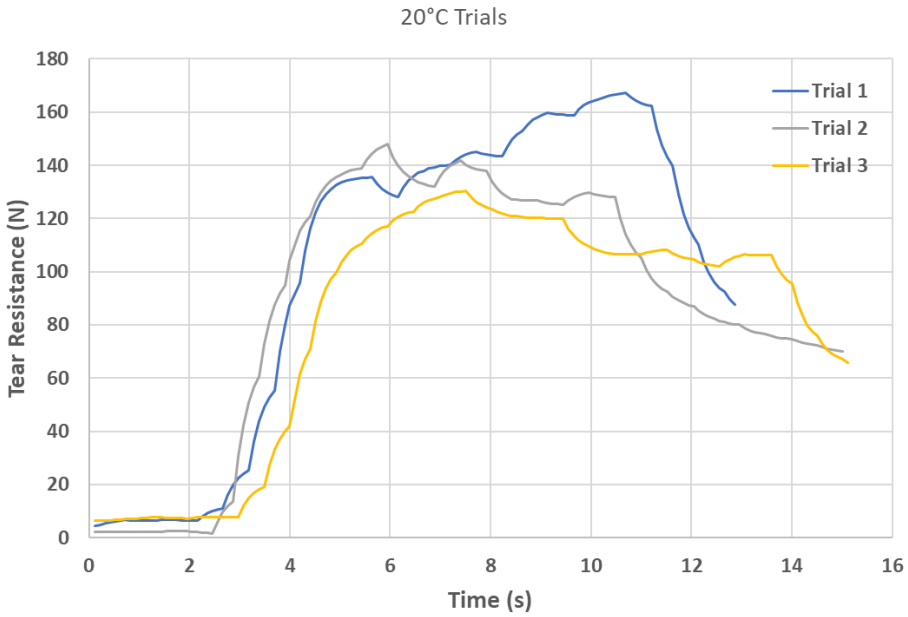

Figure 4.13 ES2 +20°C Tear Curves

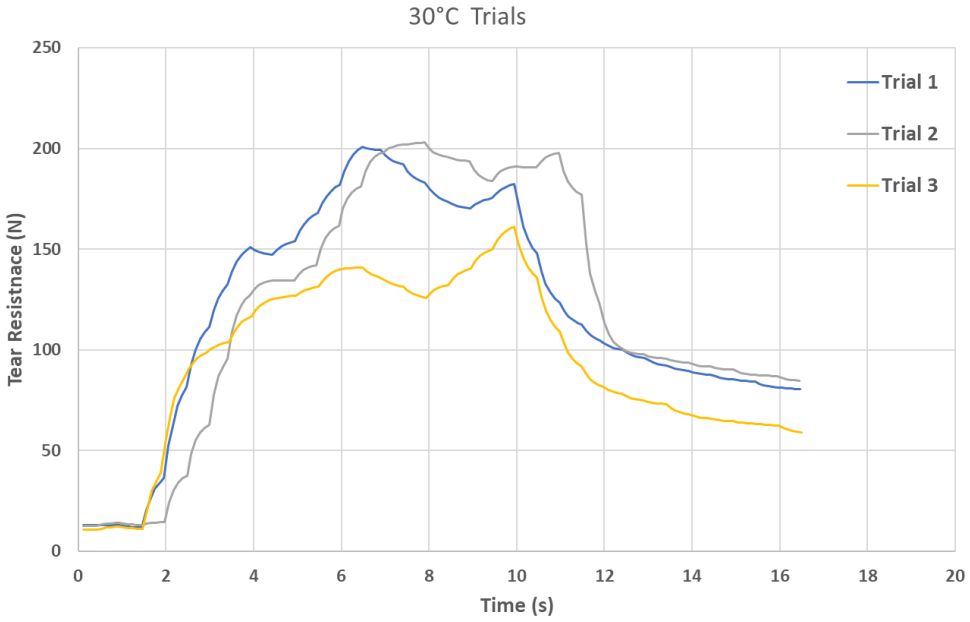

Figure 4.14 ES2 +30°C Tear Curves

4.2.2: ES4 Tear Results

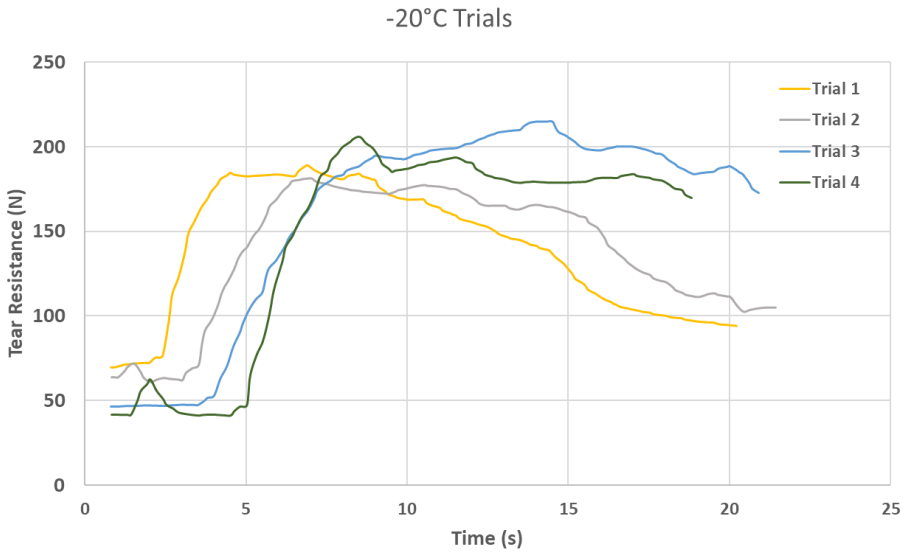

Figure 4.15 ES4 −20°C Tear Curves

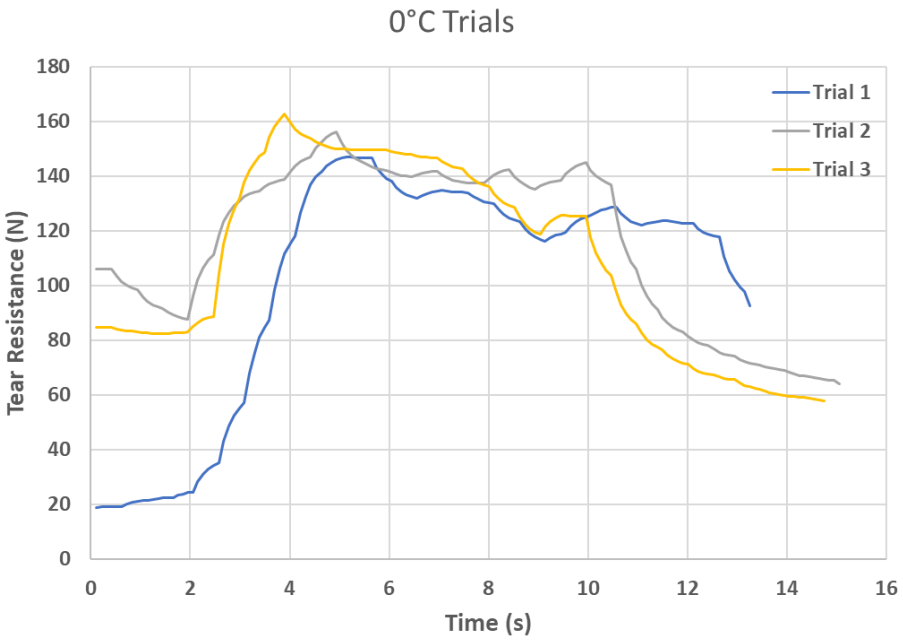

Figure 4.16 ES4 0°C Tear Curves

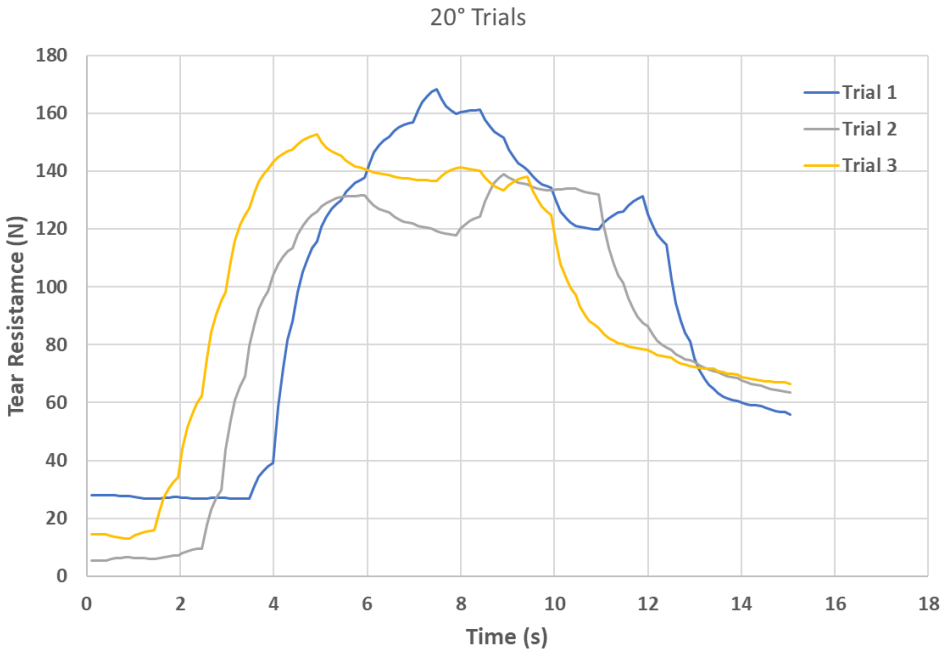

Figure 4.17 ES4 +20°C Tear Curves

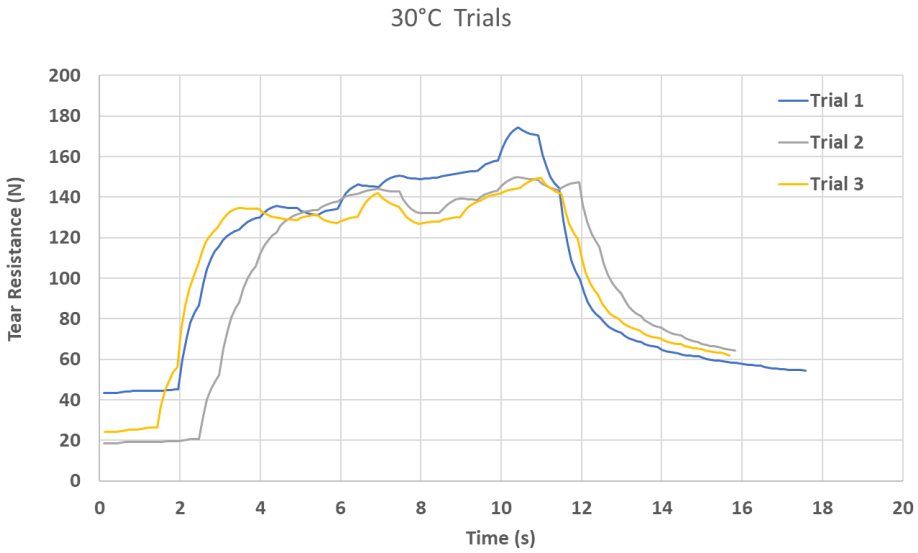

Figure 4.18 ES4 +30°C Tear Curves

4.2.3: Tear Results Discussion

Most of the variation between the samples was in the peak/post-peak responses of the samples, not the resistance values themselves. In the −20°C trials, the response of the material is very brittle, shown by the immediate peak and then fall off of resistance afterwards. There was a minimal difference between the respective peak resistances between the BGM samples while being tested

at the same temperature. Overall, the peak values in the tear experimentation did not vary by any significant margin between the ES2 and ES4 across the temperature ranges.

The ES2 samples showed peak tear resistances of 175-225 N at −20°C, and resistances of around 150-200 N at +30°C. In the responses of the ES2 sample to the different temperatures, there were two distinct differences between the high and low temperature tests. In the tests performed at −20°C, the ES2 samples reached their peak resistances nearly immediately after the tension was applied, which then trailed off as the tearing continued in the post peak portion of the tests following a brittle response. In the +30°C tests, there was a more gradual buildup to the peak tear resistance, which was held for the duration of the trial, following a more ductile response. During the 0°C and +20°C trials, the sample performed very similarly to how it did in the 30°C trials, which suggests that the performance of all tests above 0°C will show similar results.

When evaluating the tear resistance behaviour of the ES4 samples, the overall trends of the ES2 samples were still present. In the −20°C trials, the peak tear resistance ranged from 175-200 N, while displaying a similar brittle response curve to the ES2 sample. There was a very quick buildup as tension was applied and the peak was reached in the front half of the test, which then slowly dissipated out as the stroke of the apparatus completed the tear. In the +30°C testing, the peak tear resistance was found to be around 150-180 N, and again followed a similar ductile peak/post-peak response to the ES2 samples at the same temperature. There was an initial resistance as the test began which then slowly built up to the peak at the end of the tearing cycle. Again, similarly to the ES2 samples, at 0°C and +20°C, the ES4 samples performed very closely to the 30°C trials, which suggests that most tearing behaviour will be similar when the temperatures are above freezing, and in positive ranges.

When the results of this tear testing are compared to that of the product manufacturers, the values obtained in this study are substantially lower (160-180 N from this testing and 700-1200 N from manufacturer testing), however because the data are from two different tests, no further comparison can be made.

4.3: Large Scale Performance Testing Results

The large-scale performance testing results are presented based on sample and temperatures, as in the previous sections. The following graph shows the average load profile of the large-scale performance tests. All samples underwent loading as shown by the average load profile in Figure 4.19, with a +/- 50 kPa fluctuation due to the Raspberry Pi trying to maintain the applied load. It is worth noting that in all the tests, the maximum possible stress applied was limited to slightly less than 400 kPa due to the air lines available, with the average applied stress at around 350 kPa, and even with the aggressive aggregate in place, no puncture was induced in any of the experimental trials.

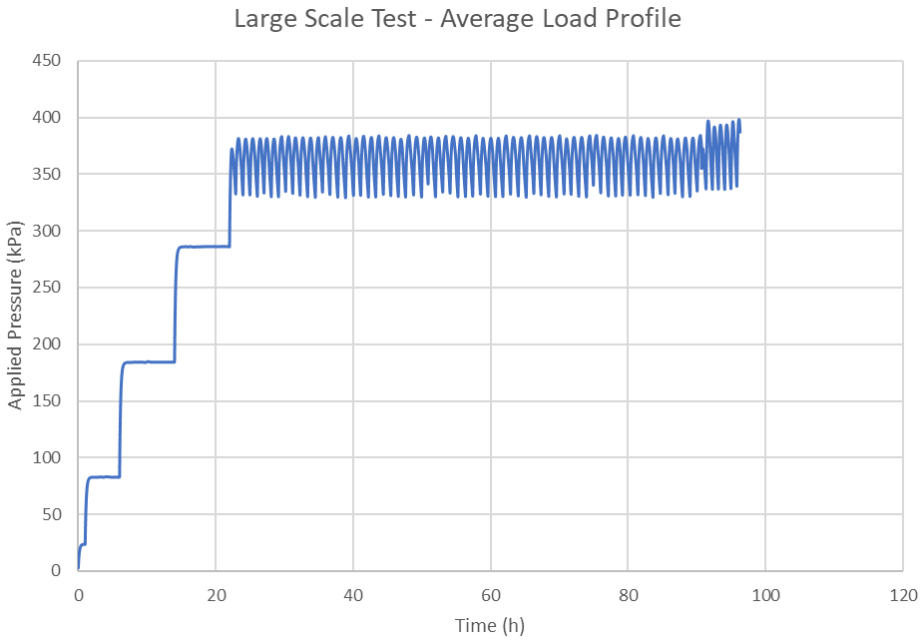

Figure 4.19 Average Large-Scale Load Profile

During the testing stages, an overburden stress is applied to the system of approximately 350 kPa (Figure 4.19), however due to the 8-10 aggressive fragments placed on the samples, point load stresses present have the potential to be significantly higher than the overall applied stresses on the sample. When the samples were evaluated after testing, one of the main things that was looked for was ‘significant deformation’. For the purposes of this research, the term ‘significant deformation’ is defined by points of indentation caused by the aggressive fragments placed on the liner that clearly penetrate deeper into the BGM than the rest of the overburden and caused more permanent deformations. These are points that have or could potentially cause holes to

form in the BGM due to point load stresses. In this section, the figures show the samples with the most points of significant deformation present in each trial for each material type, all other sample images can be found in Appendix C.

4.3.1: Results of −15°C Performance Testing

After evaluating the samples after testing at −15°C there were only 3 significant deformation points present in any of the samples, all of which occurring on the ES2 BGM material. These 3 significant points did not cause puncture but did leave permanent deformations on the surface of the sample. The following table shows the distribution of damage across all the ES2 and ES4 samples tested.

Table 4.5 Significant Deformation Distribution (-15°C)

Sample Type	ES2			ES4		
Trial	Trial 1	Trial 2	Trial 3	Trial 1	Trial 2	Trial 3
Significant Points of Deformation Present	3	0	0	0	0	0

The other surface indentations occurring on the samples are most likely due to the base aggregate under the applied load, but it appears that the BGM stiffens significantly when being tested at these sub-zero temperatures (Figure 4.20). This follows the same trends that appeared during the ASTM puncture testing, as the amount the sample deformed at the sub-zero tests was significantly less than that at the >0°C test trials. The increased stiffness of the bitumen due to the sub-zero temperatures seemed to have noticeably lessened the damage caused by the aggregate placed overtop of the sample, but could result in a more brittle failure should it occur. Having a stiff subgrade could also increase this resistance to deformation, however if the sample

is unable to deform, there could be an increase of point load stress present from aggressive point load aggregates.

Figure 4.20 ES2 Sample with Significant Deformation Points (-15°C)

4.3.2: Results of 0°C Performance Testing

Overall, there were once again only three points of deformation across all six samples that could be considered critical. All the points of deformation were only present on the ES2 samples tested. The breakdown of significant deformation present in the −0°C trials can be seen below.

Table 4.6 Significant Deformation Distribution (0°C)

Sample Type	ES2			ES4		
Trial	Trial 1	Trial 2	Trial 3	Trial 1	Trial 2	Trial 3
Significant Points of Deformation Present	0	3	0	0	0	0

At 0°C there is an increase in ductility of the sample, which is why the indentation present from the aggregate is more defined. Although the indentation at 0°C is more defined than that of the −15°C tests, it is still far from being significant deformation. When analyzing ES2 test #2, the deformation identified was isolated purely to the point of contact and did not impact the surround area through stress cracking or tearing, and the underside of the BGM was unaffected by the point of contact (Figure 4.21). The increased stiffness of the bitumen binding due to lower

temperatures seems to be a key aspect in limiting the influence of the surface deformation to the surrounding material in the sample.

Figure 4.21 ES2 Sample with Significant Deformation Points (0°C)

4.3.3: Results of +20°C Performance Testing

When examining the samples after the +20°C trials, the most significant difference between these trials and the lower temperature trials was the surface of the BGM after testing. The warmer temperatures increased the ductility of the samples compared to that of the low temperature tests, which was visually apparent from the increase in indentations across the sample. The indentations during the +20°C trials were seen to deform the samples significantly more than the other trials however a lot of the deformation was seen to be surficial as it displaced the bitumen binder. Due to the increased ductility at the higher temperature, there were more significant points of deformation present, but once again none of these significant points caused full puncture to occur. The distribution of significant deformation across the ES2 and ES4 samples can be seen in Table 4.7

Table 4.7 Significant Deformation Distribution (+20°C)

Sample Type	ES2			ES4		
Trial	Trial 1	Trial 2	Trial 3	Trial 1	Trial 2	Trial 3
Significant Points of Deformation Present	1	2	3	3	1	0

The depth of the deformations were all shallow, with the binder being displaced to the edges of the point of contact. The increase in ductility of the bitumen binding was more clearly noticeable than at the colder temperatures, but its strength and resistance to puncture remained effective. Although the damage from the fragments was slightly deeper in the +20°C tests than the others, the sites of concern were still unable to cause puncture or permanent damage to the geomembrane (Figures 4.22 and 4.23). In addition to its resistance to puncture during the test, after the tests had concluded, as the samples were left out to rest there was a visible reduction in the magnitude of all deformations and other damage to the BGM, which is most likely attributed to the self healing effect described by Clinton and Rowe (2017). This self healing effect is more visible at higher temperatures, and it is assumed that this phenomena is less prominent in sub-zero conditions.

Figure 4.22 ES2 Sample with Significant Deformation (+20°C)

Figure 4.23 ES4 Sample with Significant Deformation (+20°C)

Chapter 5 - Conclusion and Recommendations

5.1: Conclusions of the Research

This project was introduced with the objective of evaluating the short-term performance of bituminous geomembranes with respect to changes in ambient temperature, with specific objectives set out to guide the project:

- Variation in short-term performance across a temperature range of −20°C through +30°C
- Evaluate ASTM Puncture resistance for HDPE and BGM
- Evaluate ASTM Tear resistance for BGM
- Evaluate short term durability and performance for BGM
- Monitor for any leakage through the BGM as it is loaded/damaged

The first objective was to conduct tests at a range of temperature increments to evaluate how the results vary with temperature . This was conducted through two separate pieces of equipment. The first method was using the in-house climate chambers in the geo environmental lab at the college of engineering, which allowed the testing to be conducted at controlled temperatures from 0°C to +30°C. The second method used was a walk-in freezer unit. The two temperature control units used in the experimentation successfully maintained the desired temperatures for testing and allowed for proper evaluation of the geomembrane performance for each experimental approach taken throughout the project.

The second objective was to evaluate the puncture resistance of both BGM and HDPE geomembranes. In both cases there was a significant increase in puncture resistance as the temperature decreased during the experimental process. The ES2 BGMs showed puncture resistance increases of around 2x from the +30°C trials to the −20°C trials, and the ES4 BGMs showed an increase of around 2.4x in puncture resistance from +30°C to −20°C. When evaluating the HDPE geomembranes under the same conditions, there were similar results. The 1.5mm HDPE showed an increase of around 1.3x in puncture resistance, while the 3mm HDPE geomembranes showed an increase in puncture resistance of around 0.5x from +30°C to −20°C. While BGMs had a greater range of puncture resistances, the overall puncture resistance for HDPE geomembranes

was still higher than that of the BGMs. The maximum and minimum puncture resistances for each sample are as follows:

Table 5.1 Puncture Test Value Summary

Sample	Min Puncture Resistance (N)	Max Puncture Resistance (N)
ES2	337	590
ES4	498	1194
1.5mm HDPE	590	807
3mm HDPE	998	1540

In addition to the variations in puncture resistance, there was a positive correlation between the displacement of the sample before puncture and the temperature of the trial. As temperature increased, so did the displacement of the samples prior to puncture. In all sample trials, there around a 3x increase in displacements from the −20°C to +30°C trials. For the BGM samples, the displacements were elastic in nature and would slowly return to their original shape after some time, while in the HDPE trials the deformation was predominately plastic in nature and remained deformed indefinitely after the testing. It is also worth noting that the manufacturer stated puncture resistances at +20°C for ES2 and ES4 were stated to be 530 N and 650 N respectively, however during this experimentation the puncture resistances of ES2 and ES4 at +20°C were found to be 470 N and 450 N respectively.

The third objective of the research was to evaluate the tearing potential of BGM samples at different temperatures and compare the results. When evaluating the results of the tear testing there were two major points noted in the results.

1) There were not significant variations in tear resistance values of the respective samples at different temperature increments. All positive temperature tests performed similarly.

2) The main variation in the different temperature trials were the peak/post-peak responses of the samples in how they were torn.

With the first point, the ES2 and ES4 samples showed different tear resistances from sample to sample, however within each individual sample case, there were minimal changes in tear resistance between the −20°C and the +30°C trials. In the −20°C trials, for both the ES2 and ES4 samples, the peak tear resistance was reached very early on in the trials, which then trailed off as the test went on. In cold temperatures, tearing seems to occur as the load is applied, and the sample becomes weaker as the load in continuously applied. The reduction in ductility due to sub-zero temperatures seems to eliminate the samples capacity to maintain a load after tearing has occurred. When evaluating tearing of the BGMs in the +30°C trials, the reaction of the samples to tearing was more gradual. As load was applied and the sample was torn, the tear resistance reached its peak which was then fairly maintained throughout the duration of the trial. It is assumed that due to the increased ductility of the sample at higher temperatures, the bitumen binding can better maintain its tearing resistance which explains how the peak tear resistance is held.

The fourth and fifth objectives of the research can be combined into one analysis, as both were monitored during the same performance testing, and because the fifth point was found to be insignificant during the trial process. When evaluating the short-term performance of the BGM samples, there was a very clear trend in the data. As the temperature increased from −15°C to +20°C, the damage present on the BGMs became more and more noticeable, however throughout the entirety of the experimental process, there was never one complete puncture through the sample, and therefor no leakage present at any point during the experimentation. Even with stresses around 400kPa, and clear points of aggressive contact between the aggregate and the BGM, the BGM was never damaged to an extent to warrant failure of the system. Additionally, in the colder temperature trials the surface deformation of the samples were also extremely minimal, with the only noticeable points of damage being from the aggressive aggregate in place which were still considered insignificant amounts of damage.

Based on the above findings, the following conclusions can be made:

1) When evaluating the puncture resistance of HDPE and BGM samples, there are negative correlations between ambient temperature and puncture resistance. It was observed that as temperatures increased, the puncture response of the BGM transitioned from brittle to ductile In conditions in which puncture is possible during early stages of construction, colder temperatures may provide increased resistance to puncture occurring. While HDPE showed higher overall resistance to puncture, BGMs were showed a wider variety of performance capabilities which could be useful for specific application.

2) When the tearing potential of BGMs was evaluated, there was little variation between the individual sample performances at high and low temperatures, however the peak/post-peak response varied across temperatures. At sub-zero temperatures, there was a noticeably brittle response, with a ductile response occurring at positive temperatures. In general, tearing occurring at warmer temperatures seemed to maintain a higher tear resistance for most of the tests, while at cold temperatures once the peak tear resistance was reached the sample was considered failed and the resistance dropped off.

3) Based on the performance testing that was conducted on the bituminous geomembrane samples, at stresses of 400kPa and lower, the BGMs were able to perform with minimal damage present and prevent any leakage from the coarse angular gravel over liner material into the relatively deformable yet permeable sub liner material. Based on the severity of the damage present at these loads, the BGMs could potentially perform at higher levels of stress, however this was not verified and stresses over 400kPa were not reached during these trials.

To further evaluate the performance of BGMs in real life scenarios, a Boussinesq evaluation was conducted with overliner thicknesses of 300, 600, and 900mm over top of a BGM liner, while assuming a maximum allowable vertical stress of 400kPa as per the findings of this paper. Bousinnesq's equation is defined as follows:

$$Vertical\ \ stress, \sigma_z = \frac{3Q}{2\pi z^2} \frac{1}{[1 + (r/z)^2]^{5/2}} = \frac{Q}{z^2} I_B \tag{5.1}$$

Where I_B is defined as:

$$\frac{3}{2\pi} \frac{1}{[1 + (r/z)^2]^{5/2}} \tag{5.2}$$

The application is defined for a surface load over a point of interest P, as shown in the following diagram.

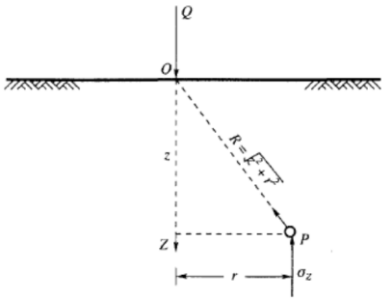

Figure 5.1 Boussinesq's Equation in Application (Murthy, 2002)

It is also assumed that the applied surface load is directly above the point of interest on the liner in this case, meaning r = 0m. Based on these assumptions, the following allowable surface loads for bituminous geomembrane liners with a maximum vertical stress allowance of 400 kPa were found to be as follows.

Table 5.2 Boussinesq's Evaluation of BGM Vertical Stress

Assuming Vertical Liner Stress of 400kPa, σ_z, at Point P	
Overliner Thickness (z)	Maximum Surface Load, Q (kN)
0.3m	75
0.6m	302
0.9m	679

When compared to these findings to those of Marcotte (2021), it appears that the allowable loading for BGMs, especially the ES4 samples, is noticeably higher than that of HDPE as the ductile bitumen binding has the potential to eliminate the risk of long-term high localised strains that can lead to puncture. In Marcotte's thesis it was found that the risk of puncture in HDPE liners was present at loads of up to 500 kPa even with the presence of heavy non-woven protection layers. The cases presented in this paper explored loads up to 400 kPa in addition to higher point load contacts on the liner with no protection layers present. Based on these findings

it may be inferred that with proper protection layers on a bituminous geomembrane liner, that the risk for puncture is significantly lower than that of HDPE geomembranes in similar conditions.

5.2: Recommendations for Future Research

The following are recommendations for future research topics on the performance of bituminous geomembranes as a barrier liner in different waste containment applications:

1) During the experimental process of this project, the ability to produce stresses higher than 400 kPa wasn't possible due to mechanical limitations of the equipment. In future testing, the focus on higher load application would be a benefit to understanding how bituminous geomembranes perform in short-term conditions.
2) The service life of geomembranes is much longer than what was investigated in this research, as these were only short-term early life tests. It is recommended that similar temperature dependent trials are completed, however for much longer terms.
    a. Trials in the magnitude of months to years would be needed to evaluate how these geomembranes perform under more realistic durations of time.
    b. Individual testing cycles could be designed to include multiple fluctuations in temperature as the tests were conducted, to simulate seasonal climate fluctuations. In addition, simple week-to-week or month-to-month temperature fluctuations could further evaluate the influence of temperature on the performance of BGM systems.

3) The potential of leakage through bituminous geomembranes was not able to be evaluated, as there was no damage present that allowed leakage to occur within the system. Experiments focused solely on leakage through BGMs separate from simulating in-situ conditions would be invaluable to the understanding of the performance of bituminous geomembranes.

References

Abdelaal, F.B., Rowe, R.K., and Brachman, R.W.I. 2014. Brittle rupture of an aged HPDE geomembrane at local gravel indentations under simulated field conditions. Geosynthetics International, **21**(1): 1–23. doi:10.1680/gein.13.00031.

Andrew Tognon, B.R., Kerry Rowe, R., and Moore, I.D. 2000. GEOMEMBRANE STRAIN OBSERVED IN LARGE-SCALE TESTING OF PROTECTION LAYERS.

ASTM FOR BGM, and ASTM. 2012. Standard Test Method for Tensile Properties of Bituminous Geomembranes (BGM). Astm, **i**(C): 7–8. doi:10.1520/D7275-07R18.2.

ASTM International. 2010. Standard Test Method for Index Puncture Resistance of Geomembranes and Related. (C): 8–11. doi:10.1520/D4833-07.2.

Axter Coletanche ® Inc. 2009. ES2 Product Data Sheet

Axter Coletanche ® Inc. 2009. ES4 Product Data Sheet

Bannour, H., Barral, C., and Touze-Foltz, N. 2013. Flow rate in composite liners including GCLs and a bituminous geomembrane. *In* The 3rd International Conference on Geotechnical Engineering. Hamamet. p. 11.

Clinton, M., and Rowe, R.K. 2017. Physical Performance of a Bituminous Geomembrane for use as a Basal Liner in Heap Leach Pads.

Fleming, Ian, and Titan Environmental Containment Ltd. 2019. "Application for a Grant." Saskatoon.

Hornsey, W.P., and Wishaw, D.M. 2012. Development of a methodology for the evaluation of geomembrane strain and relative performance of cushion geotextiles. doi:10.1016/j.geotexmem.2012.05.002.

Lambert, S., Touze, N., and Lambert, S. 2000. A test for measuring permeability of geomembranes mumolade View project A test for measuring permeability of geomembranes.

Marcotte, B. 2021. Protecting Geomembrane Liners. University of Saskatchewan.

Murthy, V. N. S. (2002). Geotechnical engineering: principles and practices of soil mechanics and foundation engineering. CRC press.

Rogal, M., Marcotte, B., Fleming, I.R., and Baht, S. 2021. Short Term Durability and Performance of Bituminous Geomembranes with Respect to Temperature.

Rowe, R.K., Brachman, R.W.I., Irfan, H., Smith, M.E., and Thiel, R. 2013. Effect of underliner on geomembrane strains in heap leach applications q. doi:10.1016/j.geotexmem.2013.07.009.

Samea, A., and Abdelaal, F.B. 2022. Geotextiles and Geomembranes Effect of elevated temperatures on the degradation behaviour of elastomeric bituminous geomembranes. Geotextiles and Geomembranes, (April). Elsevier Ltd. doi:10.1016/j.geotexmem.2022.10.010.

Tognon, A.R., Rowe, R.K., Moore, I.D. 2000. Geomembrane strains observed in large-scale testing of protection layers. Journal of Geotechnical and Geoenvironmental Engineering 126 (12): 1194-1208

Touze-Foltz, N., and Farcas, F. 2017. Long-term performance and binder chemical structure evolution of elastomeric bituminous geomembranes. Geotextiles and Geomembranes,. doi:10.1016/j.geotexmem.2017.01.003.

Touze-foltz, N., Farcas, F., and Benchet, R. 2015. Evaluation of the Ageing of Two Bituminous Geomembranes of Different Natures After 15 Years in Service. **10318**: 142–151.

Appendix A: Individual Puncture Resistance Plots

A.1: ES2 Puncture

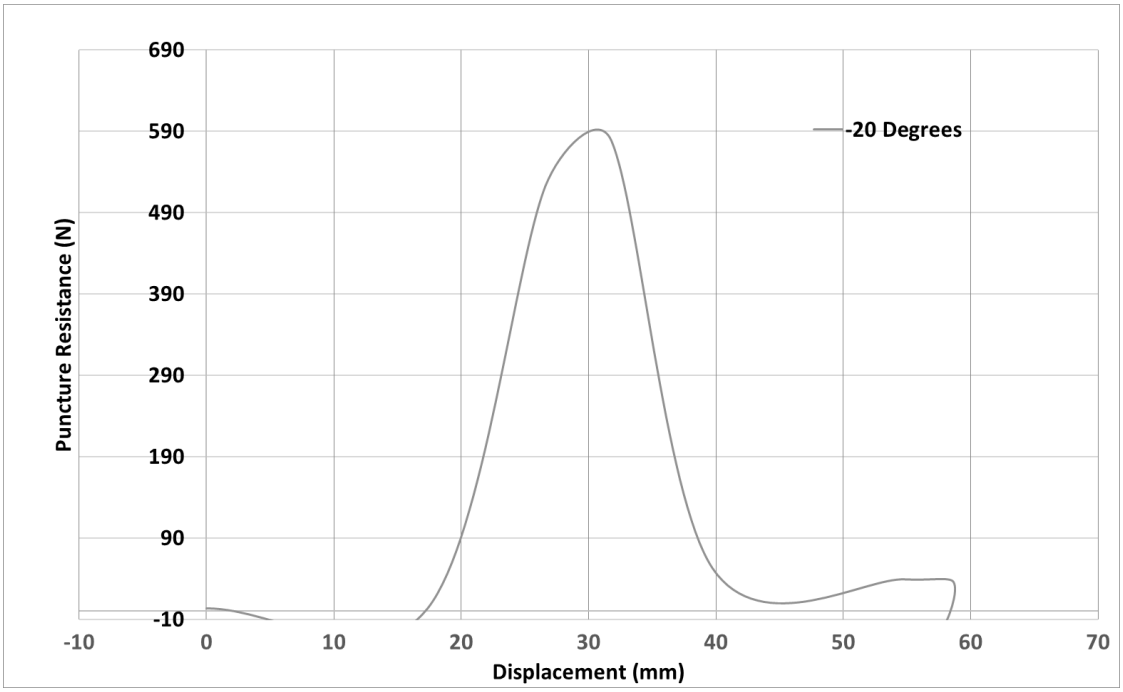

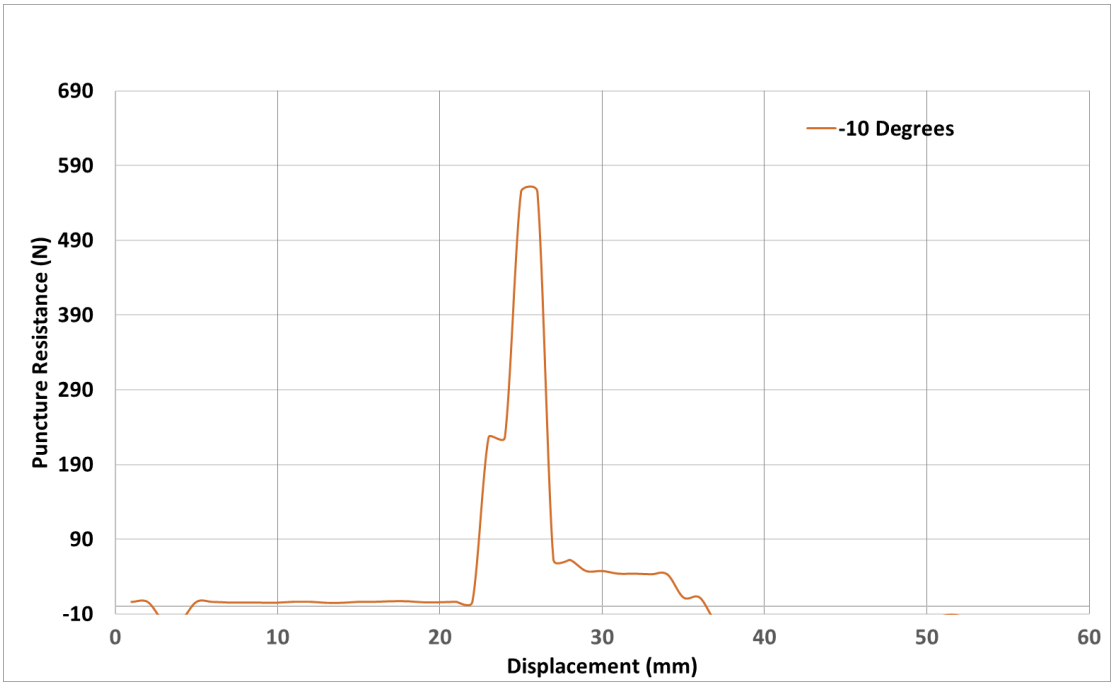

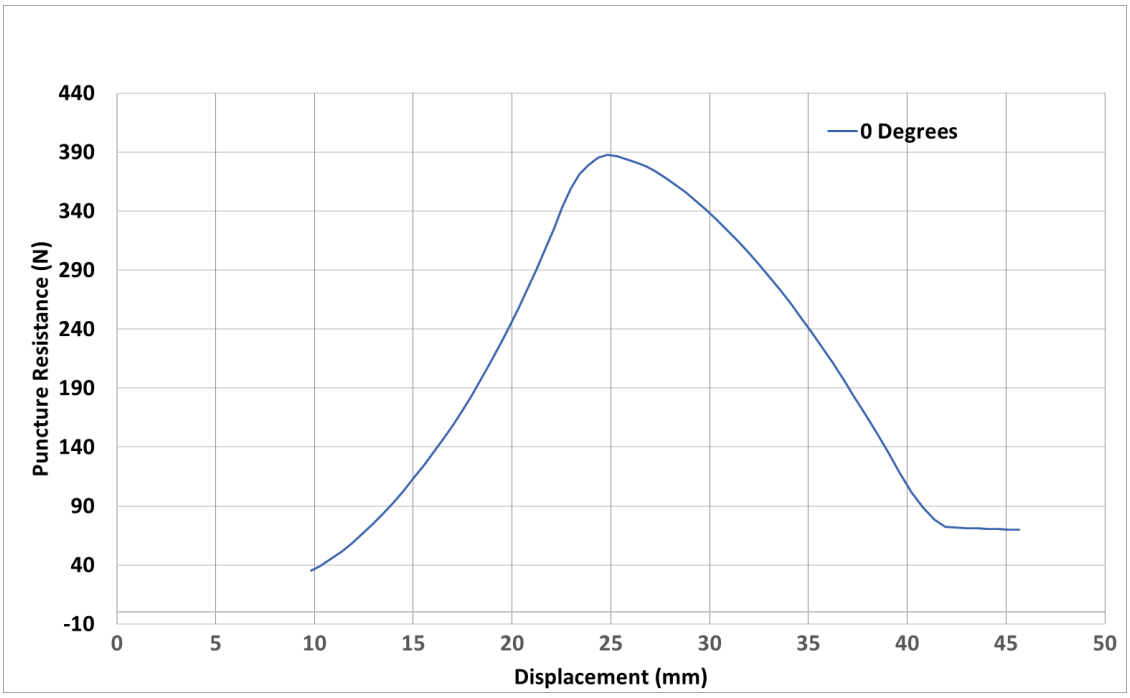
0 Degrees
Puncture Resistance (N)
440
390
340
290
240
190
140
90
40
-10
0
5
10
15
20
25
30
35
40
45
50
Displacement (mm)

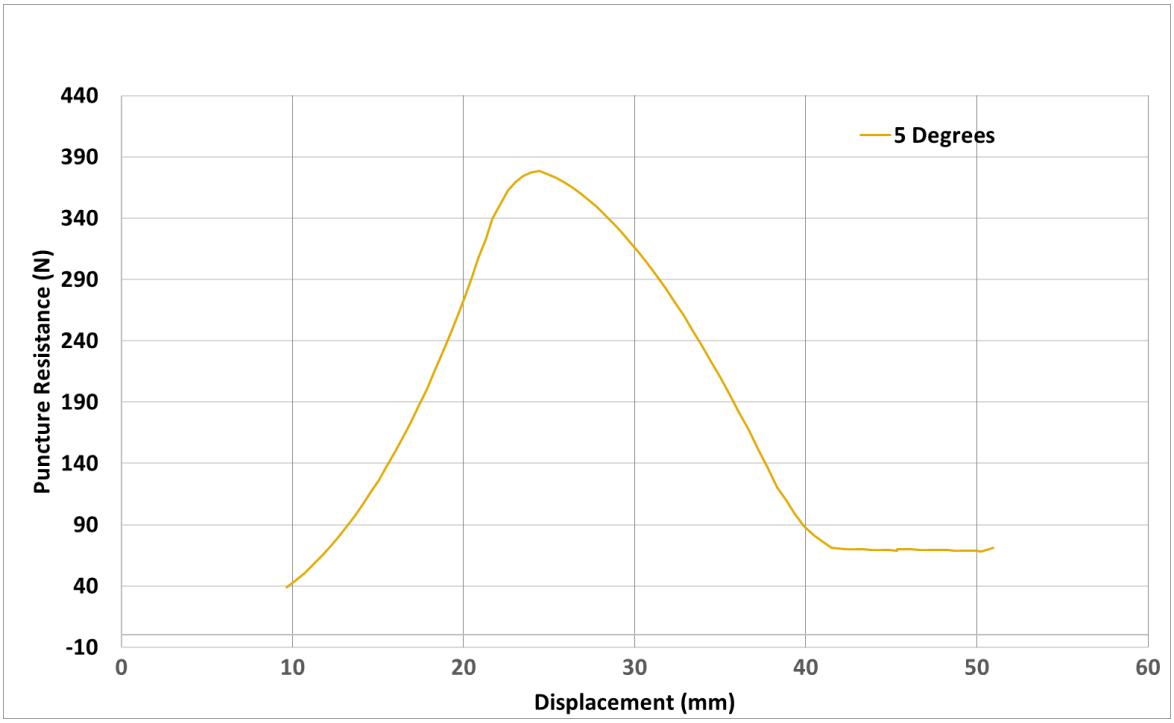
5 Degrees
Puncture Resistance (N)
440
390
340
290
240
190
140
90
40
-10
0
10
20
30
40
50
60
Displacement (mm)

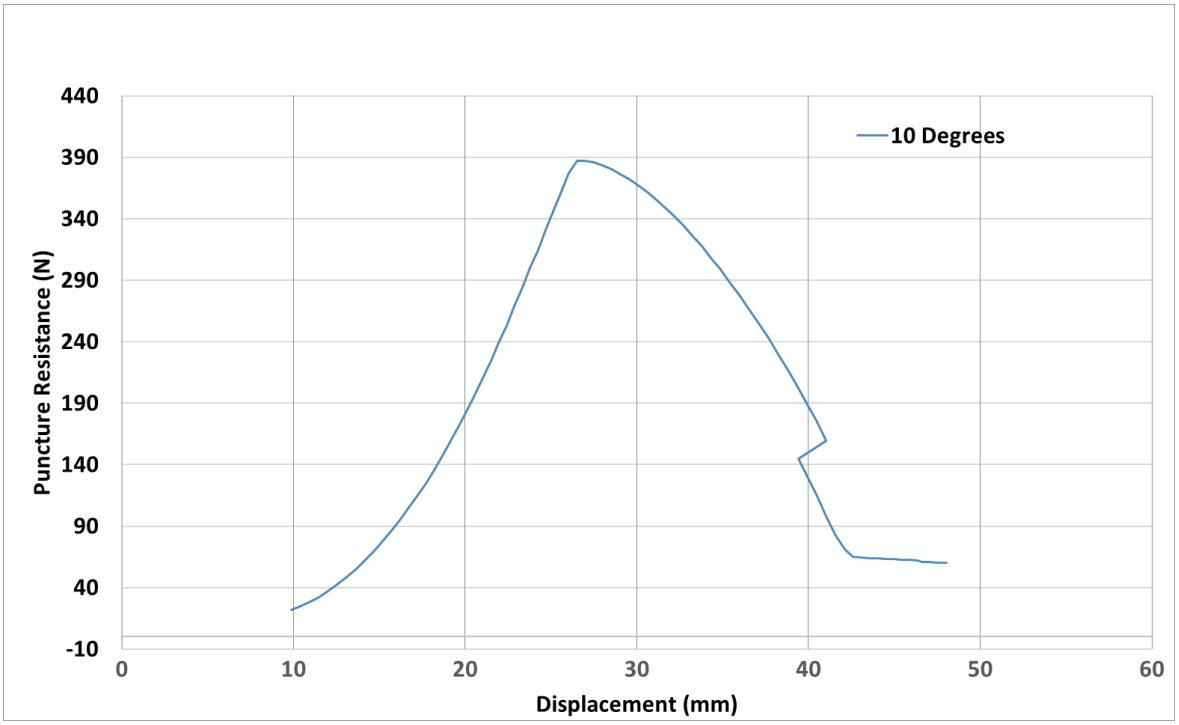
10 Degrees
Puncture Resistance (N)
440
390
340
290
240
190
140
90
40
-10
0
10
20
30
40
50
60
Displacement (mm)

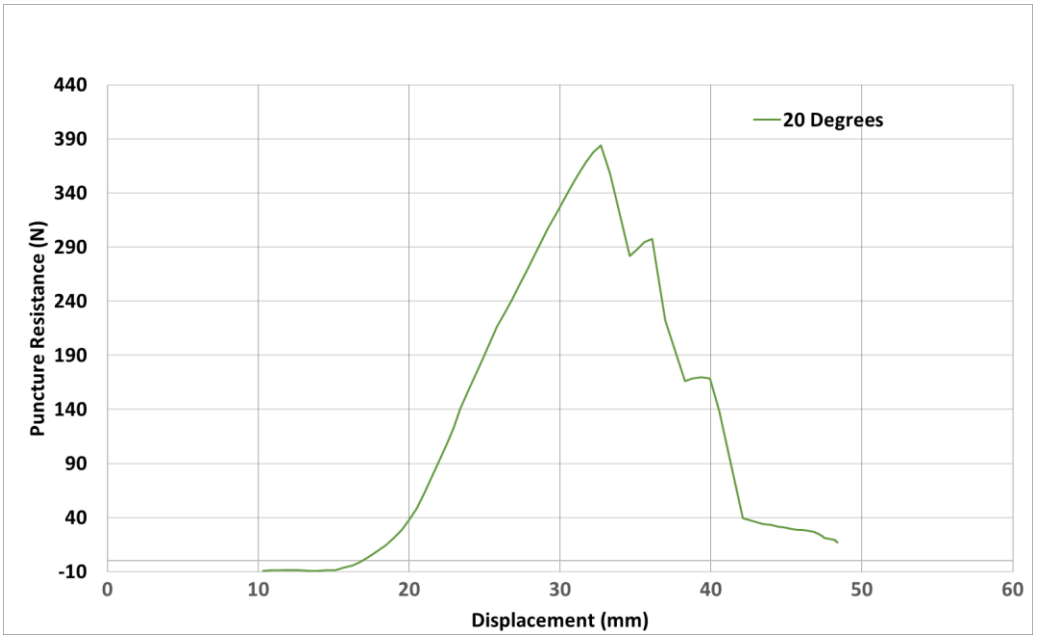
20 Degrees
Puncture Resistance (N)
440
390
340
290
240
190
140
90
40
-10
0
10
20
30
40
50
60
Displacement (mm)

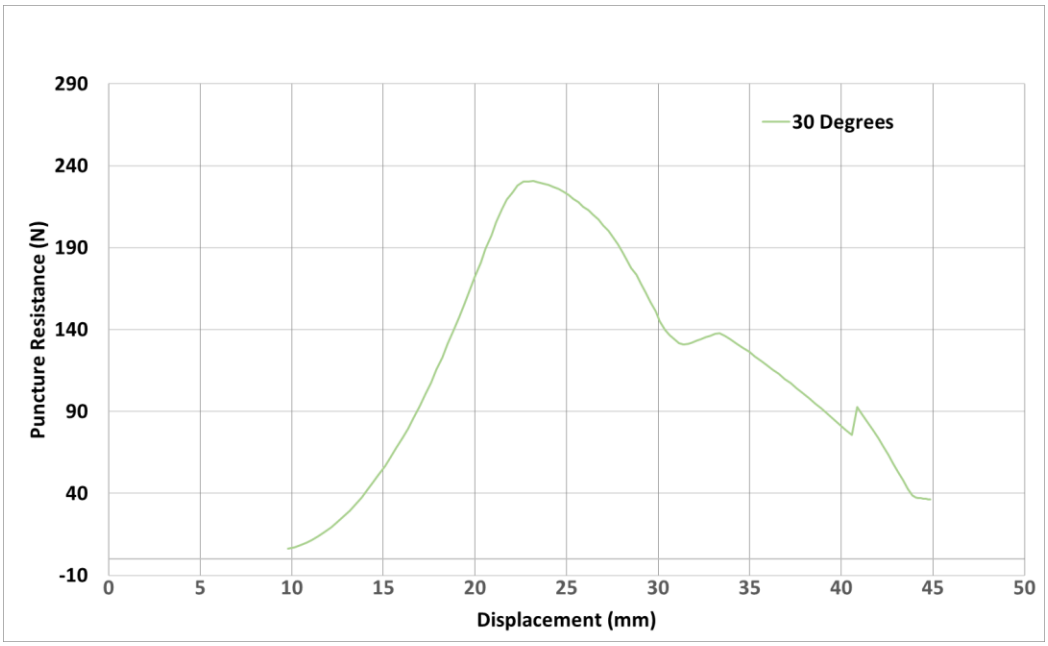

A.2: ES4 Puncture

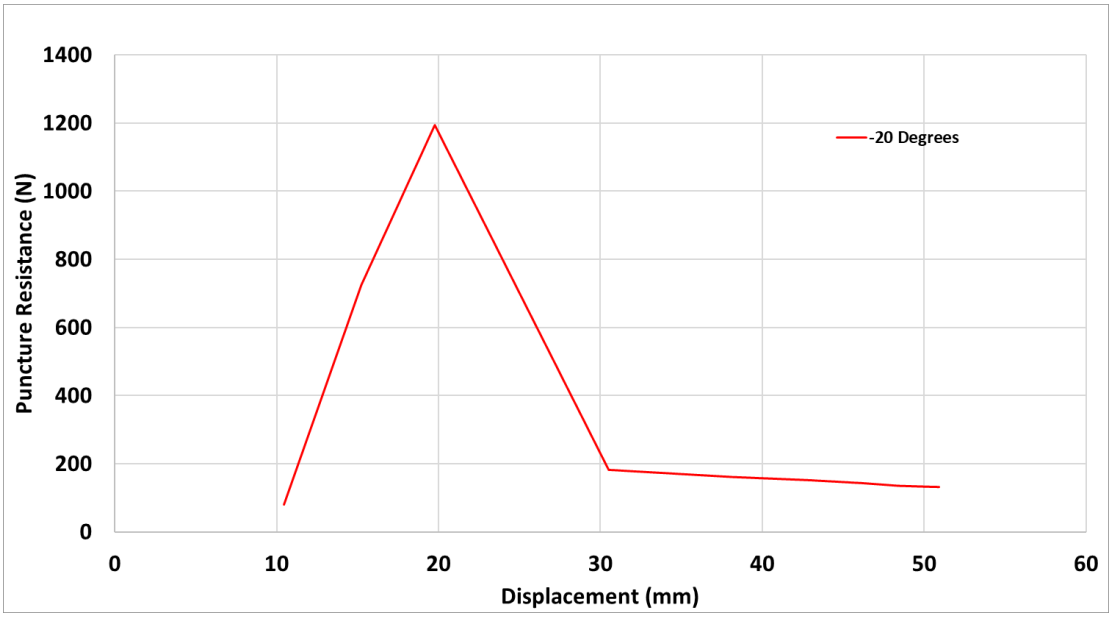

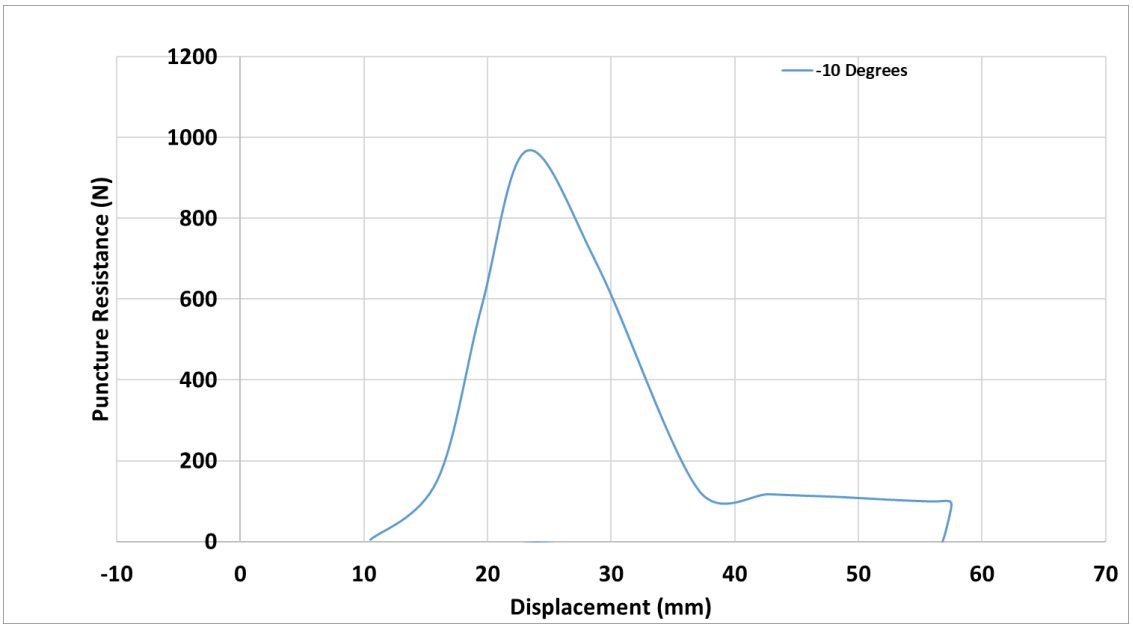
-10 Degrees
Puncture Resistance (N)
Displacement (mm)
1200
1000
800
600
400
200
0
-10
0
10
20
30
40
50
60
70

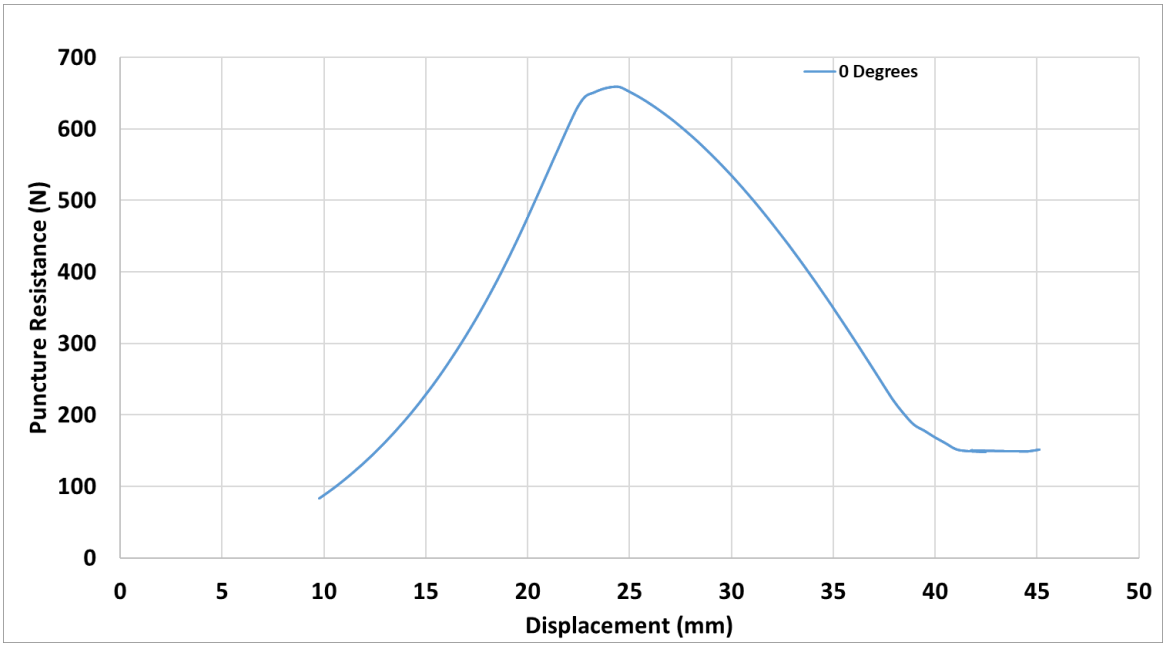
0 Degrees
Puncture Resistance (N)
Displacement (mm)
700
600
500
400
300
200
100
0
0
5
10
15
20
25
30
35
40
45
50

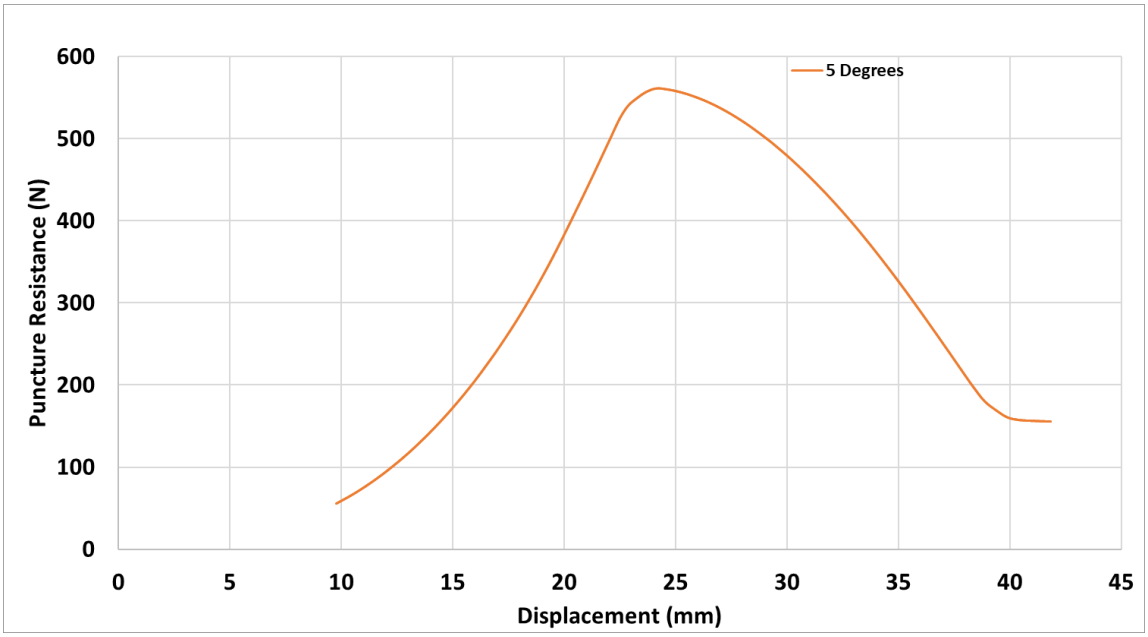
5 Degrees
Puncture Resistance (N)
Displacement (mm)
600
500
400
300
200
100
0
0
5
10
15
20
25
30
35
40
45

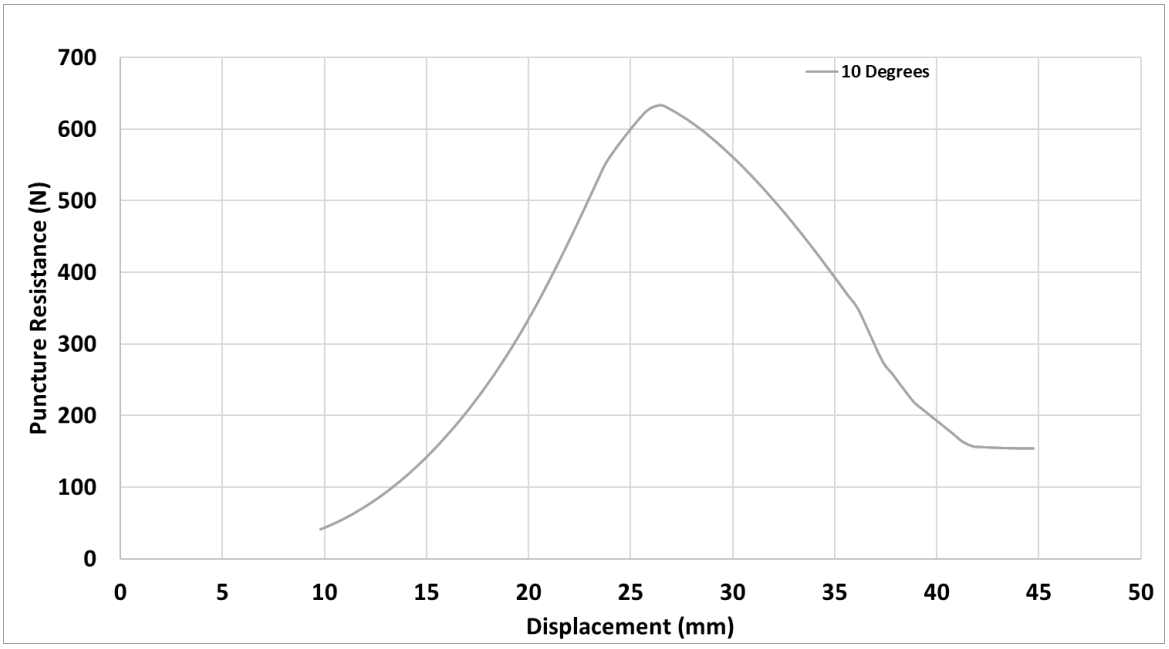
10 Degrees
Puncture Resistance (N)
Displacement (mm)
700
600
500
400
300
200
100
0
0
5
10
15
20
25
30
35
40
45
50

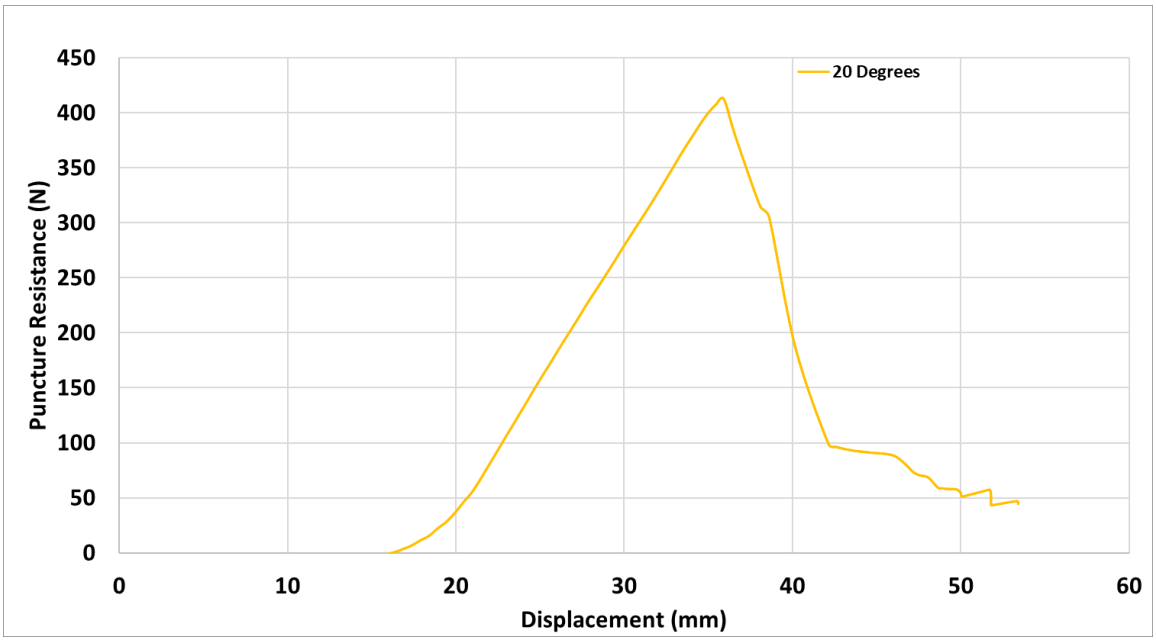
20 Degrees
Puncture Resistance (N)
Displacement (mm)
0
50
100
150
200
250
300
350
400
450
0
10
20
30
40
50
60

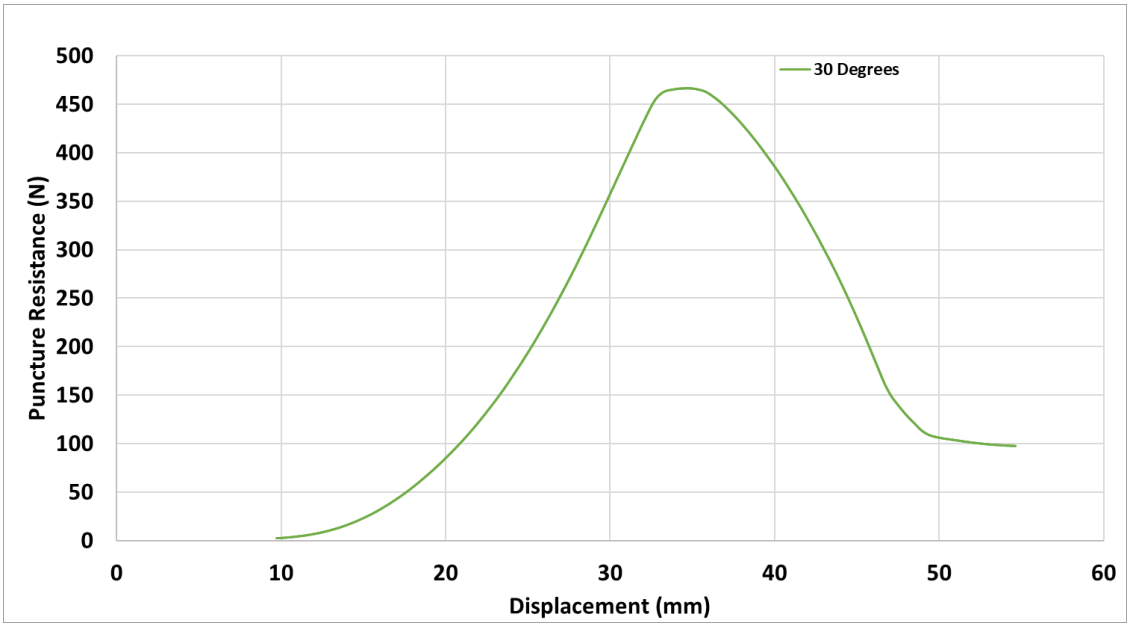
30 Degrees
Puncture Resistance (N)
Displacement (mm)
0
50
100
150
200
250
300
350
400
450
500
0
10
20
30
40
50
60

A.3: 1.5 mm HDPE Puncture

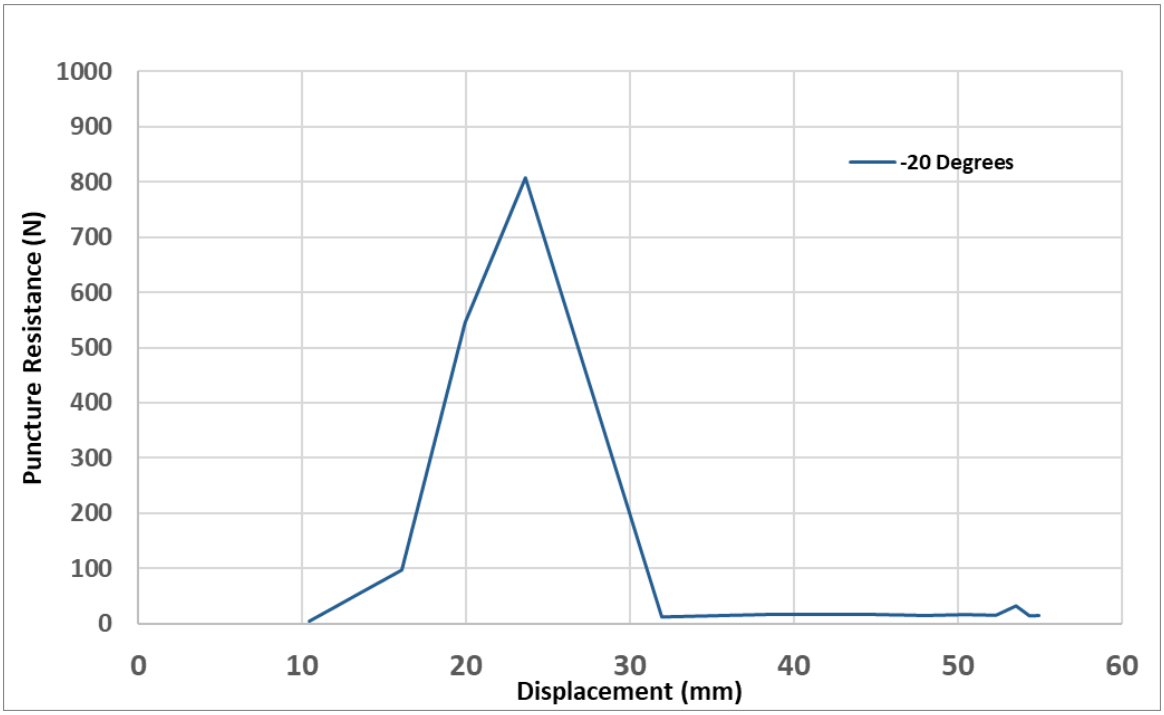

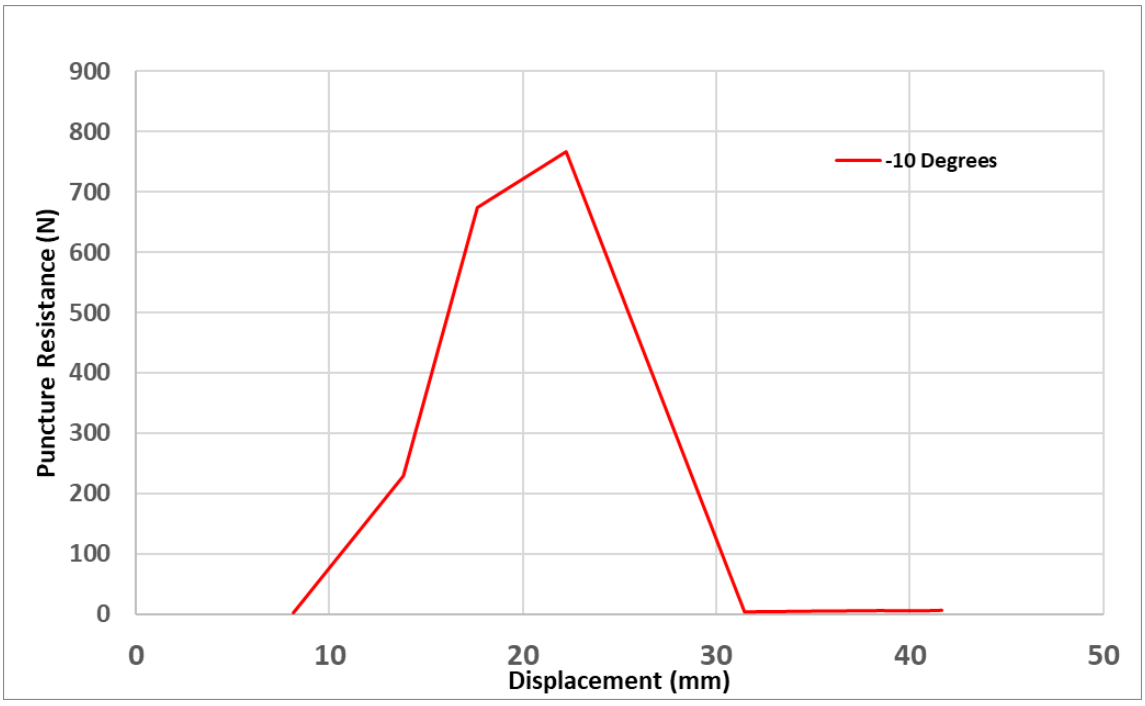

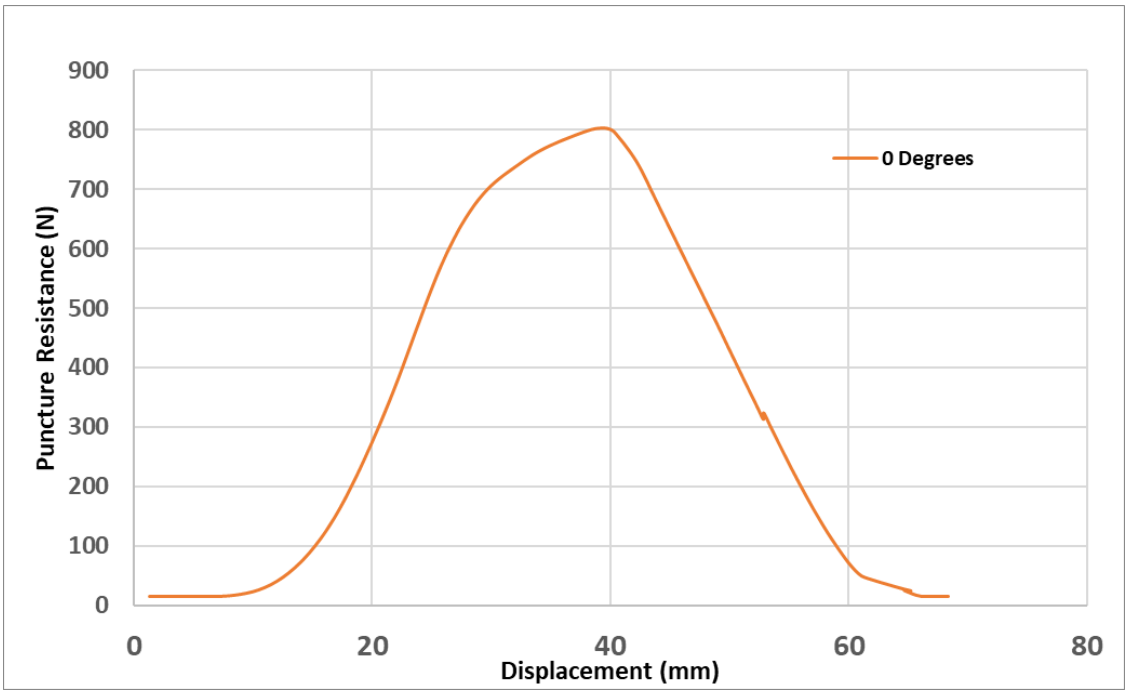
900
800
700
600
500
400
300
200
100
0
Puncture Resistance (N)
0 Degrees
0
20
40
60
80
Displacement (mm)

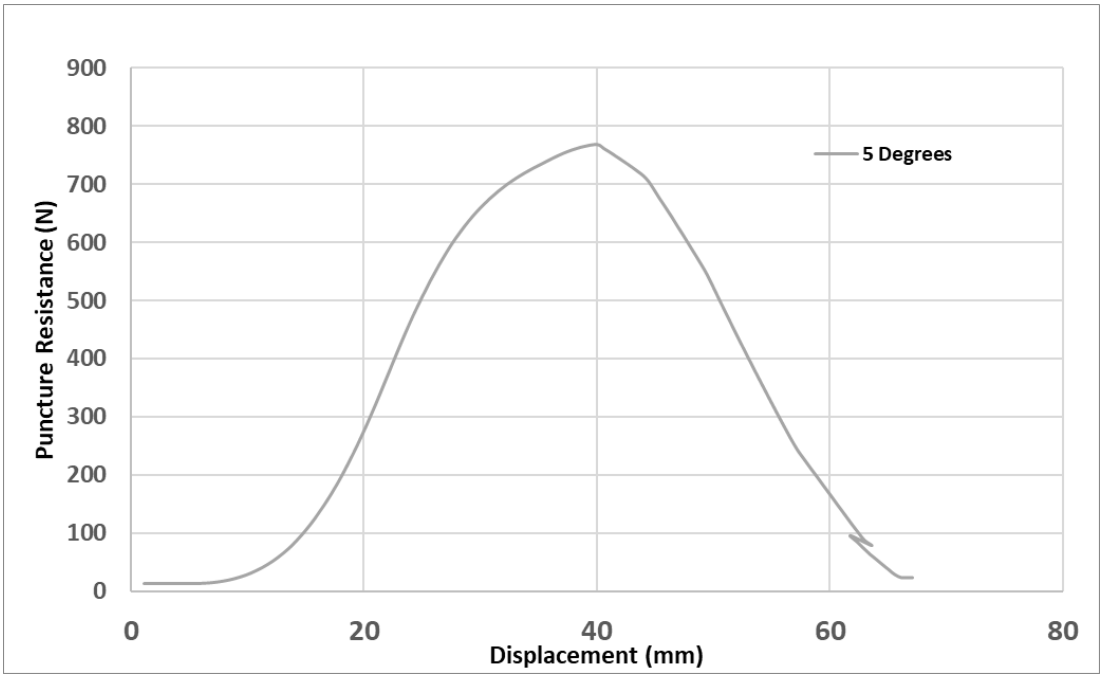
900
800
700
600
500
400
300
200
100
0
Puncture Resistance (N)
5 Degrees
0
20
40
60
80
Displacement (mm)

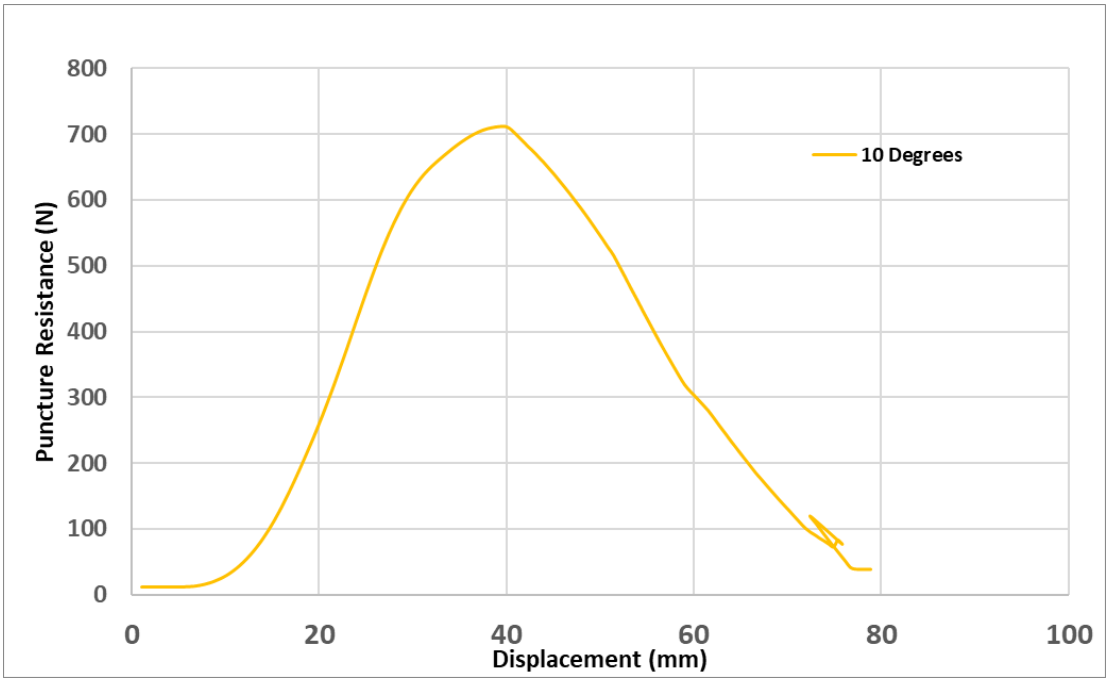
800
700
600
500
400
300
200
100
0
Puncture Resistance (N)
0
20
40
60
80
100
Displacement (mm)
10 Degrees

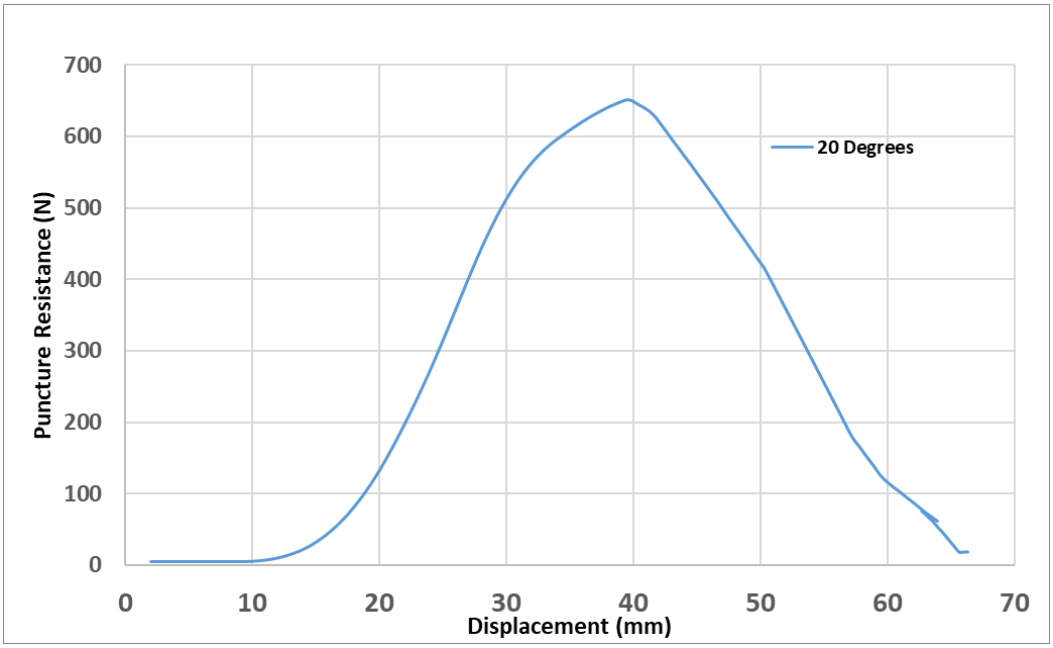
700
600
500
400
300
200
100
0
Puncture Resistance (N)
0
10
20
30
40
50
60
70
Displacement (mm)
20 Degrees

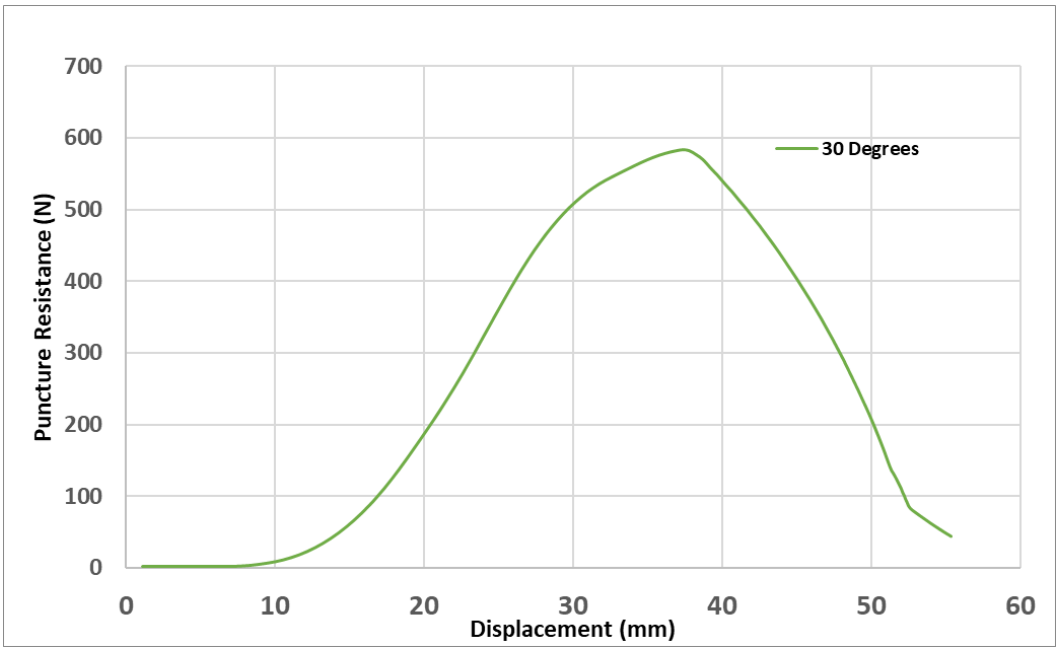

A.4: 3 mm HDPE Puncture

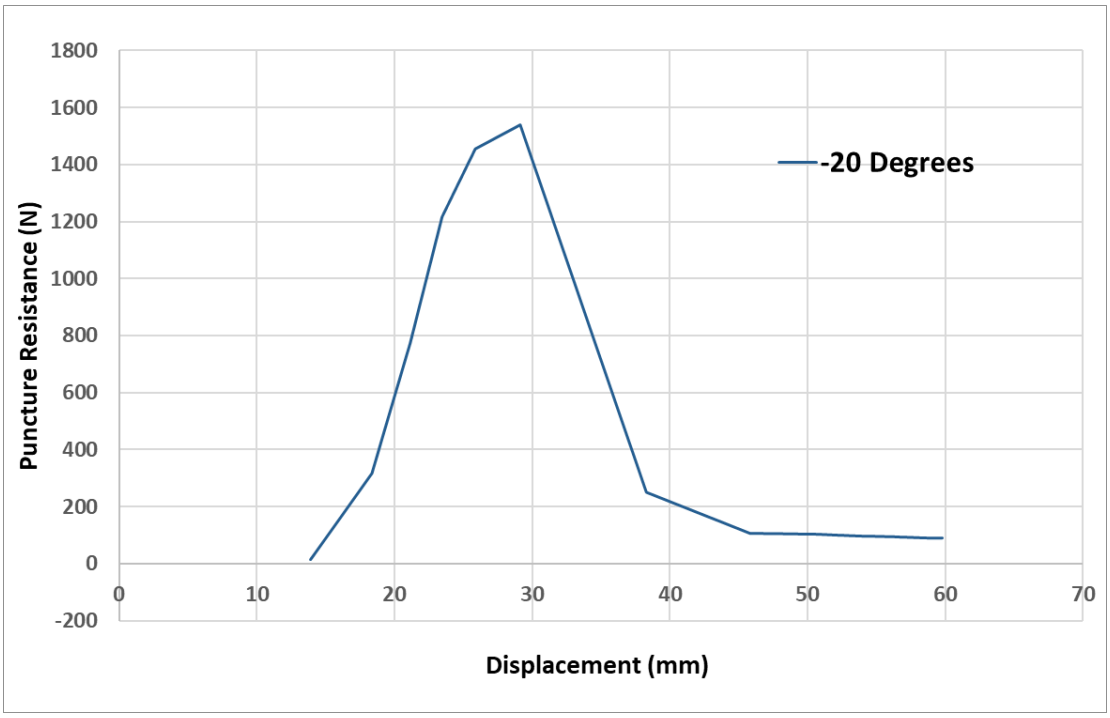

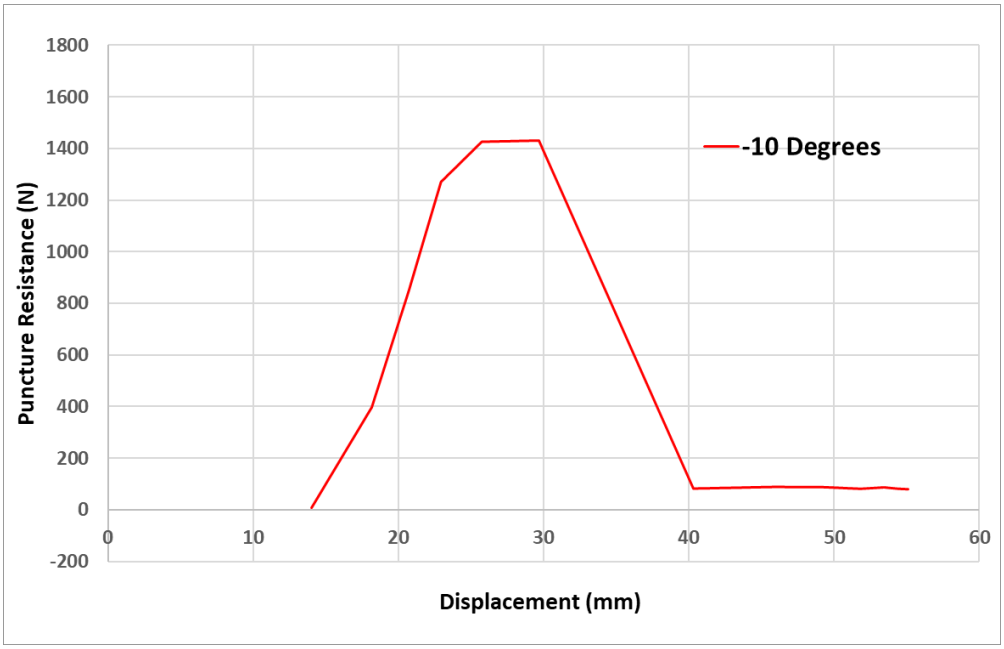
1800
1600
1400
1200
1000
800
600
400
200
0
-200
0
10
20
30
40
50
60
Puncture Resistance (N)
Displacement (mm)
-10 Degrees

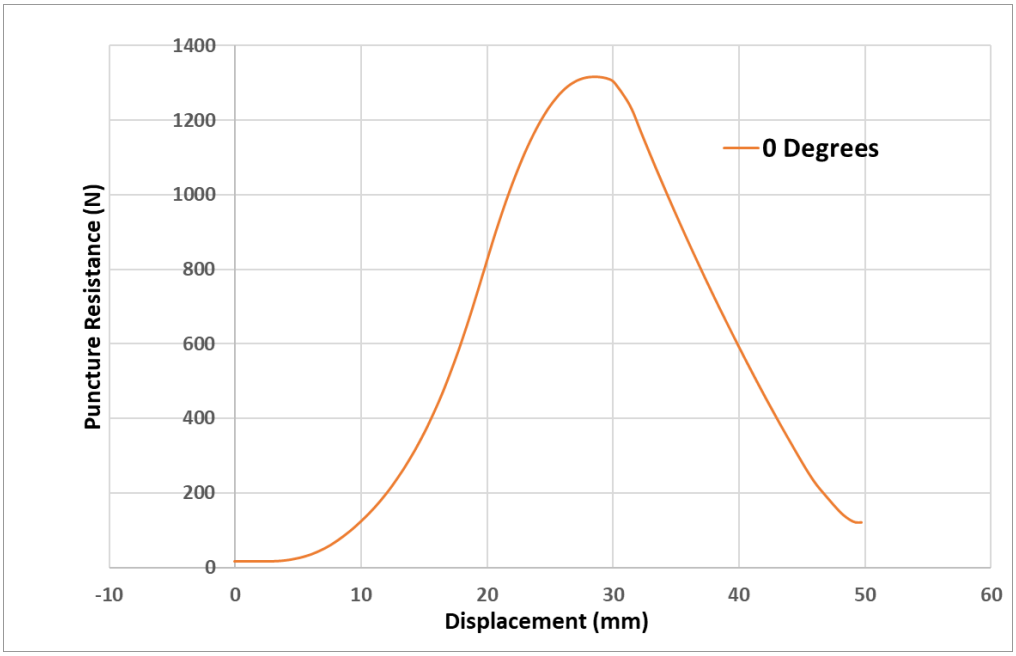
1400
1200
1000
800
600
400
200
0
-10
0
10
20
30
40
50
60
Puncture Resistance (N)
Displacement (mm)
0 Degrees

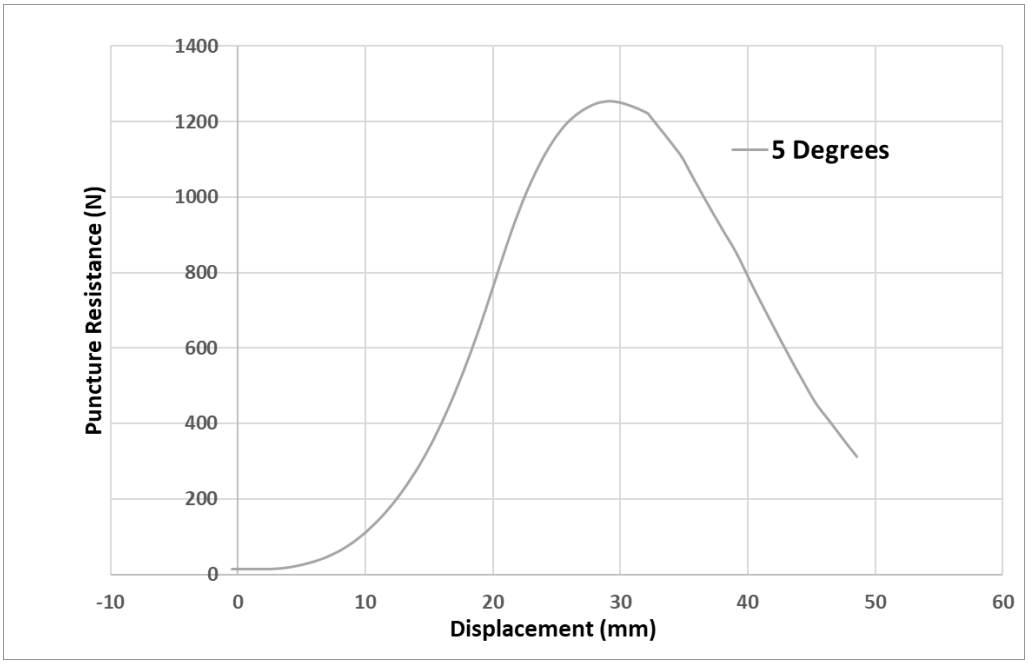
1400
1200
1000
800
600
400
200
0
Puncture Resistance (N)
-10
0
10
20
30
40
50
60
Displacement (mm)
5 Degrees

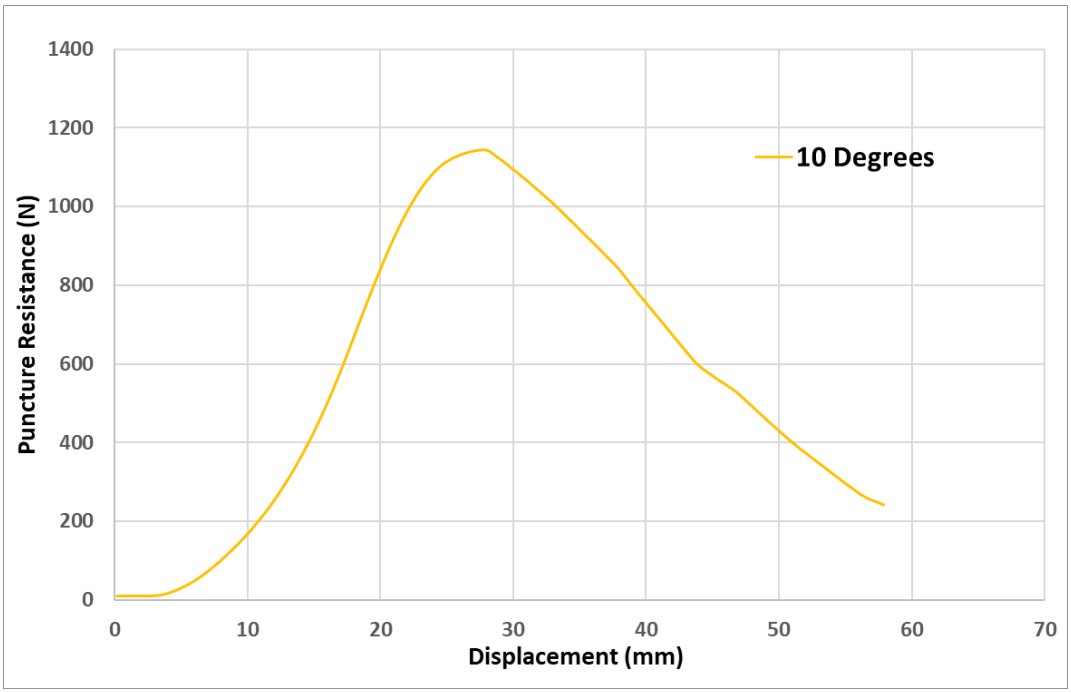
1400
1200
1000
800
600
400
200
0
Puncture Resistance (N)
0
10
20
30
40
50
60
70
Displacement (mm)
10 Degrees

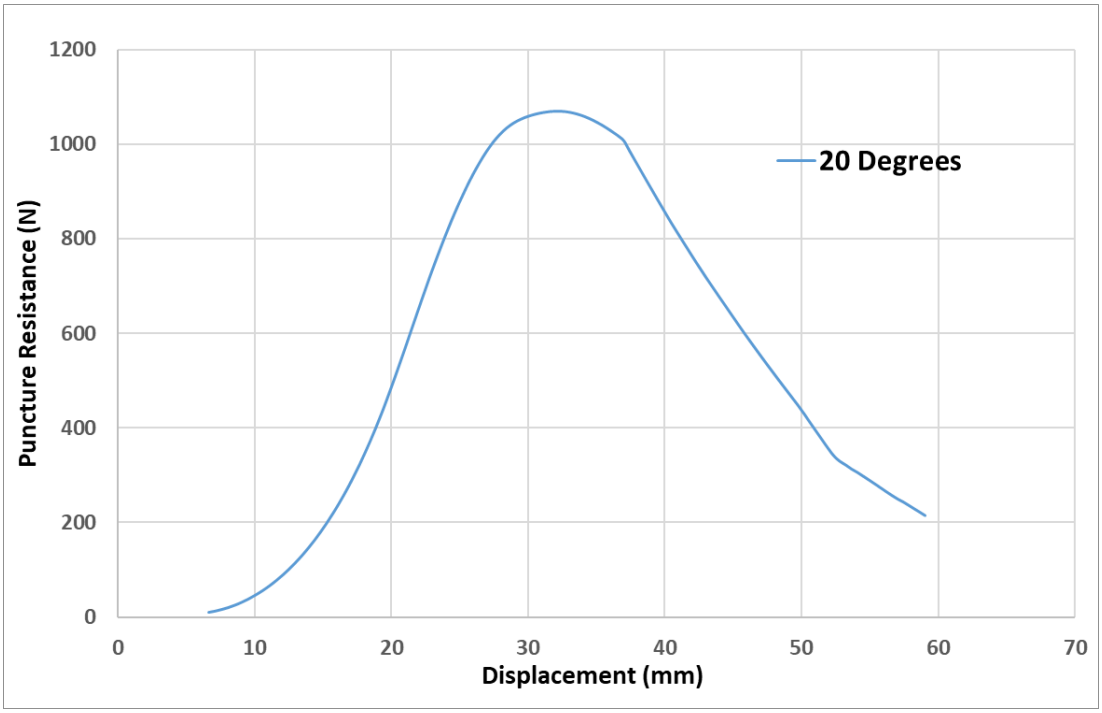
1200
1000
800
600
400
200
0
Puncture Resistance (N)
0
10
20
30
40
50
60
70
Displacement (mm)
20 Degrees

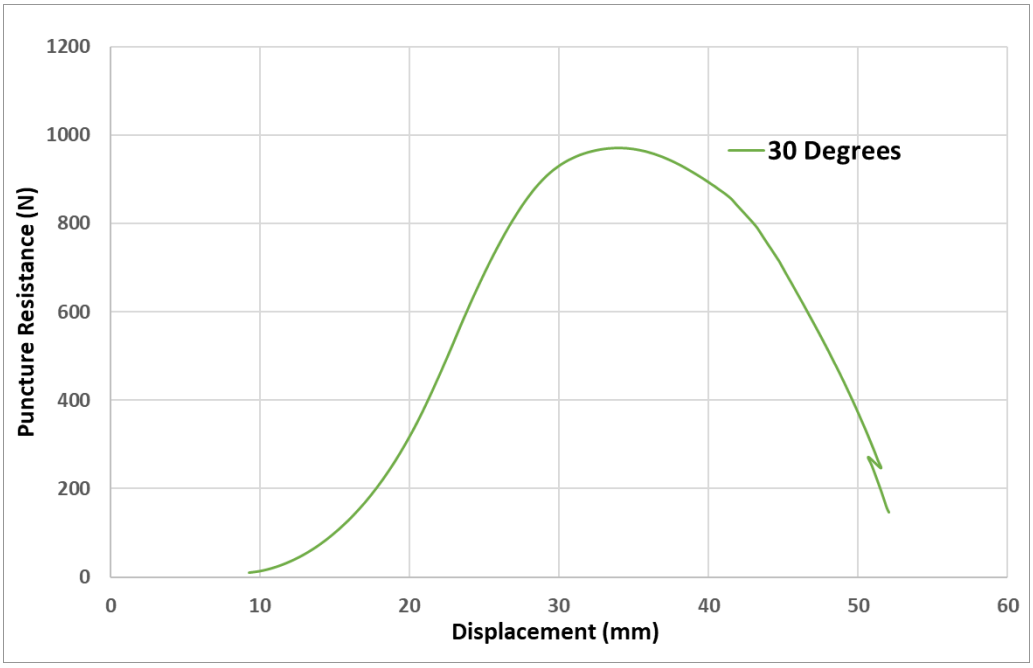
1200
1000
800
600
400
200
0
Puncture Resistance (N)
0
10
20
30
40
50
60
Displacement (mm)
30 Degrees

Appendix B: Engineering Designs of Manufactured Equipment

B.1: Individual Component Drawings

The following section contains individual component design drawings manufactured by the Engineering Shops in the College.

B.1.1: Load Apparatus Lower Body

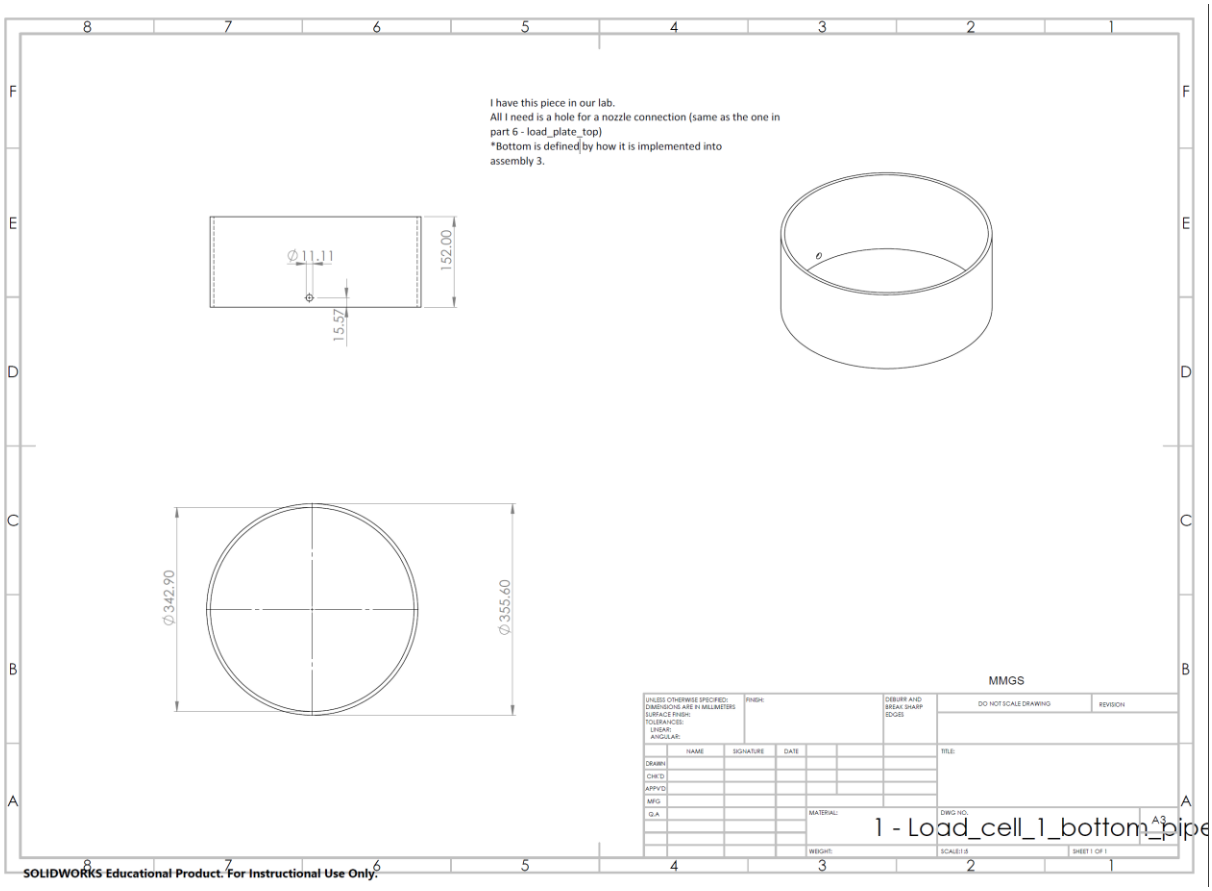

B.1.2: Load Apparatus Upper Body

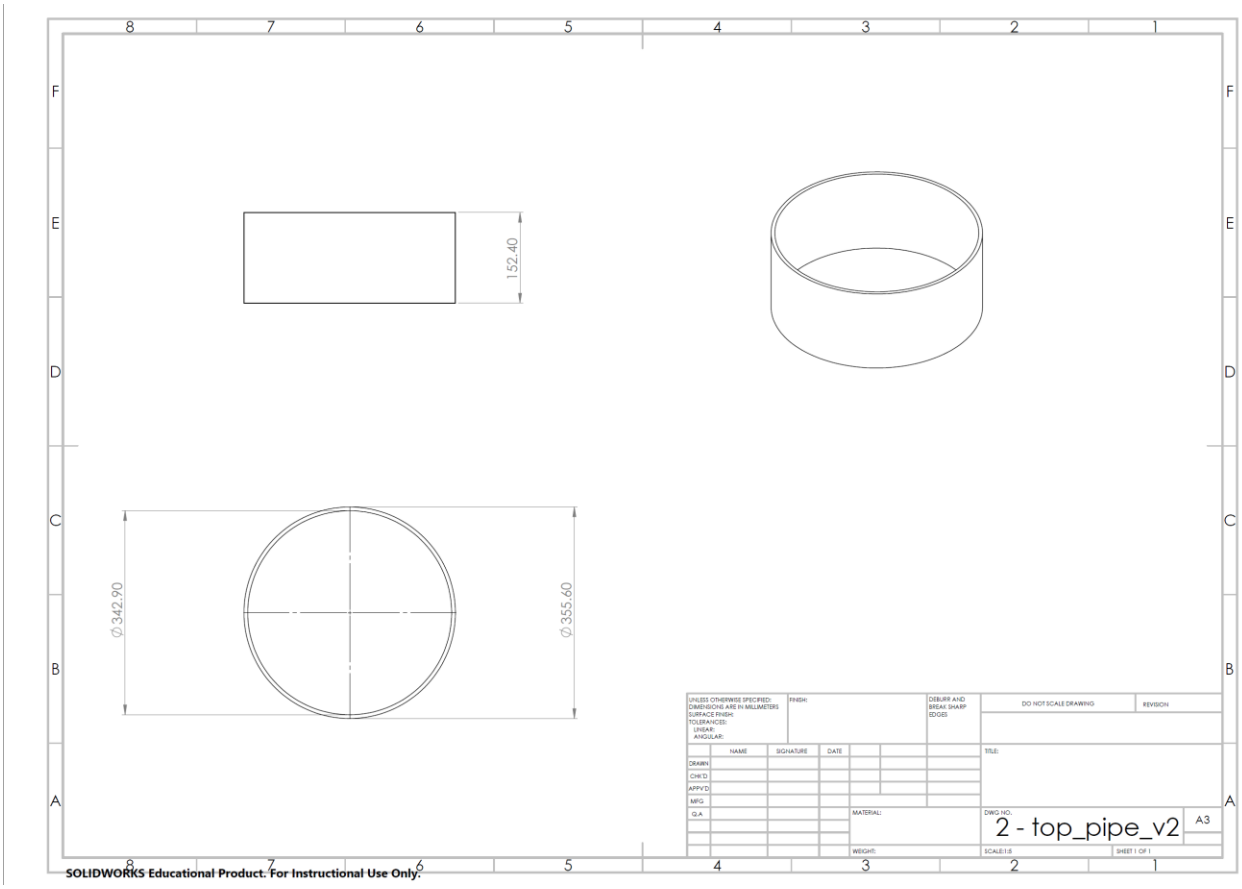

B.1.3: O-Ring Placeholder

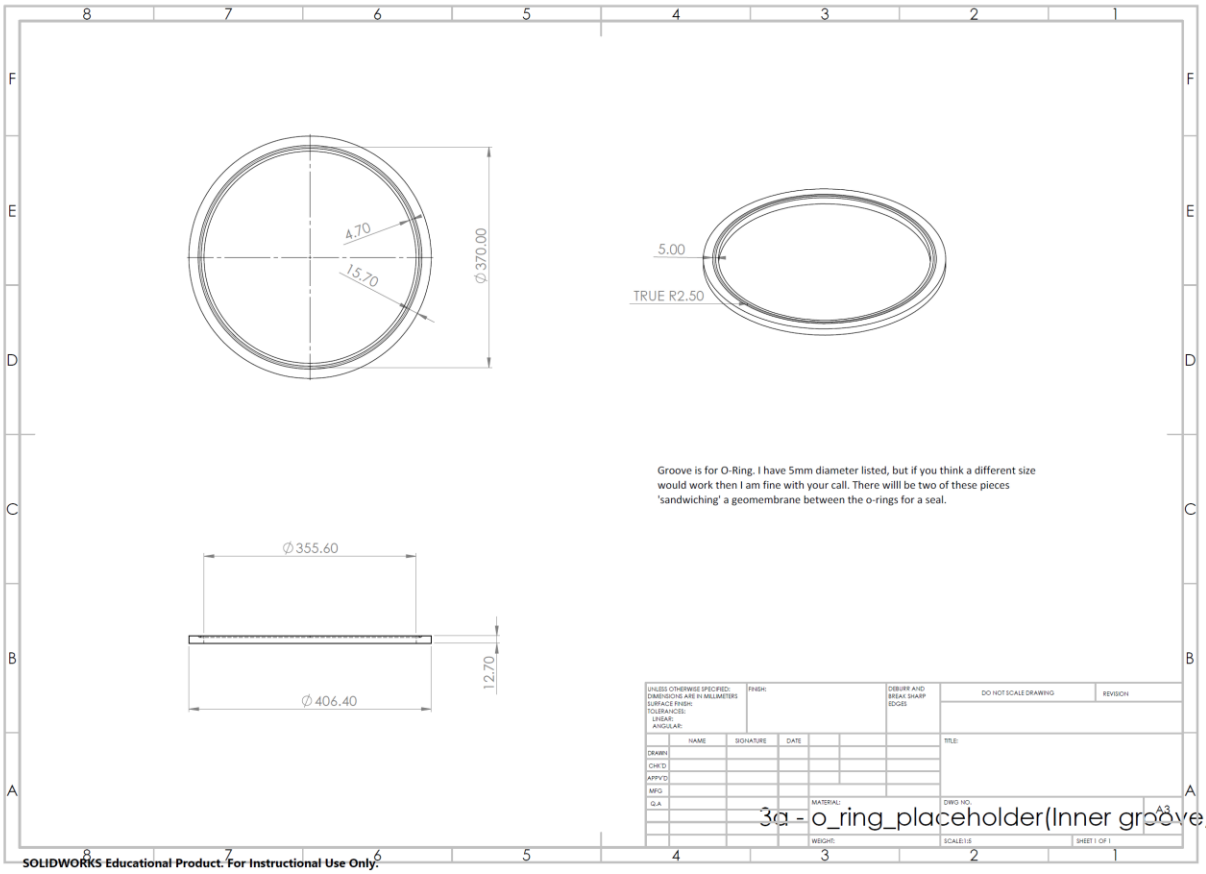

B.1.4: Upper Cap Plate

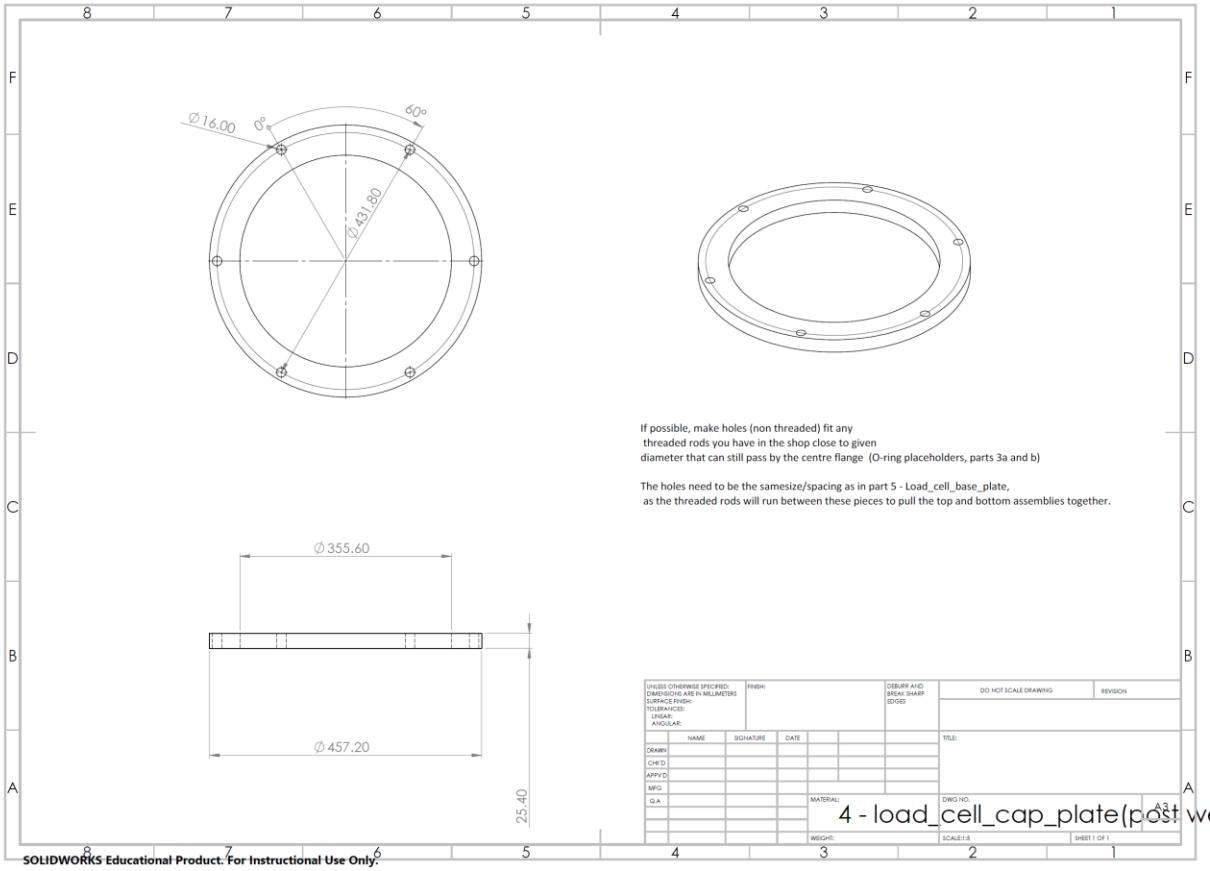

B.1.5: Lower Base Plate

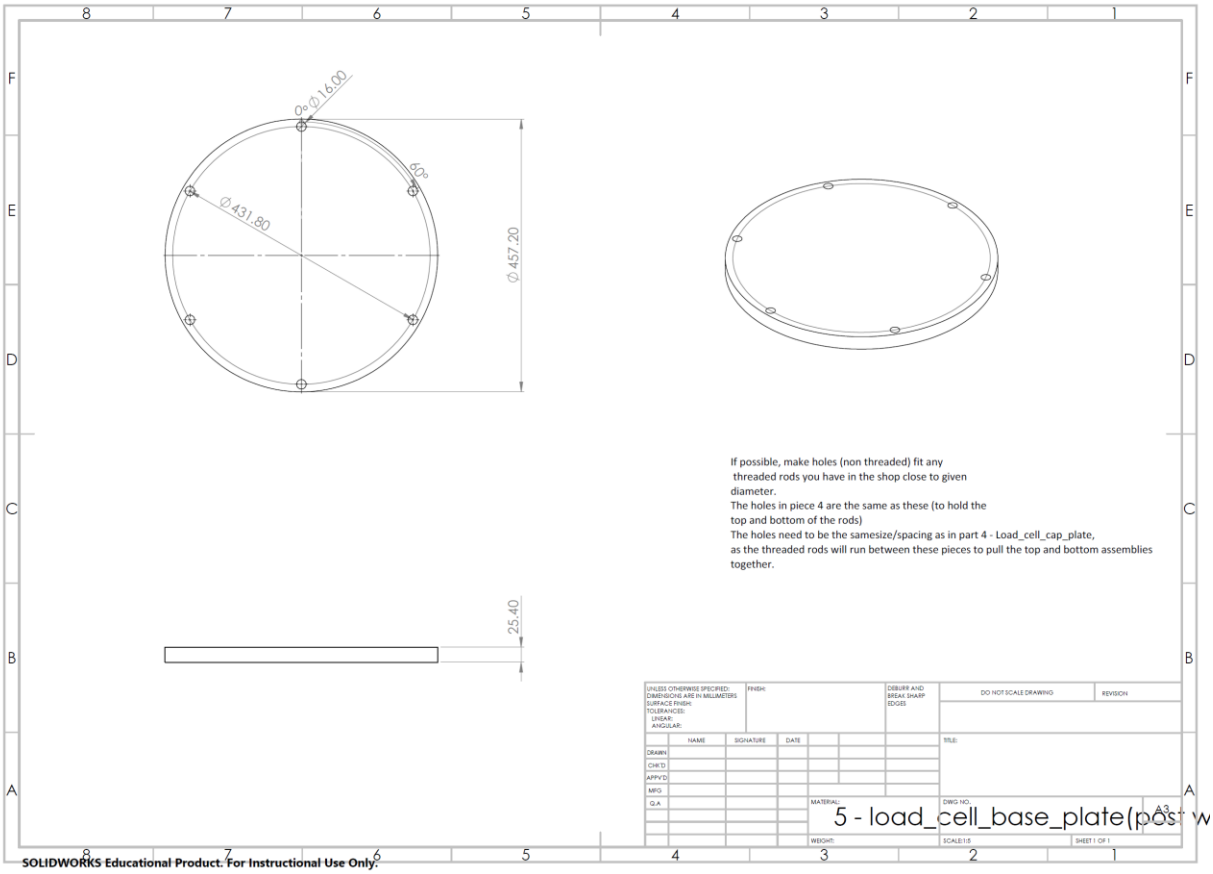

B.1.6: Load Plate Top

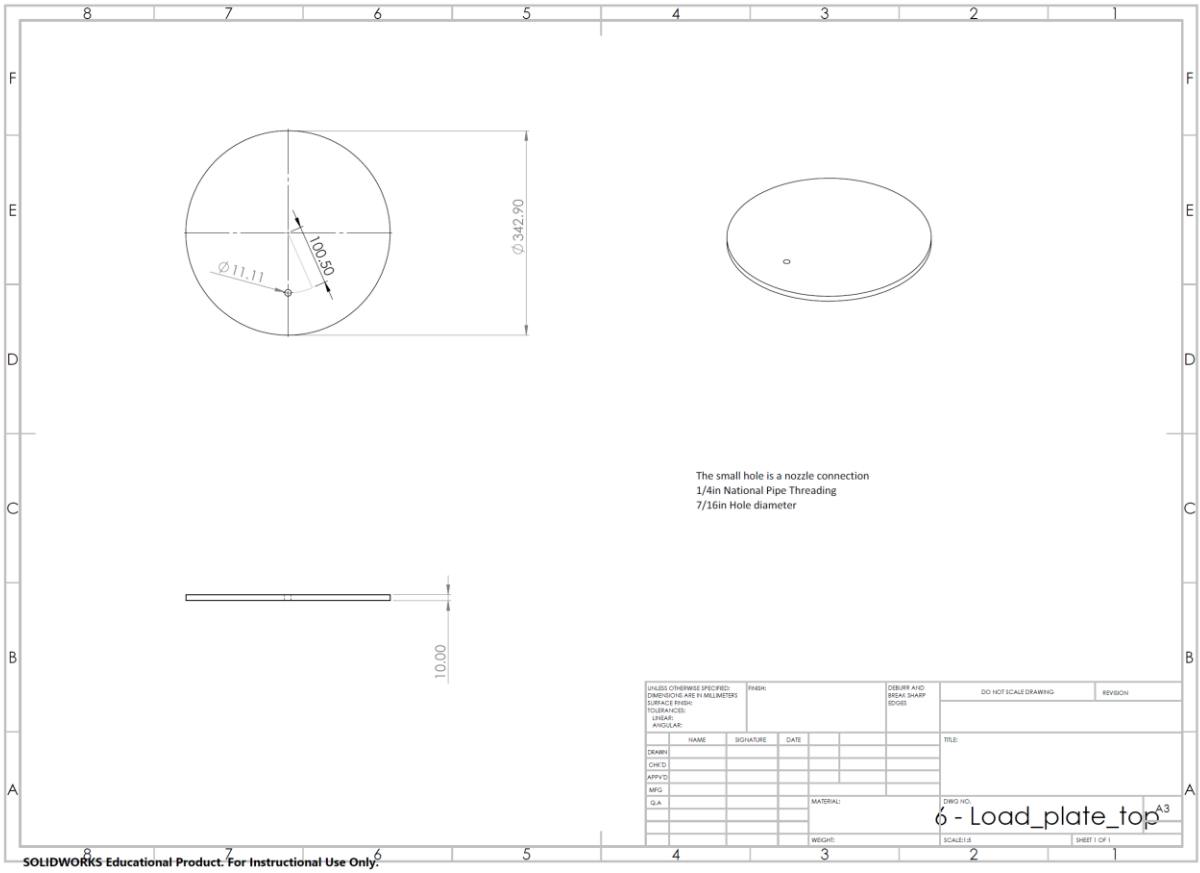

B.1.7: Load Plate Body

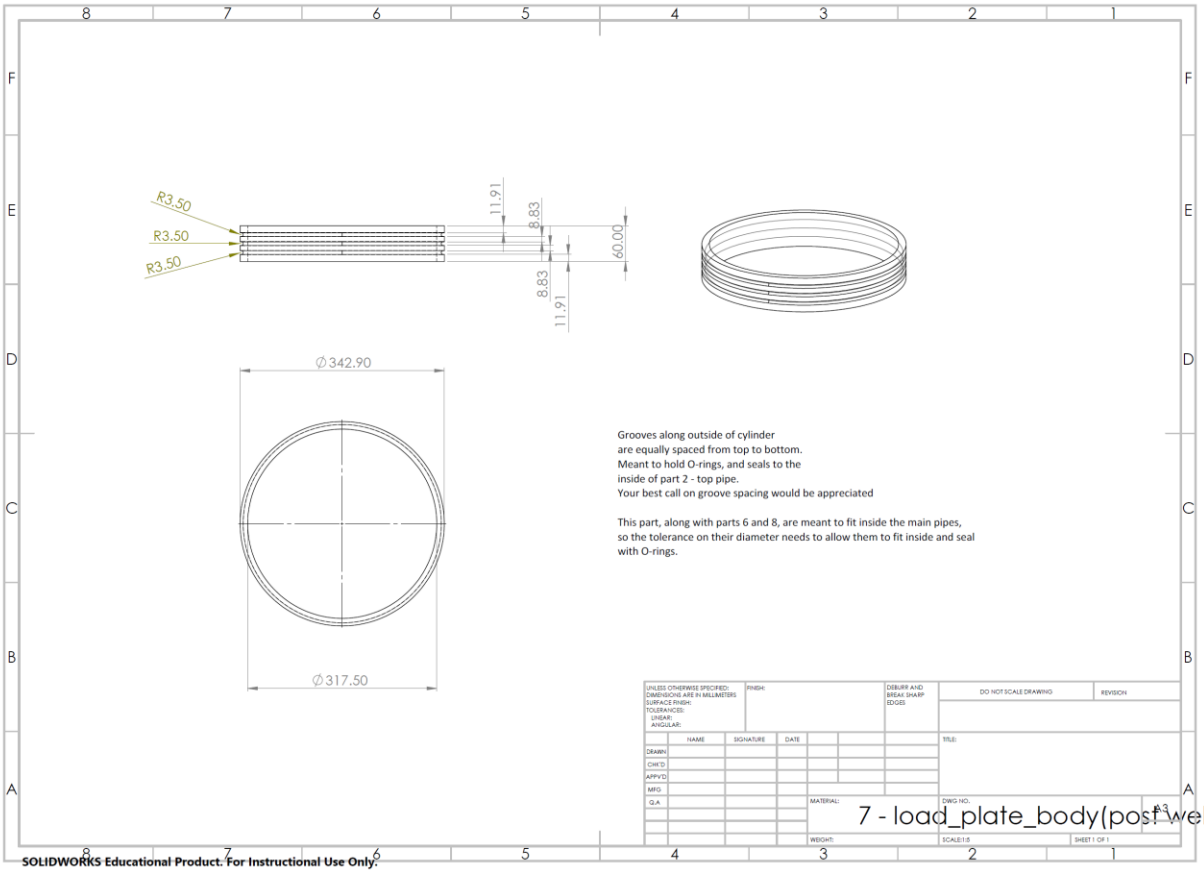

B.1.8: Load Plate Bottom

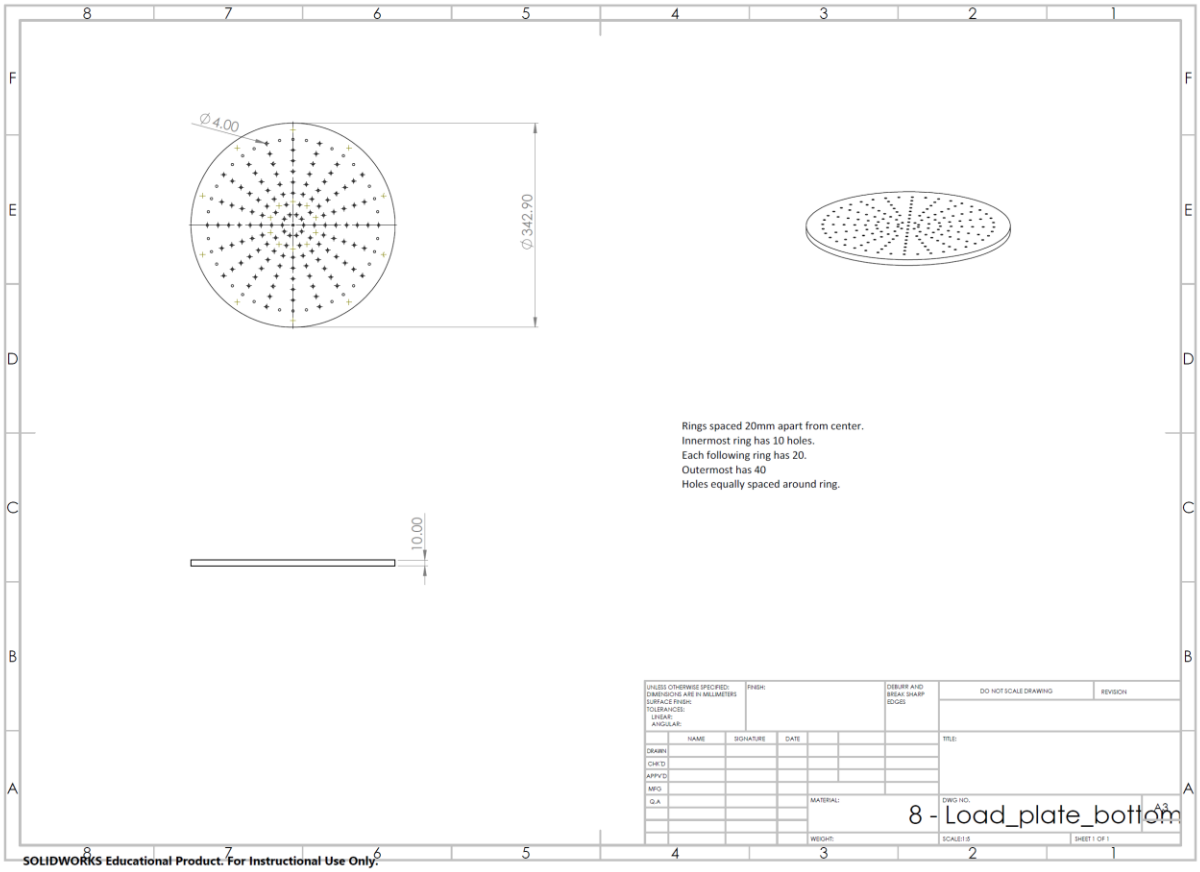

B.1.9: Load Point Attachment

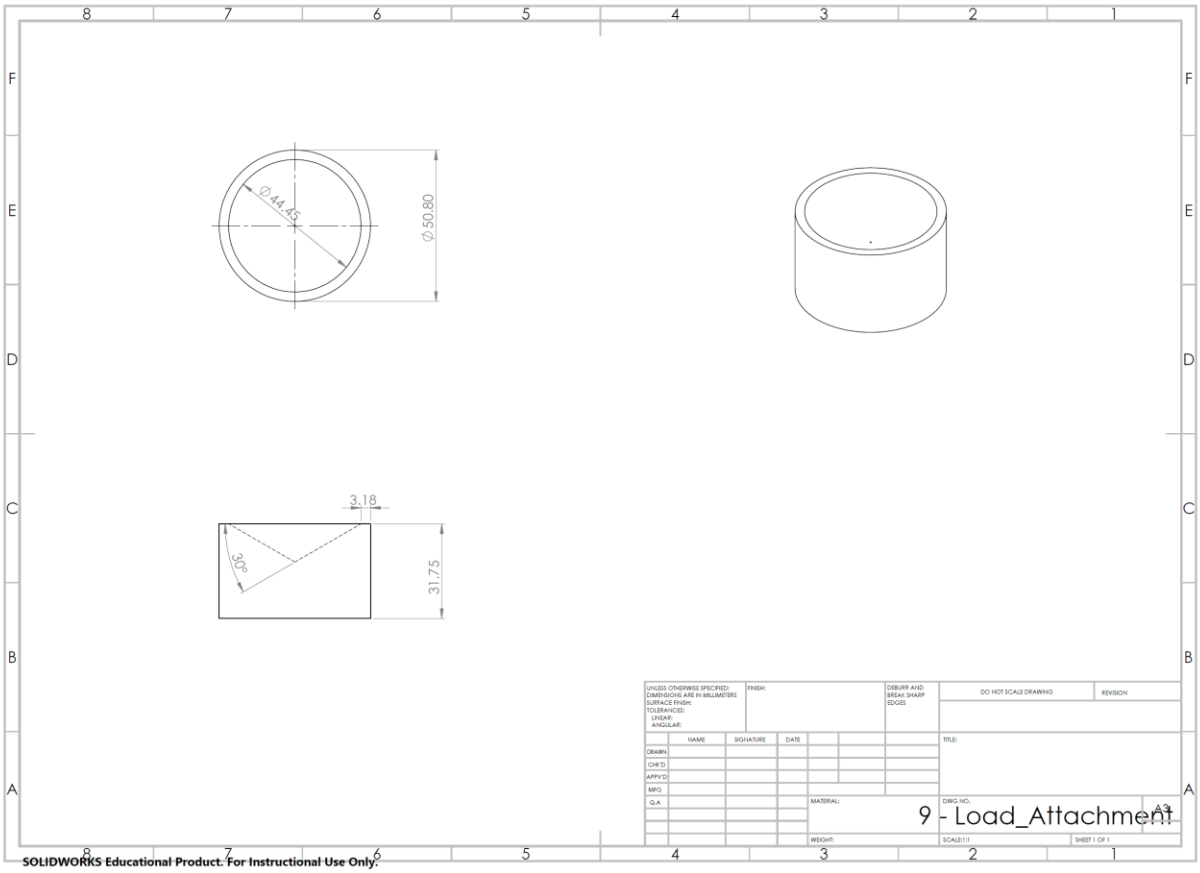

B.2: Assembly Design Drawings

It is worth noting that the upper body assembly had adjustments made after initial manufacturing. The interior diameter of the body was shaved down to very slightly loosen the tight tolerances between the body, and the load plate as initial testing resulted in the pieces being to tight to separate after testing. The results from the tests prior to this adjustment were not considered for any results.

B.2.1: Upper Body Assembly

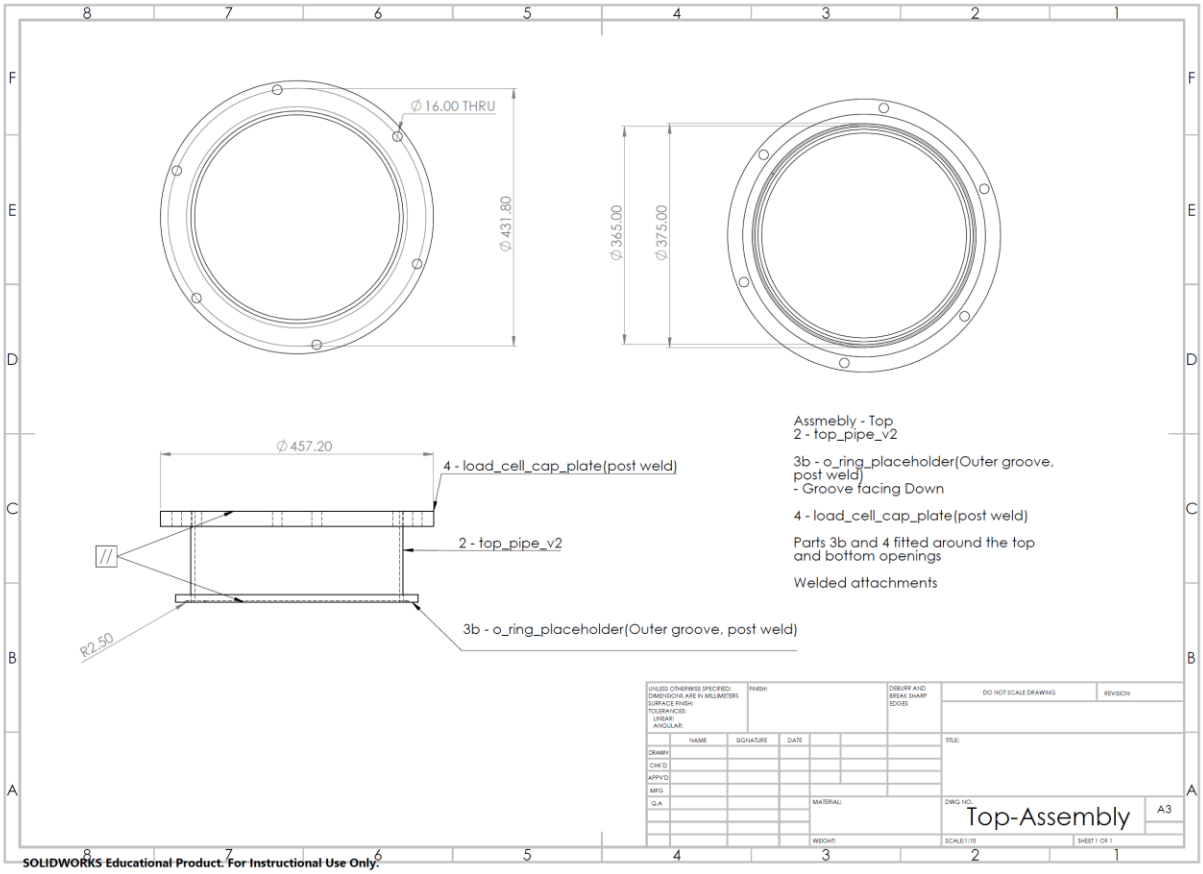

B.2.2: Lower Body Assembly

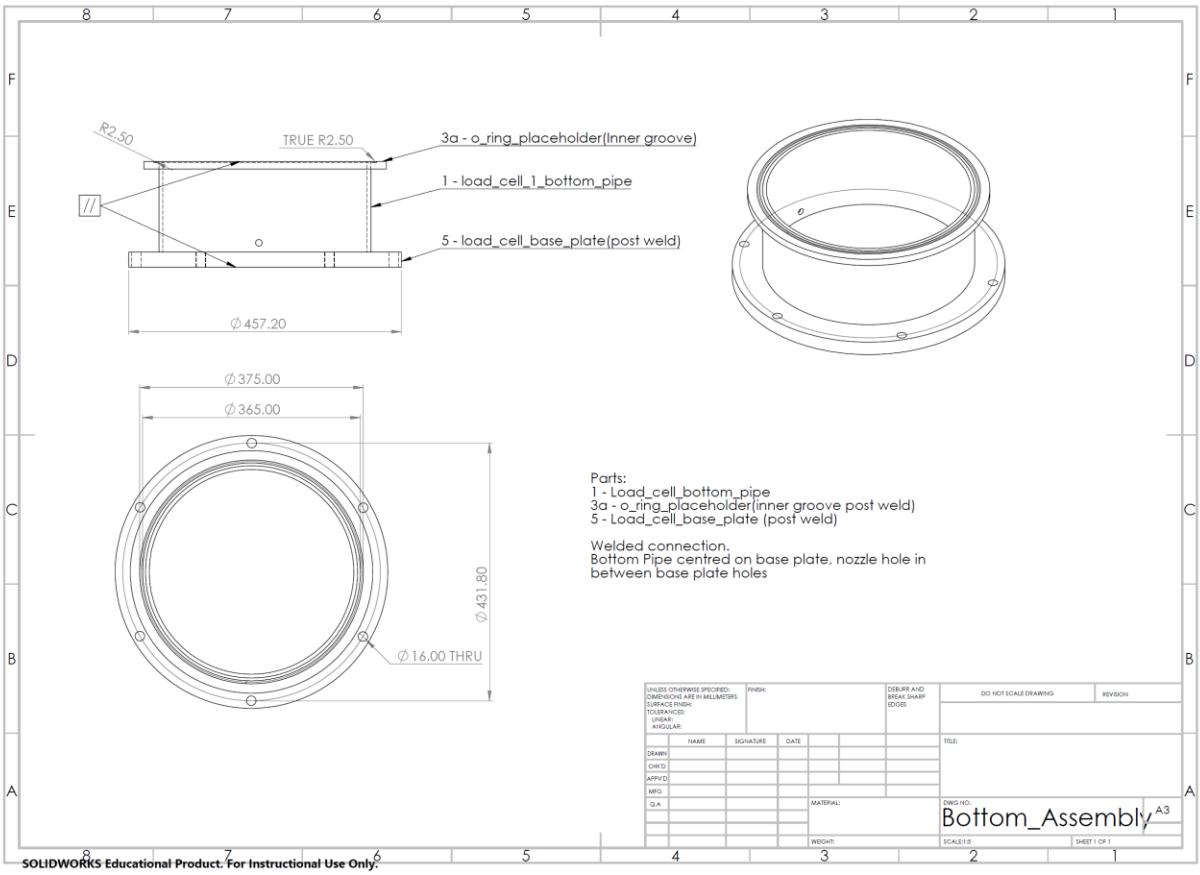

B.2.3: Load Plate Assembly

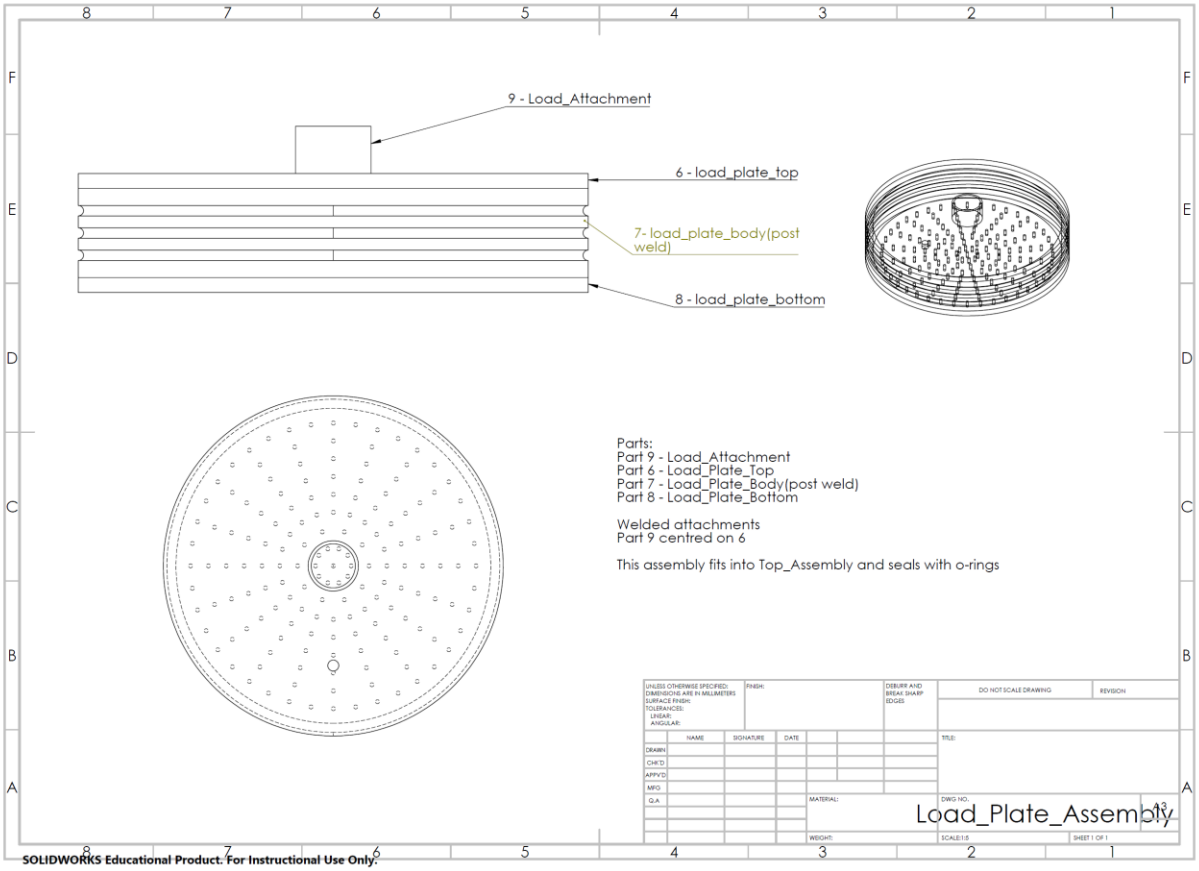

Appendix C: Extra Large Scale Sample Photos

C.1: ES2 Samples Photos (−15°C)

C.2: ES4 Samples Photos (−15°C)

C.3: ES2 Samples Photos (0°C)

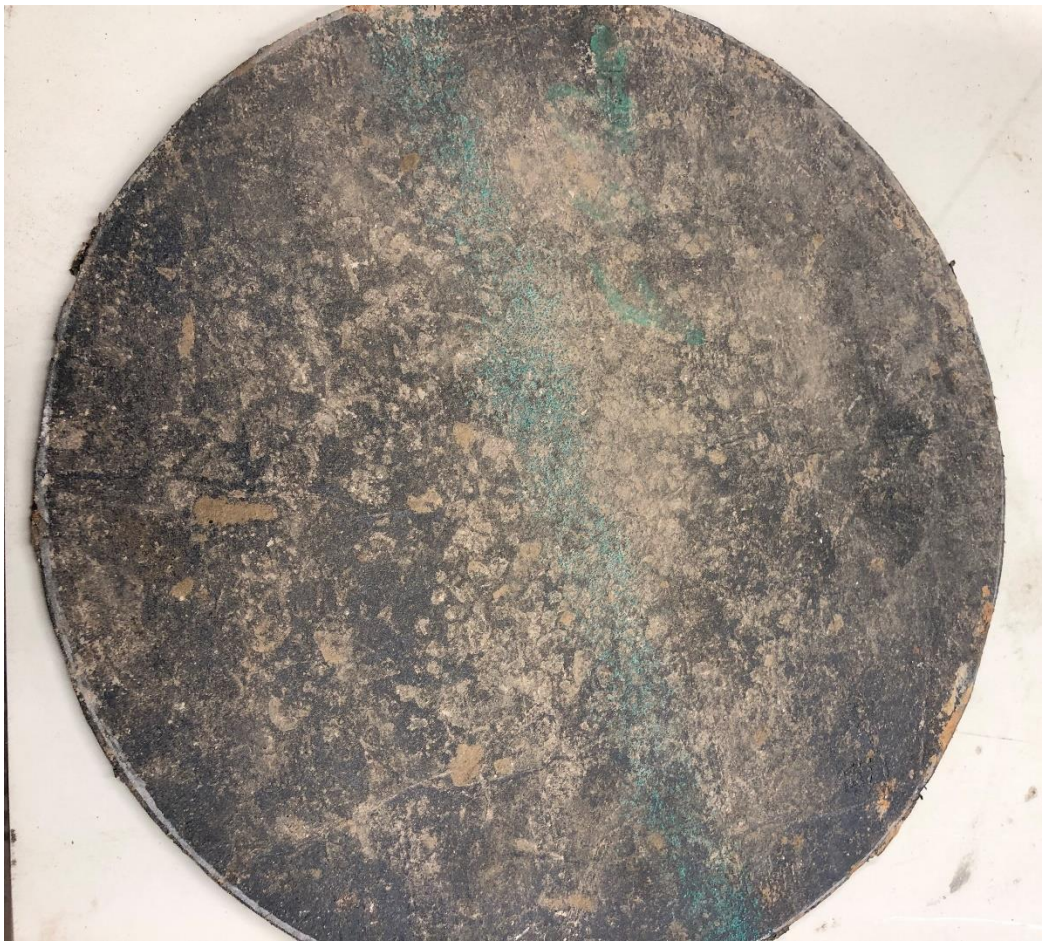

C.4: ES4 Samples Photos (0°C)

C.5 ES2 Samples Photos (+20°C)

C.6: ES4 Samples Photos (+20°C)

Appendix D: Bituminous Geomembrane Datasheets

D.1: ES2 Datasheet

COLETANCHE® by AXTER

8, Avenue Félix d'Hérelle
75016 Paris - FRANCE
www.coletanche.com

Prepared: 15/01/2018
Cancels and replaces 26/08/2016
Code : 1876901
Manufacture source Courchelettes (59-France)
Technical ref: FT AXTER ES2 ASTM

PRODUCT DATA SHEET

COLETANCHE ES 2

DESCRIPTION

COLETANCHE ES 2 is an SBS elastomeric modified bituminous geomembrane.

USE

Moderate level of mechanical resistance, for use an environmental protection and groundworks waterproofing, in particular :
- To cover landfill,
- Hydraulic ponds,
- Containment of Industrial liquid wastes,
- Canals ,
- Contamined land.

Product use must be validated by Axter

APPLICATION METHOD

By torch welding or other similar technique

STORAGE

Rolls must not be stored directly on the ground. Provide suitable supports (blocks, slides, wooden planks) with a minimum height of 35 cm to be placed under the ends of the mandrel.

COMPOSITION *(indicative)*

Reinforcement (g/m²) :	Glass mat	50
Reinforcement (g/m²) :	Non-woven geotextile	250
Binder (g/m²) :	Elastomeric SBS	4300
Surface finish (g/m²) :	Sand	250
Under surface finish (g/m²) :	Polyester antiroot film	15

CHARACTERISTICS

		STANDARD	UNITS	AVERAGE	Minimum
Dimensions	Length	-	*m*	80	79
	Width		*m*	5.10	5.01
Thickness (on finished product)		*ASTM D 5199*	mm	4.00	*3.60*
Surface mass		*ASTM D 3776*	kg/m²	4.85	*4.30*
Resistance to tearing	Longitudinal	*ASTM D 4073*	N	825	*619*
	Cross direction			700	*525*
Tensile properties : maximum tensile strength	Longitudinal	*ASTM D 7275*	kN/m	27	*20.3*
	Cross direction			24	*15*
Tensile properties : elongation	Longitudinal		%	50	*35*
	Cross direction			50	*35*
Static Puncture		*ASTM D 4833*	N	530	*477*
Flexibility at low temperature	Longitudinal	*ASTM D 5147*	°C	-20	-15
	Cross direction			-20	-15
Water permeability (liquid tightness)		*ASTM E 96*	*m/s*	6.10^{-14}	
Gas permeability (gas tightness)		*ASTM D 1434-82*	*m³/m²/j/atm*	$< 3.10^{-14}$	

NOTE: AXTER COLETANCHE INC. may modify the composition and/or utilisation of its products without prior notice. Consequently orders will be filled according to the latest specification.

AXTER afaq ISO 9001 Qualité afaq ISO 14001 Environnement

D.2: ES4 Datasheet

COLETANCHE by AXTER

143, avenue de Verdun
92130 Issy-les-Moulineaux
France
www.coletanche.com

Prepared: 24/02/2020
Cancels and replace 12/06/2018
Code : 1878M01
Manufacture source Courchelettes (59-France)
Technical ref: FT AXTER ES4 ASTM

PRODUCT DATA SHEET

COLETANCHE ES 4

Certified to NSF/ANSI 61

DESCRIPTION

COLETANCHE ES 4 is an SBS elastomeric modified bituminous geomembrane.

USE

Extreme level of mechanical resistance, for use as environmental protection and underground works waterproofing (aggressive materials,reinforced precautions), in particular :
- Railways, directly under ballast,
- Dams,

Product use must be validated by Axter.

APPLICATION METHOD

By torch welding or other similar technique.

STORAGE

Rolls must not be stored directly on the ground. Provide suitable supports (blocks, slides, wooden planks) with a minimum height of 35 cm to be placed under the ends of the mandrel.

COMPOSITION

(indicative)

Reinforcement (g/m²) :	Glass mat	50
Reinforcement (g/m²) :	Non-woven geotextile	400
Binder (g/m²) :	Elastomeric SBS	5400
Surface finish (g/m²) :	Sand	250
Under surface finish (g/m²) :	Polyester antiroot film	15

CHARACTERISTICS

		STANDARD	UNITS	AVERAGE	Min
Dimensions	Length	-	*m*	55	54
	Width		*m*	5.10	5.01
Thickness (on finished product)		*ASTM D 5199*	mm	5.60	*4.80*
Surface mass		*ASTM D 3776*	kg/m²	6.40	*5.90*
Resistance to tearing	Longitudinal	*ASTM D 4073*	N	1225	*919*
	Cross direction			1025	*769*
Tensile properties : maximum tensile strength	Longitudinal	*ASTM D 7275*	kN/m	35	*29.2*
	Cross direction			30	*23.2*
Tensile properties : elongation	Longitudinal		%	60	*45*
	Cross direction			60	*45*
Static Puncture		*ASTM D 4833*	N	650	*585*
Flexibility at low temperature	Longitudinal	*ASTM D 5147*	°C	-20	-15
	Cross direction			-20	-15
Water permeability (liquid tightness)		*ASTM E 96*	*m/s*	6.10^{-14}	<
Gas permeability (gas tightness)		*ASTM D 1434-82*	$m^3/(m^2.j.atm)$	2.10^{-4}	<

NOTE: AXTER COLETANCHE INC. may modify the composition and/or utilisation of its products without prior notice. Consequently orders will be filled according to the latest specification.

AXTER

afaq ISO 9001 Qualité AFNOR CERTIFICATION

afaq ISO 14001 Environnement AFNOR CERTIFICATION